



AN ABSTRACT OF THE DISSERTATION OF

Prashant Wadhwa for the degree of Doctor of Philosophy in Materials Science

presented on November 21, 2007.

Title: Non Newtonian Viscosity of Bulk Metallic Glass Forming Liquids and the

Ordering and Shear Rate Induced Crystallization of Undercooled

Zr<sub>41.2</sub>Ti<sub>13.8</sub>Cu<sub>12.5</sub>Ni<sub>10.0</sub>Be<sub>22.5</sub> Metallic Glass Forming Melt.

Abstract approved: \_\_\_\_\_

Ralf Busch

The influence of shear rate and temperature on the viscosity and fragility of the Zr<sub>41.2</sub>Ti<sub>13.8</sub>Cu<sub>12.5</sub>Ni<sub>10.0</sub>Be<sub>22.5</sub> (Vit1) metallic glass forming liquid is measured in the liquid and undercooled liquid state between 907 and 1300 K. The results show a complex rheological behavior of Vit1. The viscosity of Vit1 is about three orders of magnitude higher than simple metallic liquids with strong shear thinning behavior upon first heating from the amorphous state above the liquidus temperature. The shear thinning behavior decreases with increasing temperature and this kinetically strong liquid transforms to a more fragile liquid with no shear rate dependence of viscosity. The Newtonian temperature ( $T_{\text{Newtonian}}$ ) for Vit1 is measured as 1225 K. Upon cooling

this liquid the strong liquid behavior is only re-established when the melt is deeply undercooled below the liquidus temperature. This gives rise to the “hysteresis effect” in the viscosity of Vit1 as a function of temperature. The difference in viscosity and the shear thinning behavior is also seen depending on the initial state of the material (amorphous or crystalline). The shear thinning and strong to fragile transition is attributed to the destruction of medium range order (MRO) in the liquid state whereas the reformation of order in the supercooled region is much more complex. Secondly, the effect of ordering and shear rate on the crystallization kinetics of undercooled  $Zr_{41.2}Ti_{13.8}Cu_{12.5}Ni_{10.0}Be_{22.5}$  metallic-glass-forming melts is investigated. The study quantitatively shows the shift of the TTT diagram of Vit1 to shorter crystallization times with increasing shear rates. The classical nucleation and growth theory is applied by incorporating the change in various factors such as viscosity, driving force for crystallization and entropy change as a function of shear rate. It is found that the change in crystallization kinetics can not be explained quantitatively by the classical nucleation and growth theory. The order present in the melt immensely influences the crystallization and the material with higher order crystallizes sooner than the material with smaller order. The ordered clusters are formed faster at higher shear rates and hence the material crystallizes sooner at higher shear rates making the TTT diagram shift to the left.

Finally, the viscosities of two bulk metallic glass forming liquids  $Zr_{57}Cu_{15.4}Ni_{12.6}Al_{10}Nb_5$  (Vit106) and  $Pd_{43}Ni_{10}Cu_{27}P_{20}$  are measured and compared with the viscosity of Vit1. The main goal of this study was to investigate whether high viscosity and shear thinning behavior is just associated with Vit1 or the other BMG

forming liquids also show such behavior. It is shown that all these glass formers show higher viscosities than monoatomic metallic liquids and surprisingly the non-Newtonian shear thinning behavior. Vit1 exhibits the highest viscosity with the largest drop in viscosity on shearing from  $0.1 \text{ s}^{-1}$  to  $250 \text{ s}^{-1}$  at the temperatures above  $T_{\text{liq}}$ . Vit106 shows lower viscosities than Vit1, however, a stronger non-Newtonian behavior on shearing from  $0.1 \text{ s}^{-1}$  to  $143 \text{ s}^{-1}$  at the temperatures between 1130 K and 1305 K is seen. Surprisingly, this non-Newtonian behavior disappears at higher shear rates where the viscosity stays constant. The melt viscosity of the  $\text{Pd}_{43}\text{Ni}_{10}\text{Cu}_{27}\text{P}_{20}$  shows a lower viscosity and much smaller shear thinning behavior than the Zr-based alloys. The viscosity data of Vit106 and  $\text{Pd}_{43}\text{Ni}_{10}\text{Cu}_{27}\text{P}_{20}$  indicate a possibility to reach a steady state viscosity if high enough shear rates are applied to the melt of Vit1 at the temperatures between 1075 K and 1225 K. In all the three alloys, this non-Newtonian behavior gets weaker with increasing temperature and the material starts to behave like a Newtonian liquid. This behavior is attributed to the presence of MRO and short range order (SRO) in the melt of these alloys. The MRO present in the melt can be reduced by shearing and more effectively destroyed to SRO by increasing the temperature which leads to a Newtonian liquid with smaller viscosity.

©Copyright by Prashant Wadhwa

November 21, 2007

All Rights Reserved

Non Newtonian Viscosity of Bulk Metallic Glass Forming Liquids and the Ordering  
and Shear Rate Induced Crystallization of Undercooled  $Zr_{41.2}Ti_{13.8}Cu_{12.5}Ni_{10.0}Be_{22.5}$

Metallic Glass Forming Melt

by

Prashant Wadhwa

A DISSERTATION

submitted to

Oregon State University

in partial fulfillment of  
the requirements for the  
degree of

Doctor of Philosophy

Presented November 21, 2007

Commencement June 2008

Doctor of Philosophy dissertation of Prashant Wadhwa presented on November 21,  
2007.

APPROVED:

---

Major Professor, representing Materials Science

---

Director of the Material Science Program

---

Dean of the Graduate School

I understand that my dissertation will become part of the permanent collection of Oregon State University libraries. My signature below authorizes release of my dissertation to any reader upon request.

---

Prashant Wadhwa, Author

## ACKNOWLEDGEMENTS

None of this work would have been possible without the guidance and motivation of Dr. Ralf Busch. His profound knowledge and determined advice guided me and lead to the success in this work. My special thanks go to Dr. Christopher Way, who trained me on using the viscometer and provided support in this work to bring the elaborateness in the work. I sincerely thank Dr. William Warnes for his cooperation and encouragement during my work at OSU. I would like to extend my gratitude to Dr. Isabella Gallino for the support and motivation she provided me during my stay in Germany. I would also like to thank the following people, my friends and my family for their contribution and support through my academic & personal development – alphabetical order.

Steve Adams

Dr. Max Launey

Herman Altmeyer

Ben Legg

Gaurav Bajaj

Dr. Vinod Narayanan

Dr. Belinda Batten

Dr. Willie “Skip” Rochefort

Dr. Manish Bothara

Vardan Rathi

Dr. Dave Cann

Dr. Andrew Ross

Manfred Dettrich

Chandan Sarkar

Heather Glover

Dr. Jan Schroers

Deeksha Grover

Minalben Shah

Pranav Joshi

Dr. Jay Kruzic

I dedicate this manuscript to  
my Family and VasudevShriKrishana

## TABLE OF CONTENTS

		<u>Page</u>
1	INTRODUCTION.....	1
2	LITERATURE REVIEW AND BACKGROUND – BULK METALLIC GLASSES.....	5
2.1	History and Development of Bulk Metallic Glasses .....	5
2.1.1	Processing of Metallic Glasses.....	7
2.2	Metallic Glass and the Glass Transition.....	9
2.3	Glass Forming Ability in Multicomponent Alloys.....	11
2.4	Thermodynamics and Kinetics of Metallic Glasses.....	13
2.4.1	Thermodynamics of Metallic Glasses .....	14
2.4.2	Kinetics and Viscosity of Metallic Glasses .....	22
2.4.2.1	Angell Plot.....	23
2.4.2.2	Adam-Gibbs Entropy Model for Viscous Flow.....	25
2.5	Crystallization of Supercooled Metallic Liquids and Glasses.....	26
2.5.1	TTT Diagram.....	26
2.6	Viscosity Measurement of Bulk Metallic Glasses.....	31
2.6.1	Below the Liquidus Temperature.....	31
2.6.2	Above the Liquidus Temperature.....	32
2.7	Purpose of this Work.....	36
3	EXPERIMENTAL METHODS AND INITIAL WORK.....	38
3.1	Materials Preparation.....	38

## TABLE OF CONTENTS (Continued)

		<u>Page</u>
3.1.1	Differential Scanning Calorimetry.....	39
3.1.2	Differential Thermal Analysis.....	40
3.2	Viscosity Measurements.....	40
3.2.1	Measurement Equipment.....	40
3.3	Initial Work.....	44
	References.....	64
4	MANUSCRIPT I.....	68
	Abstract.....	69
	References.....	91
5	MANUSCRIPT II.....	93
	Abstract.....	94
	References.....	116
6	SUMMARY AND CONCLUSIONS.....	118
	References.....	126
7	REFERENCES.....	127

## LIST OF FIGURES

<u>Figure</u>	<u>Page</u>	
1	<p>Specific volume as a function of temperature for a liquid, which can form either glass or crystal. Formation of glass or crystal depends on the cooling rate. At the smaller cooling rates, the material follows (-----) and form crystal whereas at faster cooling rates (-) path is followed and glass formation takes place. In the figure <math>T_g</math> and <math>T_m</math> designate glass transition temperature and melting temperature respectively [25] .....</p>	10
2	<p>Differential Scanning Calorimeter (DSC) thermogram of <math>Zr_{41.2}Ti_{13.8}Cu_{12.5}Ni_{10}Be_{22.5}</math> (Vit1) from 500 to 1150 K using the scan heating rate of 10 K/min [31]. The onset of the glass transition, crystallization temperature, eutectic melting point and liquidus temperatures are depicted by <math>T_g</math>, <math>T_x</math>, <math>T_{eut}</math> and <math>T_{liq}</math> respectively.....</p>	16
3	<p>Heat capacity curves of the <math>Zr_{41.2}Ti_{13.8}Cu_{12.5}Ni_{10}Be_{22.5}</math> (Vit1) glass, the corresponding liquid and crystalline solid as a function of temperature [31].....</p>	18
4	<p>The Gibbs free energy difference between crystal and supercooled liquid for different various glass forming liquids. Vit1 with the smallest cooling rate shows the smallest free energy difference [26].</p>	21
5	<p>Equilibrium viscosity as a function of temperature for the supercooled liquid of <math>Zr_{41.2}Ti_{13.8}Ni_{10}Cu_{12.5}Be_{22.5}</math> (Vit1) in an Arrhenius plot [7].....</p>	23
6	<p>TTT Diagram for <math>Zr_{41.2} Ti_{13.8} Cu_{12.5} Ni_{10.0} Be_{22.5}</math> showing the liquidus temperature, glass transition temperature, super cooled liquid region, and the crystalline nose [26]. The samples have not been sheared during the experiment.....</p>	28
7	<p>Viscosity as a function of shear rate at various temperatures between 1071 K and 1156 K for Vit1. The data shown were collected by Tyler Shaw and Christopher Way [49, 50]. A strong shear thinning effect reflected in a pronounced decrease in viscosity with increasing shear rate can be seen. ....</p>	34

## LIST OF FIGURES (Continued)

<u>Figure</u>		<u>Page</u>
8	Schematic of high-temperature high-vacuum viscometer (from Tyler Shaw [49]).....	41
9	Isothermal viscosity vs. shear rate upon heating from 1075 K to 1300 K in 25 K increments. It shows the high viscosity and shear rate dependence above $T_{liq}$ for this alloy. With increasing temperature both of these behaviors reduce and become constant above 1225 K.....	47
10	Comparison of the isothermal viscosity vs. shear rate on initially amorphous material shown for two different temperature scans. The solid red symbols represent first temperature scan in which the viscosity upon heating the initially amorphous alloy from 1075 to 1275 K. At this point the sample was cooled to 1075 K and held isothermally for one hour. A second temperature scan from 1075 K to 1300 K, indicated by the open blue symbols, was then performed.....	49
11	Comparison of the isothermal viscosity vs. shear rate between initially amorphous (solid red symbols) and initially microcrystalline (open symbols) Vit1. At 1075 K there is a large difference between the viscosities of two samples, which decreases with increasing temperature. At 1175 K, the viscosities of both samples become the same and continue to be same with increasing temperature.....	51
12	Non-Newtonian behavior vs. temperature of initially amorphous Vit1 for a first (■) and a second (●) temperature scans. After first melting from the initially amorphous state, the alloy exhibits a pronounced shear thinning behavior that weakens with increasing temperature. Above 1225 K there is no longer a shear rate dependence of the viscosity. After cooling back to 1075 K and holding isothermal for one hour, the material is still Newtonian over the investigated temperature range.....	53

## LIST OF FIGURES (Continued)

<u>Figure</u>		<u>Page</u>
13	<p>Viscosity vs. temperature during undercooling experiment with an average cooling rate of <math>2 \text{ K}\cdot\text{s}^{-1}</math> using a constant clockwise shear rate. When the material is cooled from 1125 K (<math>\square</math>), the viscosity stays about two orders of magnitude higher than when cooled from 1225 K (<math>\circ</math>). Data shown by (<math>\Delta</math>) is represented by isothermal viscosity measurements.....</p>	55
14	<p>Angell plot showing the combined isothermal (<math>\bullet</math>, <math>\Delta</math>) and viscosity measurements obtained while cooling at <math>2 \text{ K}\cdot\text{s}^{-1}</math> from 1125 K (<math>\square</math>) and 1225 K (<math>\circ</math>). This shows the temperature hysteresis effect seen in the viscosity of Vit1. Also shown are the data of <math>\text{SiO}_2</math> and o-terphenyl. (<math>\bullet</math>) represents data collected at a shear rate of <math>10 \text{ s}^{-1}</math> while (<math>\Delta</math>) represents the viscosity collected at <math>100 \text{ s}^{-1}</math> upon cooling from 1300 K. This is done because the sensitivity of the torque sensor does not allow for accurate data at low shear rates. ....</p>	58
15	<p>Viscosity (<math>\blacksquare</math>) and temperature (-) signal with respect to recorded time upon cooling below <math>T_{\text{liq}}</math>. The onset of recalescence associated with crystallization occurs over 60 K below the temperature at which the increasing viscosity trips the torque sensor.....</p>	59
16	<p>Expanded Angell plot of combined isothermal (<math>\bullet</math>) and viscosity measurements obtained at a constant clockwise shear rate while cooling at <math>2 \text{ K}\cdot\text{s}^{-1}</math> from both 1125 K (<math>\circ</math>) and 1225 K (<math>\square</math>). VFT fitting has been performed and shows the strong (<math>\cdots</math>) and fragile (<math>---</math>) boundaries for Vit1. The viscosity hysteresis shows the transition between these two boundaries with respect to temperature. Also shown is TMA low viscosity measurements (<math>\Delta</math>) obtained from three point beam bending experiments with an estimated shear rate of <math>10^{-5} \text{ s}^{-1}</math> [14]. This viscosity data matches the predicted strong VFT fits thus indicating a similar ordered state both below and above <math>T_{\text{liq}}</math>.....</p>	61

## LIST OF FIGURES (Continued)

<u>Figure</u>		<u>Page</u>
17	<p>Angell plot showing the isothermal (●, Δ) viscosity data and viscosity measurements obtained upon continuous cooling at 2 K/s from 1125 K (□) and 1250 K (○). (●) represents data collected at a shear rate of 10 s<sup>-1</sup> while (Δ) represents the viscosity collected at 100 s<sup>-1</sup> upon cooling from 1300 K. This is done because the sensitivity of the torque sensor does not allow for accurate data at low shear rates. The viscosity hysteresis can be seen upon heating and cooling. Upon heating the material makes a transition from a strong liquid to a weak liquid(●) where as upon cooling a reverse transition from fragile to strong in the supercooled liquid region can be seen (○). The plot also shows the viscosity of SiO<sub>2</sub> (strong liquid) and o-terphenyl (fragile liquid) plotted as a function of inverse temperature normalized by the glass transition .....</p>	76
18	<p>Viscosity (□) and temperature (-) during undercooling experiment are shown. The maximum measured viscosity related to maximum torque output is observed at 907 K whereas the recalescence associated with the onset of crystallization occurs more than 60 K below 907 K.....</p>	79
19	<p>Continuous cooling data shown for two different samples cooled from 1125 K and 1250 K. The data reported by Schroers et al is also shown. The recalescence at different time and temperature are measured. Inset in the figure shows the isothermal measurements from 930 K to 970 K in the increments of 10 K at the shear rates of 10, 50 and 150 s<sup>-1</sup>. The initial increase in viscosity shows the onset of reordering and maximum viscosity reached indicates the crystallization event.....</p>	82
20	<p>Time–temperature-transformation as a function for different shear rates reflecting the onset of reordering and crystallization. A strong impact of shear rate on the reordering are observed.....</p>	84

## LIST OF FIGURES (Continued)

<u>Figure</u>		<u>Page</u>
21	<p>Viscosity as a function of shear rate at isothermal temperatures from 1075 K to 1275 K in 25 K increments for initially amorphous and remelted Vit1. The high viscosity and shear rate dependence above <math>T_{liq}</math> for this alloy decreases with increasing temperature. Hollow symbols show the viscosity data obtained cooling the sample to 1075 and reheating to 1275 by 25 K increments. The difference between the first and second temperature scans show a strong temperature dependence of the viscosity.....</p>	101
22	<p>Isothermal viscosity vs. shear rate upon heating from 1155 K to 1335 K in 25 K increments for initially amorphous and remelted Vit 106. It shows strong shear rate dependence above <math>T_{liq}</math> for this alloy. At the shear rate of above <math>143 \text{ s}^{-1}</math>, the viscosity approximately reaches a constant value and non Newtonian behavior disappears. The non Newtonian behavior disappears completely at the temperatures equal to and above 1305 K.....</p>	103
23. a	<p>Shear thinning exponent, <math>n</math>, vs. temperature of initially amorphous and remelted Vit1 obtained by fitting the power law to the data shown in Fig. 1. After melting the alloy exhibits a pronounced shear thinning dependence of viscosity which vanishes above 1225 K.....</p>	107
23. b	<p>Shear thinning exponent, <math>n</math>, vs. temperature of initially amorphous and remelted Vit106 obtained by fitting the power law to the data shown in Fig. 2. At each isotherm, the power law was applied to the range to which the shear rate dependence of viscosity is seen. After melting the alloy exhibits much stronger shear thinning behavior which vanishes above 1305 K.....</p>	107
23. c	<p>A much larger shear thinning exponent, vs. temperature of initially amorphous and remelted <math>\text{Pd}_{43}\text{Ni}_{10}\text{Cu}_{27}\text{P}_{20}</math>. The larger value to <math>n</math> indicates much smaller shear rate dependence. At the temperature above 975 K the material becomes completely Newtonian.....</p>	107

## LIST OF FIGURES (Continued)

<u>Figure</u>		<u>Page</u>
24	Isothermal viscosity vs. shear rate of all the three alloys upon heating above the $T_{\text{liq}}$ . Vit1 shown by open symbols shows the higher viscosity than Vit106 and $\text{Pd}_{43}\text{Ni}_{10}\text{Cu}_{27}\text{P}_{20}$ .....	109
25	Fragility plot of viscosity of Vit106 ( $\square$ ) and $\text{Pd}_{43}\text{Ni}_{10}\text{Cu}_{27}\text{P}_{20}$ ( $\circ$ ). The viscosities of $\text{SiO}_2$ and o-terphenyl. ( $\Delta$ ) shows a strong and a weak behavior. The data was fitted by VFT relations as indicated by the solid lines and the results are tabulated in table I. ....	114
26	Schematic quasibinary Gibbs free energy diagram for a fragile strong transition below the critical temperature. At concentration $C_1$ polyamorphism occurs, where as at $C_2$ the fragile liquid decomposes into two strong liquids with different medium range orders. ....	120
27. a	Schematic binary cut through the metastable fragile-strong liquid phase diagram that would result from the Gibbs free energy curves drawn in Fig. 1 with two medium range ordered states.. ....	122
27. b	Schematic binary cut through metastable fragile-strong phase diagram with only one strong liquid. There is a large region in which the fragile liquid decomposes into a strong and a fragile liquid. The arrows in both figures indicate where polyamorphism is possible.....	114

## LIST OF TABLES

<u>Figure</u>		<u>Page</u>
1	Table showing the viscosity at various temperatures and shear rates. Time for onset of ordering are also depicted.....	83
2	The fragilities of three different bulk metallic glass formers are obtained by fitting the viscosity data as a function of inverse temperature using VFT equation [2].....	113

## 1. INTRODUCTION

Over the past two decades, bulk metallic glasses have emerged as interesting engineering materials due to their perfectly elastic behavior, a high strength to weight ratio, as well as a low coefficient of friction, and a higher corrosion resistance than their crystalline counterparts [1-3]. Metallic glass formation from the liquid state was first reported by Duwez and co-workers in 1960 [4] when they processed thin ribbons of AuSi at extremely fast cooling rate of  $10^5$ - $10^6$  K/s to suppress crystallization. Extensive research conducted during the past two decades has led to the development of several new families of multicomponent glass forming alloys based on Lanthanum, Magnesium, Zirconium, Palladium, Iron, Platinum, Copper and Nickel [5-10]. Many of these alloys exhibit excellent glass forming ability (GFA) and can be processed in bulk amorphous form (section thickness >1mm) [11]. These metallic glasses are known as Bulk Metallic Glasses (BMGs) and show a higher thermal stability to crystallization than the conventional metallic glasses [12]. Although some of the bulk metallic glasses are used for various applications, there is still a need to devote considerable efforts to unravel the glass forming ability of these materials which could further help in the alloy development and easy processing. The glass forming ability (GFA) of a BMG is governed by several thermodynamic and kinetic factors. Viscosity is one such factor which reflects the kinetic slowdown, when a liquid is supercooled below its melting point. Therefore, it is very important

to investigate the viscosity of BMGs in order to completely understand the GFA. Although viscosity near the glass transition temperature has been reported for several alloys [13, 14], only limited data are available above the liquidus temperature. In addition, the knowledge of high temperature viscosity has significant engineering importance for processing techniques like injection molding and composite infiltration.

The first viscosity study on a BMG above the liquidus temperature was conducted by Johnson and co-workers on  $Zr_{41.2}Ti_{13.8}Cu_{12.5}Ni_{10.0}Be_{22.5}$  (Vit1). Contrary to the monatomic and binary simple metallic liquids which exhibit low viscosities of about  $10^{-3}$  Pa·s [15] at the melting point, the viscosity of  $Zr_{41.2}Ti_{13.8}Cu_{12.5}Ni_{10.0}Be_{22.5}$  (Vit1) was found to be about 3 orders of magnitude higher than that of a simple liquid. This study assumed a Maxwell model for the kinetics that predicts extremely small relaxation times on the order of  $10^{-10}$  s at liquidus temperature ( $T_{liq}$ ). Due to this high mobility and small relaxation time, it was assumed that the system would reach equilibrium rapidly and that there would be no shear rate dependence of the viscosity above  $T_{liq}$ . Later in 2004, the viscosity of Vit1 was revisited by Busch and co workers and surprisingly a pronounced shear rate dependence of the viscosity for temperatures above the  $T_{liq}$  [16] was observed. The results of this study suggested that there is an order of magnitude drop in viscosity for a two order of magnitude increase in shear rate indicating a non-

Newtonian shear thinning behavior. The research that is described here seeks to further understand the viscosity behavior and crystallization in the BMG forming liquids. It will be shown that especially the kinetics in Vit1 is even far more complex than previously anticipated.

This manuscript comprises of three parts, the first part has introduction with initial work, and last two parts have two publications, to be published in scientific journals, which demonstrates the non Newtonian viscosity of  $Zr_{41.2}Ti_{13.8}Cu_{12.5}Ni_{10}Be_{22.5}$ ,  $Zr_{57}Cu_{15.4}Ni_{12.6}Al_{10}Nb_5$  and  $Pd_{43}Ni_{10}Cu_{27}P_{20}$  bulk metallic glass forming liquids and the ordering and shear rate induced crystallization of the undercooled  $Zr_{41.2}Ti_{13.8}Cu_{12.5}Ni_{10.0}Be_{22.5}$  metallic glass forming melt. The first part gives the introduction and describes the initial work conducted on “the influence of shear rate and temperature on the viscosity of the  $Zr_{41.2}Ti_{13.8}Cu_{12.5}Ni_{10.0}Be_{22.5}$  metallic glass forming liquid”. This section demonstrates that the viscosity of initially amorphous Vit1 is more than 3 orders of magnitude higher than the simple metallic liquids and shows a shear thinning behavior above the liquidus temperature. This shear thinning behavior decreases with increasing temperature and disappears at the temperatures above 1225 K. It is also shown that the initial state of the sample (amorphous or crystalline) substantially effect the viscosity due to the presence of different order in the melt. In the first publication (second part), “ordering and shear rate induced crystallization of undercooled  $Zr_{41.2}Ti_{13.8}Cu_{12.5}Ni_{10.0}Be_{22.5}$  metallic-

glass-forming melts”, effect of shearing on the crystallization kinetics of the  $\text{Zr}_{41.2}\text{Ti}_{13.8}\text{Cu}_{12.5}\text{Ni}_{10.0}\text{Be}_{22.5}$  is reported. The time temperature transformation diagram of  $\text{Zr}_{41.2}\text{Ti}_{13.8}\text{Cu}_{12.5}\text{Ni}_{10.0}\text{Be}_{22.5}$ , has been measured as a function of shear rate. It demonstrates the occurrence of ordering and crystallization events as a function of shear rate, isothermal annealing time and temperature in the undercooled liquid. It is found that the TTT diagram shifts to shorter times with increasing shear rates. It is shown that the classical nucleation and growth model can not completely explain the shift in this TTT diagram. Finally, the second publication (third part) “non Newtonian viscosity of the  $\text{Zr}_{41.2}\text{Ti}_{13.8}\text{Cu}_{12.5}\text{Ni}_{10}\text{Be}_{22.5}$ ,  $\text{Zr}_{57}\text{Cu}_{15.4}\text{Ni}_{12.6}\text{Al}_{10}\text{Nb}_5$  and  $\text{Pd}_{43}\text{Ni}_{10}\text{Cu}_{27}\text{P}_{20}$  bulk metallic glass forming liquids” compares the non-Newtonian viscosity of two additional BMGs with the results on Vit1. The viscosity, fragility and the amount of shear thinning occurring in these melts are measured and discussed.

## 2. LITERATURE REVIEW AND BACKGROUND – BULK METALLIC GLASSES

### 2.1 History and Development of Bulk Metallic Glasses

The first major breakthrough in metallic glass formation came in 1960 when Duwez and co workers discovered that liquid  $\text{Au}_{80}\text{Si}_{20}$  could be turned into an amorphous solid by direct quenching from the melt with a cooling rate of  $10^6$  K/sec [4]. At that time, one of the well known factors required for the glass formation was very high cooling rate [17]. The cooling rate required to avoid crystallization and form a metallic glass is termed as the critical cooling rate,  $R_c$ . The thickness of the metallic glass is inversely proportional to the square root of  $R_c$ .

$$t \propto \frac{1}{\sqrt{R_c}} \quad (1)$$

Conventional metallic glasses required cooling rates of  $10^5$ - $10^6$  K/s to suppress crystallization and form a glass [18]. The high critical cooling rates limited the dimension of the samples to thin sheets or ribbons. Later, Cohen and Turnbull

suggested that the formation of amorphous  $\text{Au}_{80}\text{Si}_{20}$  is related to the deep eutectic in the AuSi alloy system near the 25 at. % Si coupled with rapid solidification rate [19]. In 1984, the first bulk metallic glass was reported by Drehman et al by quenching ternary Pd-Ni-P alloy. Heterogeneous nucleation sites on the surface were dissolved, by repeated melting in a boron oxide flux. As a result, glass formation at cooling rates below 10 K/s and glassy ingots with sizes up to 10 mm in diameter were obtained [20]. Today bulk metallic glass (BMG) is defined in the community as a metallic glass sample with its smallest dimension being at least 1 mm thick.

In 1993, Peker and Johnson discovered an exceptionally good glass forming system; Zr-Ti-Cu-Ni-Be. In particular  $\text{Zr}_{41.2}\text{Ti}_{13.8}\text{Cu}_{12.5}\text{Ni}_{10}\text{Be}_{22.5}$  which is commercially known as Vitreloy1<sup>TM</sup>, exhibits a critical cooling rate of 1K/s and can be cast up to several centimeters in diameter [8]. This alloy has a combination of excellent mechanical properties and processability and is therefore used widely in several applications ranging from sporting goods to defense equipment. However, the presence of toxic beryllium in this alloy limits its use. Johnson and co-workers further enlarged the Zr-based alloy family by developing another group of easily processible BMG system Zr-Ti(Nb)-Cu-Ni-Al alloys;  $\text{Zr}_{52.5}\text{Ti}_5\text{Cu}_{17.9}\text{Ni}_{14.6}\text{Al}_{10}$  and  $\text{Zr}_{57}\text{Cu}_{15.4}\text{Ni}_{12.6}\text{Al}_{10}\text{Nb}_5$  [21]. Even though their critical cooling rate is higher than Vitreloy1<sup>TM</sup>, they still have good mechanical properties and do not contain beryllium.

### 2.1.1 Processing of Metallic Glasses

Although metallic glasses are thermodynamically metastable, there are many processing routes, in which they can be processed. We can use gases (vapor deposition), liquids, or even crystals (solid state amorphization) as the starting material. Some of the methods that use liquid alloys as a starting materials are the following.

The first amorphous metal was prepared by gun quenching [4]. In this process, the molten sample is held in a non-reactive crucible with a small hole at the bottom and small droplets are driven out of the hole by a shock wave. The droplets then impinge onto a highly conductive metal substrate such as copper, spread out and form a film. Although this method provides the highest cooling rate of about  $10^6$ - $10^8$ K/sec, the irregularity of the foil thickness makes the sample to be a mixture of amorphous and crystalline structure. The average thickness of the film formed by this method ranges from 5 to 25 $\mu$ m.

Another method to obtain foils of thickness ranging from 20 to 50 $\mu$ m is the hammer-anvil method [22]. In this process, two metallic pistons are propelled

towards each other at high speed and a molten drop of alloy is quenched to a foil between the two metallic pistons. This process also provides high cooling rates.

A major advancement in processing came with the development of twin roll technique. This technique was potentially the first continuous process to produce metallic glasses. The thin ribbons of metallic glasses are obtained when a molten metal is fed into the nip of two rapidly rotating wheels. However in this process, it is difficult to keep the liquid from either solidifying too early (before the minimum separation between the wheels occurs) resulting in cold worked strips, or solidifying too late (i.e. leaving the nip partially liquid).

To date, the most accepted continuous processing technique of making metallic glass ribbons is melt spinning. In this technique a stream of molten metal is directed at a rapidly rotating copper wheel. This process provides high cooling rates and the ribbons with the thickness ranging between 20 and 100 $\mu\text{m}$  can be produced [23].

The most widely used technique to process (the novel) bulk metallic glasses both in industry and research is casting. This is a relatively simple technique, in which the molten material is poured into the mold with a desired pattern. It is only used for processing bulk metallic glasses due to the limited cooling rates. This

technique has been widely employed at the university laboratories [24] and in the industry such as Liquid Metal Technologies for the mass production of parts.

## **2.2 Metallic Glass and the Glass Transition**

A crystalline solid exhibits a long-range order where the atoms are arranged in a pattern that repeats periodically in three dimensions to a large or infinite extent. In contrast, metallic glass refers to a vitreous or amorphous alloy which lacks a long ranging periodicity of atoms and only short or medium-range order exists, which means that the atoms arrange themselves into small groups which are not repeated consistently throughout the bulk of the sample. This kind of structure is normally called a glass or a “frozen liquid”. Like all other amorphous solids it exhibits a glass transition.

When a liquid is cooled below its melting point, either crystallization takes place or the liquid becomes an undercooled or interchangeably a supercooled liquid. The path taken by the liquid depends on the cooling rate. For a slow cooling rate, the atoms have enough time to arrange themselves and form a crystalline solid. But for a cooling rate faster than a certain critical value,  $R_c$ , crystallization is avoided to obtain a supercooled liquid. This supercooled liquid is characterized by a higher viscosity, which means a higher resistance to flow, than the liquid above the melting point. As

the supercooled liquid is cooled further, its viscosity increases and the atoms move so slowly that they finally freeze and form a glass. Unlike the crystallization of a liquid, the glass formation is a continuous process and occurs over a range of temperatures.

The glass transition can be observed by monitoring the volume of the liquid as a function of temperature as shown in Fig. 1

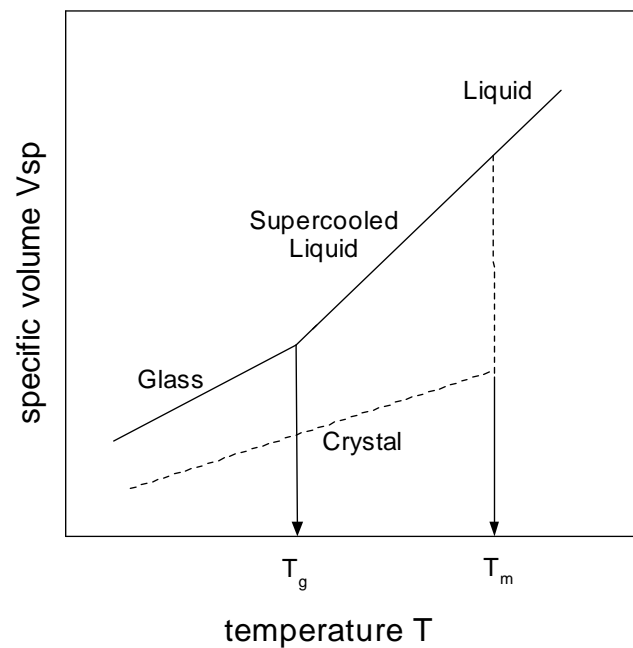


**Figure 1:** Specific volume as a function of temperature for a liquid, which can form either glass or crystal. Formation of glass or crystal depends on the cooling rate. At the smaller cooling rates, the material follows (-----) and form crystal whereas at faster cooling rates (-) path is followed and glass formation takes place. In the figure  $T_g$  and  $T_m$  designate glass transition temperature and melting temperature respectively [25].

During crystallization there is an abrupt change in volume at the melting point,  $T_m$ , whereas the glass formation is characterized by a change in the slope at a temperature called the glass-transition temperature,  $T_g$ . Between  $T_g$  and  $T_m$ , the material is in a metastable state with respect to the crystallization. This region is termed as the supercooled liquid region. Below this region, it is the metallic glass, which is in a nonequilibrium state. The thermodynamic variables such as volume, entropy and enthalpy all exhibit a change in slope at  $T_g$ . This implies that at  $T_g$  there should be a discontinuity in the derivative variables such as [25]:

Heat capacity, ( $C_p = (\partial H / \partial T)_p$ ) and

Thermal expansivity, ( $\alpha = \partial \ln V / \partial T$ ).

Although several attempts have been made to understand the glass transition, no theory has yet been able to completely describe the glass transition.

### **2.3 Glass Forming Ability in Multicomponent Alloys**

BMGs are dense liquids with very high viscosity and smaller free volumes than other metallic systems [26]. The compositions of BMGs are selected in proximity of deep eutectic. Chen and Turnbull proposed that the destabilization of

crystalline structure near the eutectic composition determines the stability and the ease of glass formation [27].

Size mismatch between the components is another factor that influences the glass forming ability. In a multicomponent glass forming system, species with different atomic sizes are alloyed together. The corresponding crystalline alloy suffers with the increase in chemical disorder due to the local atomic strains arising from the atomic mismatch as well as the difference in valence electron configuration. Also, the probability of forming a new crystal structure and a chance of acquiring long range ordered structure progressively decreases in the multi component systems.

Another factor predicted by Turnbull [28] in improving the glass-forming ability is the reduced glass transition temperature,  $T_{rg}$ , which is the ratio of the glass transition temperature  $T_g$  to the melting temperature  $T_m$  of an alloy. High values of  $T_{rg}$  are associated with the good glass forming ability. This means that as  $T_g$  gets closer to  $T_m$ , the homogeneous nucleation of crystals in the undercooled liquid become sluggish on the laboratory time scale and crystallization is suppressed.

Inoue later proposed three empirical rules governing the good glass forming ability of the bulk metallic glass [29];

- Considerable size mismatch (12% or more in 3 main components)

- Multicomponent systems with three or more than three components which reduces the free volume and increases viscosity
- Negative heat of mixing among the three main constituent elements

## **2.4 Thermodynamics and Kinetics of Metallic Glasses**

BMGs have a unique combination of superior mechanical properties in the domain of high-strength metals and processability like plastics which makes them interesting engineering materials. The kinetics and thermodynamics of metallic glasses have been subject to studies for a long time. However, due to the low thermal stability of metallic glass forming liquids only data close to the glass transition or in the equilibrium melt could be obtained. The development of BMGs allow us to study the thermophysical properties such as heat capacity, viscosity, surface tension, and emissivity of metallic melts in the supercooled liquid region. This is because of their high thermal stability to crystallization and a large supercooled liquid region above the glass transition temperature than the conventional metallic glasses [30].

There are several theoretical approaches to describe the thermodynamics and kinetics of supercooled liquids. The thermodynamics are represented by the change of specific heat capacity, entropy, enthalpy and Gibbs free energy upon undercooling

and the kinetics can be investigated by the measuring the viscosity above the liquidus temperature and in the supercooled liquid region.

#### **2.4.1 Thermodynamics of Metallic Glasses**

Bulk metallic glass formers allow us to investigate the thermodynamic functions of supercooled metallic liquids on a broader time and temperature scale. The thermodynamic functions of the supercooled liquid with respect to the crystal can be determined in a Differential Scanning Calorimeter (DSC) and in a Differential Thermal Analyzer (DTA). This is done by measuring the heat of fusion, heat of crystallization and specific heat capacity data of the supercooled liquid and crystal [30-33].

The phase transformations that occur upon heating the material lead to the absorption or release of energy. This energy can be recorded as a heat flow as a function of temperature in DSC and DTA. Figure 2 depicts the phase transitions that occurred during the heating of material in a DTA. The initial endothermic peak corresponding to the glass transition,  $T_g$ , provides a qualitative proof for amorphous state of the sample. Upon further heating, crystallization occurs exothermally at the crystallization temperature,  $T_x$ . The amount of heat released during crystallization is known as the heat of crystallization,  $\Delta H_x$ . When the sample is heated further an

endothermic peak showing the melting of the sample can be seen in this figure.

The onset of melting is shown by eutectic temperature,  $T_{\text{eut}}$  and the end is depicted by  $T_{\text{liq}}$ . By integrating the area under these endothermic events, the enthalpy of fusion,  $\Delta H_f$ , can be calculated [31]. The entropy of fusion,  $\Delta S_f$ , can be calculated from  $\Delta H_f$  by using [34] :

$$\Delta S_f = \frac{\Delta H_f}{T_m} \quad (2),$$

where  $\Delta H_f$  is the enthalpy of fusion,  $T_m$  is the melting temperature.

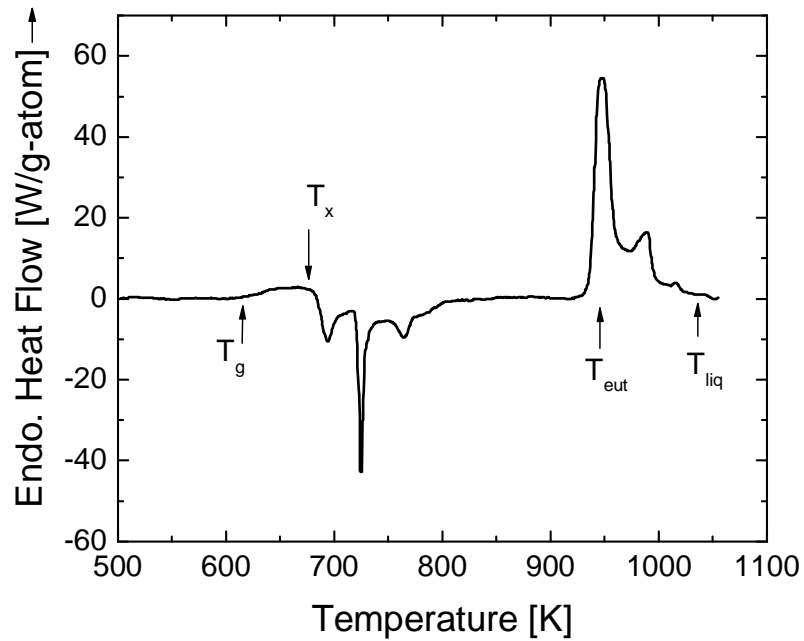


**Figure 2:** Differential Scanning Calorimeter (DSC) thermogram of  $\text{Zr}_{41.2}\text{Ti}_{13.8}\text{Cu}_{12.5}\text{Ni}_{10}\text{Be}_{22.5}$  (Vit1) from 500 to 1150 K using the scan heating rate of 10 K/min [31]. The onset of the glass transition, crystallization temperature, eutectic melting point and liquidus temperatures are depicted by  $T_g$ ,  $T_x$ ,  $T_{\text{eut}}$  and  $T_{\text{liq}}$  respectively.

The specific heat capacities at constant pressure,  $c_p$ , of the glassy, crystalline and supercooled liquid state are also measured in DSC with changing temperatures. Specific heat at constant pressure,  $c_p$  is the amount of heat required to raise the temperature of the substance by one degree Kelvin at constant pressure and is given by [25],

$$C_p = \left( \frac{\partial Q}{\partial T} \right)_p = T \left( \frac{\partial S}{\partial T} \right)_p \quad (3),$$

where,  $dQ$  is the heat absorbed by a unit mass of material to raise the temperature by  $dT$  and  $dS$  is the entropy change. Figure 3 depicts the heat capacity curves for a glass, the corresponding liquid and the crystalline solid as a function of temperature for Vit1 [31].

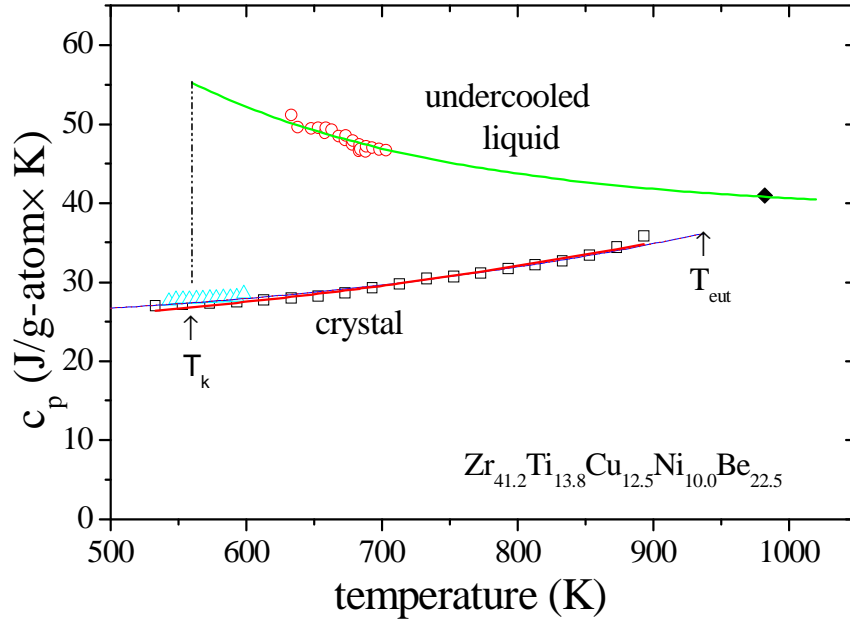


**Figure 3:** Heat capacity curves of the  $\text{Zr}_{41.2}\text{Ti}_{13.8}\text{Cu}_{12.5}\text{Ni}_{10.0}\text{Be}_{22.5}$  (Vit1) glass, the corresponding liquid and crystalline solid as a function of temperature [31].

The sudden increase in the heat capacity of the glass upon heating is the thermal manifestation of the glass transition. Thermodynamically, the glass transition,  $T_g$ , is defined as the point of inflection of the rising heat capacity. The specific heat of the crystal and liquid,  $c_{p,\text{xtl}}$  and  $c_{p,\text{liq}}$  can be represented by the following equations:

$$C_{p,\text{xtl}} = 3R + aT + bT^2 \quad (4),$$

and

$$C_{p,xTl} = 3R + cT + dT^{-2} \quad (5),$$

where R is the universal gas constant, a, b, c and d are the fitting parameters. For Vit1 the fitting parameters are reported as;  $a = -9.653 \times 10^{-3}$ ,  $b = 2.321 \times 10^{-5}$ ,  $c = 7.560 \times 10^{-3}$  and  $d = 8.167 \times 10^6$  in the appropriate units [31].

The entropy difference,  $\Delta S^{l-x}$ , between the liquid and crystal as a function of temperature can be calculated by integrating the specific heat using [9]

$$\Delta S^{l-x}(T) = \Delta S_f(T_m) - \int_T^{T_{liq}} \frac{\Delta C_p(T')}{T'} dT' \quad (6),$$

where  $\Delta S_f$  is the entropy of fusion, T is the temperature, and  $\Delta c_p = c_{p,liq} - c_{p,xTl}$ . Similar to entropy, variation of enthalpy,  $\Delta H^{l-x}$ , with temperature is calculated with the knowledge of specific heat

$$\Delta H^{l-x}(T) = \Delta H_f(T_m) - \int_T^{T_{liq}} \Delta C_p(T') dT' \quad (7).$$

By knowing the enthalpy, entropy of fusion and the specific heat capacity difference between supercooled liquid and crystalline mixture,  $\Delta c_p$ , the thermodynamic functions are calculated by integrating  $\Delta c_p$  as discussed above. This results in the Gibbs free energy difference between supercooled liquid and crystal,

$$\Delta G_{l-x}(T) = \Delta H_f - \Delta S_f \cdot T - \int_T^{T_f} \Delta c_p^{l-x}(T') dT' + T \int_T^{T_f} \frac{\Delta c_p^{l-x}(T')}{T'} dT' \quad (8),$$

where  $\Delta H_f$  and  $\Delta S_f$  are the enthalpy and entropy of fusion, respectively, at the temperature  $T_f$ . This gives us an approximation of the thermodynamic driving force for crystallization. Figure 4 shows a plot of the Gibbs free energy difference for some of the metallic glass forming systems as a function of undercooling [26]. The temperatures are normalized to the melting temperature of the respective alloy. The alloys plotted have the different critical cooling rates.

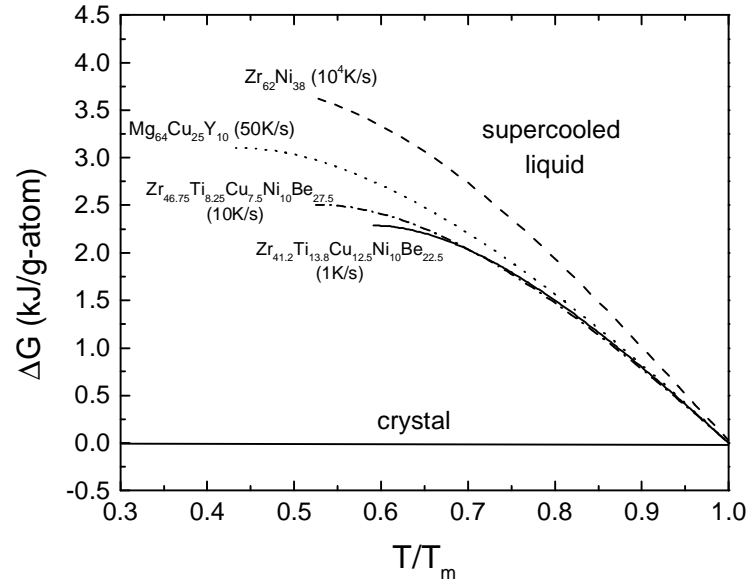


**Figure 4:** The Gibbs free energy difference between crystal and supercooled liquid for different various glass forming liquids. Vit1 with the smallest cooling rate shows the smallest free energy difference [26].

It can be seen in the plot that the best glass former with the lowest critical cooling rate of 1K/s (Vitrelloy1) has smaller Gibbs free energy differences than the other glass formers whereas the binary  $Zr_{62}Ni_{38}$  with the critical cooling rate of about  $10^4$  K/s has the highest Gibbs free energy difference. This is consistent in all the glass formers shown in the Fig. 4 and the glass former with smaller critical cooling rate has a smaller driving force for crystallization. Therefore in order to understand the glass forming ability of the alloys, it is a prerequisite to understand the thermodynamic conditions for good glass formation as well as its relation to the kinetics in the supercooled liquids.

### 2.4.2 Kinetics and Viscosity of Metallic Glasses

Along with thermodynamics it is also essential to study kinetics in the proximity of glass transition region and above the liquidus temperature in order to understand the glass forming ability of BMGs. In terms of kinetics, the glass transition temperature can be understood as the temperature at which the viscosity ( $\eta$ ) of the undercooled liquid reaches about  $10^{12}$  Pa·s [35]. At such high viscosities, atomic motions are retarded and the relaxation time for atomic rearrangement becomes comparable to or greater than the experimental time scale.

Viscosity reflects the kinetic slowdown, when a liquid is supercooled below its melting point. Contrary to the monatomic and binary simple metallic liquids which exhibit low viscosities of about  $10^{-3}$  Pa·s [36] at the melting point, BMGs are expected to possess much higher viscosities. For example, the viscosity of Vit1 is more than 3 orders of magnitude higher than that of a simple liquid. If we assume that the diffusivity is given by the Stokes Einstein equation as  $D \propto T/\eta$ , it is apparent that the crystallization kinetics is substantially retarded in an alloy with high viscosity. Therefore it has been argued that in Vit1, high viscosity is a major contributing factor to the high glass forming ability, because high viscosity implies a slow nucleation and growth kinetics in the supercooled liquid region.

### 2.4.2.1 Angell Plot

Glass formation has been studied in a large variety of materials. An empirical concept to describe the sensitivity of the viscosity to temperature changes for different materials in the supercooled liquid state was developed by Angell [37]. Figure 5 shows an Angell plot which describes the temperature dependence of viscosity for various materials.

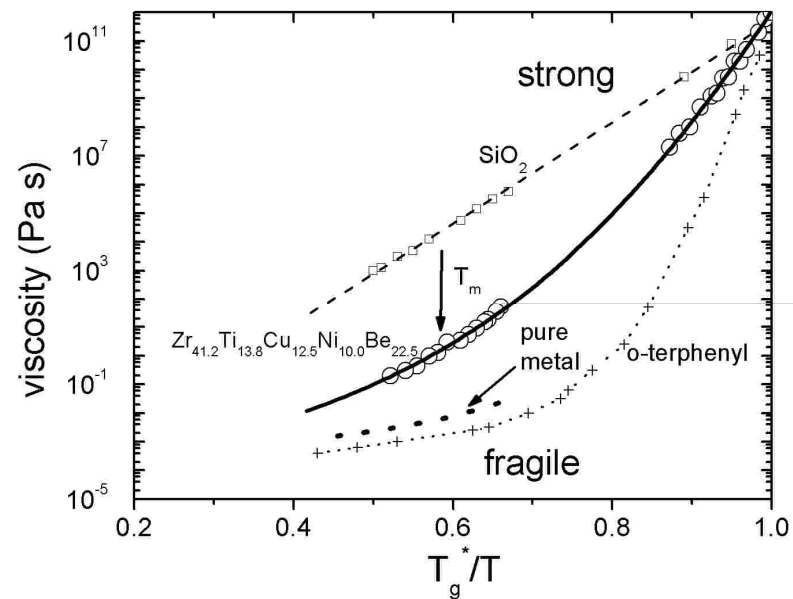


**Figure 5:** Equilibrium viscosity as a function of temperature for the supercooled liquid of  $\text{Zr}_{41.2}\text{Ti}_{13.8}\text{Ni}_{10}\text{Cu}_{12.5}\text{Be}_{22.5}$  (Vit1) in an Arrhenius plot [7].

The temperature dependence of viscosity can differ substantially among different materials. For example, the viscosity of SiO<sub>2</sub>, which is an open random network glass, can be described well with an Arrhenius law [25]. Other substances such as materials with van der Waals bonds are best described by a Vogel-Fulcher-Tammann (VFT) relation with a VFT-temperature very close to the glass transition. The VFT- equation is given as,

$$\eta = \eta_0 \cdot \exp\left(\frac{D^* \cdot T_0}{T - T_0}\right) \quad 9,$$

where,  $\eta_0$  is a constant of about  $4 \cdot 10^{-5}$  Pa·s,  $D^*$  is the fragility parameter and  $T_0$  is the VFT temperature, where the barriers with respect to flow would go to infinity. “Strong” liquids, like SiO<sub>2</sub>, have high melt viscosities and a  $D^*$  of about 100 whereas the other extreme are "fragile" liquids that show a VFT temperature close to the glass transition temperature, as well as low melt viscosities and a  $D^*$  of less than 10. Conventional metallic glasses were considered fragile liquids with  $D^*$  less than 10 and it was not possible to perform viscosity measurements in the vicinity of glass transition due to their poor stability against crystallization. The development of BMG forming liquids made it possible to measure the viscosity by three point beam bending [38], parallel plate rheometry [39-41] as well as rotating cup viscosimetry [15, 42].

Early viscosity measurements on  $Zr_{41.2}Ti_{13.8}Cu_{12.5}Ni_{10.0}Be_{22.5}$  (Vit1) showed that Vit1 exhibits a “strong” as opposed to “fragile” liquid behavior, in contrast to what was previously assumed for metallic liquids [15]. It was proposed that this high viscosity has an important influence on the crystallization kinetics and glass forming ability of multicomponent glass forming alloys, because it implies smaller diffusivities than in very fluid liquids. The viscosity data obtained in this work are also analyzed on the Angel plot and fragility parameters for various alloys are obtained by fitting viscosity as a function of temperature using VFT relation.

#### **2.4.2.2 Adam-Gibbs Entropy Model for Viscous Flow**

The Adam-Gibbs Entropy Model for viscous flow relates the amount of configurational entropy present in the liquid with its viscosity. The model states that the viscosity,  $\eta$ , can be expressed as

$$\eta = \eta_0 \exp\left(\frac{C}{(T \cdot S_c)}\right) \quad (10),$$

[43] where  $\eta_0 = 4 \times 10^{-5}$  Pa·s [44] is a constant pre-exponential factor,  $C$  is the effective free enthalpy barrier for viscous flow, and  $S_c$  is the configurational entropy of the system.

## **2.5 Crystallization of Supercooled Metallic Liquids and Glasses**

### **2.5.1 TTT Diagram**

In order to study crystallization kinetics, the time-temperature-transformation (TTT) diagrams from the supercooled liquid into the crystalline state are studied. In a TTT diagram, the temperature is plotted on the vertical axis and the time on the horizontal axis on a logarithmic scale. A TTT diagram is obtained through isothermal experiments at various temperatures, and the time required by the material to crystallize at each isothermal temperature is plotted. Various curves, such as the onset (1%), intermediate (~50%) and end (99%) time of crystallization, are represented by such TTT diagrams. As described in section 2.2, a glass is formed by avoiding crystallization of the material below its melting point. Although the driving force for crystallization increases as the material is cooled more and more below its melting point, the diffusivity of the components in the alloy decreases with decreasing temperature. The decreasing kinetics (reduced diffusivity) below the liquidus temperature and the increasing driving force for crystallization are antagonistic and result in the characteristic “C” shape to the TTT diagram. As the

material is cooled below its liquidus temperature the time taken for initiation of crystallization decreases. The increase in the driving force for crystallization controls the crystallization process. This trend continues till the nose of the TTT diagram is reached. The nose corresponds to the minimum amount of time required to begin crystallization at any undercooling. Below the nose sluggish kinetics of the system takes over and governs the crystallization onset. The crystallization proceeds in different manner in various alloys. Figure 6 shows a TTT diagram of (not sheared) Vit1, where the isothermal onset of crystallization has been determined in the entire supercooled liquid for a metallic liquid.

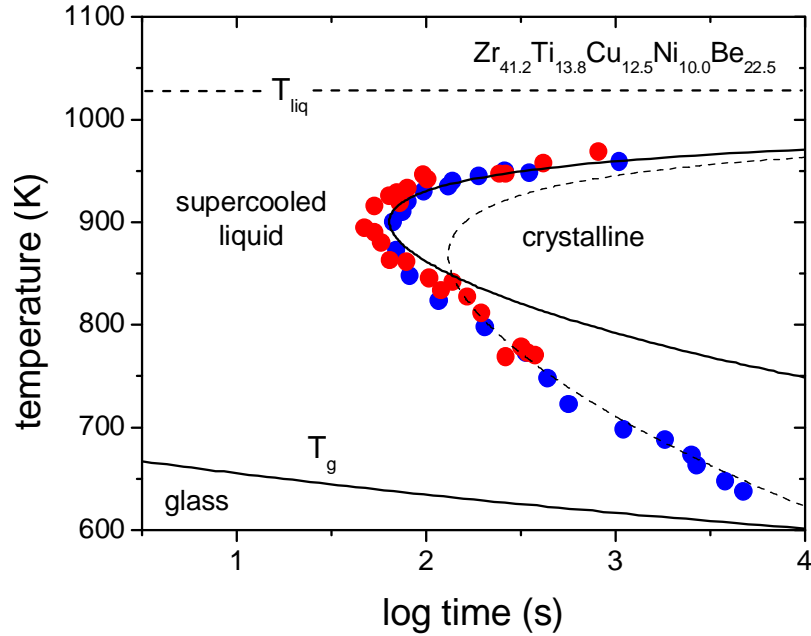


**Figure 6:** TTT Diagram for  $Zr_{41.2}Ti_{13.8}Cu_{12.5}Ni_{10.0}Be_{22.5}$  showing the liquidus temperature, glass transition temperature, super cooled liquid region, and the crystalline nose [26]. The samples have not been sheared during the experiment. The solid line and dashed line show the fits obtained by using  $D_{eff} \propto 1/\eta$  and  $D_{eff} \propto \exp(-Q_{eff}/k \cdot T)$  [26].

The TTT diagram is analyzed by applying classical nucleation and growth models and taking the measured thermodynamic and kinetic quantities into account. The results can then be compared with the experimentally determined number of nucleation and growth events provided by the microstructure analyses.

According to the classical nucleation theory [46, 47], the time for the crystallization,  $t_x$ , is given by

$$t_x = \left( \frac{3 \cdot x}{\pi \cdot I_{ss} \cdot u^3} \right)^{1/4} \quad (11),$$

where  $x$  is a small volume fraction to crystallize,  $I_{ss}$  is the steady state nucleation rate and  $u$  is the growth velocity. The steady state nucleation rate,  $I_{ss}$ , can be described by,

$$I_{ss} = A \cdot D_{eff} \cdot \exp\left(\frac{-\Delta G^*}{k_B \cdot T}\right) \quad (12),$$

where  $D_{eff}$  is the effective diffusivity,  $A$  is a fitting parameter,  $k_B$  is a Boltzmann's constant and  $\Delta G^*$  is the activation energy barrier for nucleation.  $D_{eff}$  can be calculated from the Stokes-Einstein equation given by

$$D = \frac{k_B \cdot T}{3 \cdot \pi \cdot \eta \cdot a} \quad (13),$$

where  $T$  is the temperature,  $\eta$  is the viscosity, and  $a$  is average atomic distance. The viscosity  $\eta$  as a function of temperature is taken from the experimental data.

The nucleation barrier  $\Delta G^*$  is given as

$$\Delta G^* = \frac{16 \cdot \pi \cdot \sigma^3}{3 \cdot \Delta G^2} \quad (14),$$

where  $\sigma$  is the interfacial energy and  $\Delta G$  is the driving force for crystallization and is approximated as the Gibbs free energy difference,  $\Delta G^{l-x}$ , of the supercooled liquid with respect to the crystalline mixture.  $\Delta G$  is experimentally calculated from enthalpy, entropy and specific heat data by using the method explained in section 2.4.1.  $\sigma$  is used as a fitting parameter to model the experimental data. Similarly, the growth velocity,  $u$ , can be calculated by

$$u = \frac{f \cdot D_{eff}}{l} \left( 1 - \exp\left(-\frac{v_m \cdot \Delta G}{k_B \cdot T}\right) \right) \quad (15),$$

where  $l$  is the average atomic diameter,  $v_m$  is the atomic volume,  $k_B$  is the Boltzmann constant,  $f$  is the fraction of sites at the liquid-crystal interface,  $T$  is the temperature and  $\Delta G$  is the same Gibbs free energy difference between the liquid and crystalline phase stated above.

In the first paper of the manuscript presented in this work we determined the change in TTT diagram at various shear rates. The above mentioned classical nucleation model was used in order to analyze the shift in TTT diagram as a function of shear rate.

## 2.6 Viscosity Measurement of Bulk Metallic Glasses

### 2.6.1 Below the Liquidus Temperature

The viscosity of some BMGs near the glass transition temperature has been reported by investigating the deformation of amorphous beams by the three point beam bending method. The three point beam bending consists of a beam that is supported at the ends by sharp edges. The beam is deflected with a constant force ( $M$  in kg) applied in the center of the beam. From the deflection rate ( $v$  in m/s) the viscosity is determined by the equation

$$\eta = -\frac{gL^3}{2.4I_c v} \left[ M + \frac{\rho AL}{1.6} \right] \quad (16),$$

where  $g$  is the gravitational constant in  $m/s^2$ ,  $I_c$  is the cross-section moment of inertia in  $m^4$ ,  $\rho$  is the density of glass in  $kg/m^3$ ,  $A$  is the cross-section and  $L$  is the support span. In case of bulk metallic glasses, viscosities between  $10^7$  and  $10^{14}$  Pa·s have been previously obtained by this method. Waniuk et al obtained the viscosity of Vit1 in the super cooled region by using three point beam bending method. They reported a decrease from  $10^{13}$  Pa·s at 600 K to  $10^7$  Pa·s at 700 K and upon primary

crystallization the viscosity increased by 1.5 orders of magnitude indicating a decrease in the atomic mobility [48]. Similar studies have also been conducted on some other kinds of BMGs [38, 39].

### **2.6.2 Above the Liquidus Temperature**

Little is known about the viscosities of BMGs above the liquidus temperature. Previous theories determined that a metallic system in the liquid state has a low viscosity on the order of  $10^{-3}$  Pa·s . The first viscosity study in BMGs above the liquidus temperature was conducted by Johnson and coworkers on Vit1. They assumed a Maxwell model relationship that predicts extremely small relaxation times on the order of  $10^{-10}$  s at  $T_{liq}$ . Due to this high mobility and small relaxation time, it was therefore assumed that the system would reach equilibrium rapidly and that there would be no shear rate dependence of the viscosity above  $T_{liq}$ . These experiments were performed by using a Couette Concentric Cylinder and were done over shear rate and temperature range of  $30-300$  s<sup>-1</sup> and  $927-1173$  K respectively. Experimental procedures included constant temperature shearing experiments from high to low temperatures. A constant clockwise and counter clockwise rotation was applied in order to obtain an average torque signal

The next viscosity study of Vit1 above the melting point was performed between 2001 to 2004 by Tyler Shaw and Christopher Way at Oregon State University (OSU) [42, 49, 50]. Similar equipment Couette Concentric Cylinder viscometer as previous study was designed and built at OSU [42, 49] with a wider range of shear rates and temperature. Shear rates from  $10^{-3}$  to  $10^2$   $s^{-1}$  and temperatures from 1090-1172 K, respectively were applied. In the study the experiments were performed at constant temperatures and variable shear rates and surprisingly showed a strong shear thinning behavior as shown in Fig. 7, which is rather surprising for a metallic system.

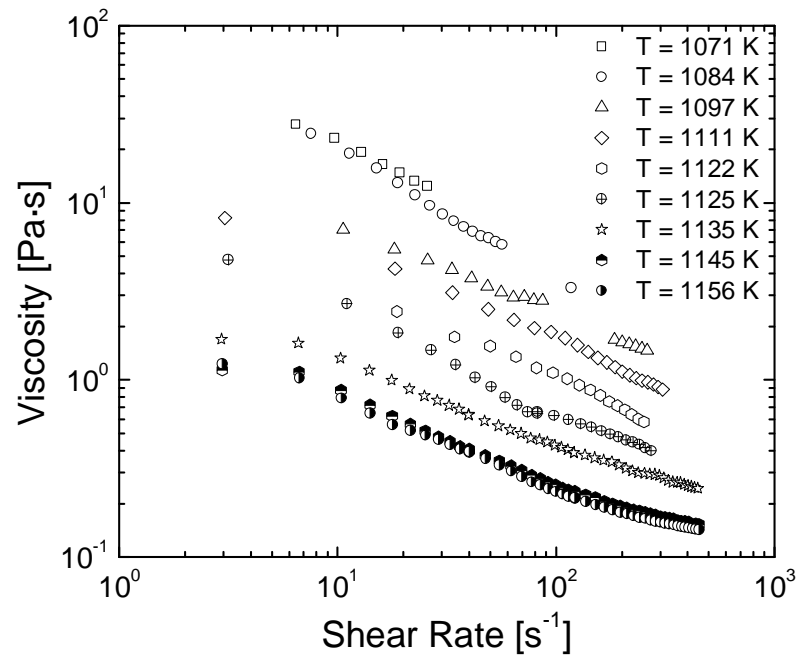


**Figure 7:** Viscosity as a function of shear rate at various temperatures between 1071 K and 1156 K for Vit1. The data shown were collected by Tyler Shaw and Christopher Way [49, 50]. A strong shear thinning effect reflected in a pronounced decrease in viscosity with increasing shear rate can be seen.

This shear thinning behavior was attributed to the presence of short and medium range order, which remains after melting and can be destroyed by shearing. Due to the presence of shear thinning behavior in the melt a shear rate correction factor has been applied on the torque vs. rotational speed data to obtain the corrected shear rates. Further experiments indicated that the starting measurement temperature and processing time may affect the viscosity. The viscosity measurements were

performed in the shear cell made machined from graphite. The details are given in the next section. Therefore, the investigation of Vit1 interaction with graphite was also performed. Optical microscopy of the sectioned shear cells after testing showed a distinct separation between the melt and graphite. Electron Microprobe Analysis (EMPA) of these sectioned shear cells confirmed no detectible diffusion of the melt deep into the graphite.

However following were the two major concerns in the studies done at OSU until 2004

1. The results were not repeatable even within the same experiments.
2. The measurements at the temperatures above 1175K could not be performed because the material started to form bubbles and came out of the shear cell. This is due to the presence of hydrogen in Vit1 which diffuses into the alloy during manufacturing. When this alloy is re-melted, hydrogen diffuses out and forms bubbles which made the measurements impossible at higher temperatures.

## **2.7 Purpose of this Work**

The role of the viscosity as one of the most important factors to determine the glass forming ability of supercooled liquids has been discussed in the previous sections. Particularly, there have been very few in-depth studies on the viscosity of supercooled liquids above the liquidus temperature. Therefore, this research attempts to better understand the viscosity of bulk metallic glass forming alloys especially at high temperatures around the melting point. There are three main reasons to study the viscosity. Firstly, the viscosity of the material above the liquidus temperature and in the supercooled liquid region plays a vital role in crystal nucleation and growth. As discussed earlier, the atomic mobility in the liquid state is inversely proportional to the viscosity and the higher the atomic mobility is, the faster is the crystallization kinetics. Secondly, the viscosity of the amorphous material can be related to the thermodynamic functions by means of the entropy model for viscous flow. This model states that an increase in viscosity is directly linked to the configurational entropy [eq.10]. Lastly, the study of the viscosity of amorphous metals is important from the processing standpoint. For processing in the liquid state, such as during injection molding, viscosity becomes a critical parameter for determining the energy necessary for complete mold filling. Knowing the viscosity, we can predict the

processing parameters in terms of: fluid flow behavior, time, melt temperature, mold temperature, pressure and other transport properties.

### 3. EXPERIMENTAL METHODS AND INITIAL WORK

#### 3.1 Materials Preparation

In this study the viscosity of three different alloys namely  $Zr_{41.2}Ti_{13.8}Cu_{12.5}Ni_{10}Be_{22.5}$  (Vit1),  $Zr_{57}Cu_{15.4}Ni_{12.6}Al_{10}Nb_5$  (Vit106) and  $Pd_{43}Ni_{10}Cu_{27}P_{20}$  over a large temperature range above their respective liquidus temperatures have been investigated. Following is the processing technique used for these alloys.

#### $Zr_{41.2}Ti_{13.8}Cu_{12.5}Ni_{10.0}Be_{22.5}$ (Vit1)

Three different kinds of Vit1 samples were investigated in this study; (I) as cast amorphous pellets of  $Zr_{41.2}Ti_{13.8}Cu_{12.5}Ni_{10.0}Be_{22.5}$  (Vit1) obtained from Liquid Metal Technologies, Lake Forest, CA (II) dehydrogenated amorphous Vit1 samples; these samples were processed from the pellets obtained from Liquid Metal Technologies. The as received samples were dehydrogenated by melting them under a high vacuum of  $10^{-3}$  Pa in a water cooled copper boat. The samples were quenched to attain an amorphous state in a Bühler MAM Arc melter. (III) dehydrogenated

crystalline Vit1; these samples were dehydrogenated and prepared in a similar way as II but were allowed to crystallize in the water cooled copper boat itself. The dehydrogenation was necessary in samples (II) and (III) to prevent hydrogen from emerging from the molten sample during the subsequent viscosity measurement and adversely affecting the viscosity measurements. The amorphous and crystalline nature of all the samples was confirmed in DSC.

### **Zr<sub>57</sub>Cu<sub>15.4</sub>Ni<sub>12.6</sub>Al<sub>10</sub>Nb<sub>5</sub> (Vit106) and Pd<sub>43</sub>Ni<sub>10</sub>Cu<sub>27</sub>P<sub>20</sub>**

Amorphous master alloys of Vit106 with the nominal composition of Zr<sub>57</sub>Cu<sub>15.4</sub>Ni<sub>12.6</sub>Al<sub>10</sub>Nb<sub>5</sub>, were prepared by mixing the elements of high purity ranging from 99.9 % to 99.995% in a Bühler MAM Arc melter. All the elements were cut in an uncontaminated environment and were ultrasonically cleaned in the bath of acetone followed by ethanol. This was done in order to avoid the presence of any particle which could cause the heterogeneous nucleation. Similarly, amorphous pieces of Pd<sub>43</sub>Ni<sub>10</sub>Cu<sub>27</sub>P<sub>20</sub> were prepared.

#### **3.1.1 Differential Scanning Calorimetry**

Prior to viscosity measurements, Differential Scanning Calorimetry (DSC) was performed on all the samples by using a Perkin Elmer Pyris 1 DSC. This was

done in order to investigate the amorphous or crystalline state of the sample. Samples ranging from 20 to 50 mg were ultrasonically cleaned in a bath of acetone followed by ethanol. Temperature scans were then done at 20 K/min from 323 K to 853 K in 99.999% pure argon flowing during testing.

### **3.1.2 Differential Thermal Analysis**

The Differential Thermal Analysis (DTA) analysis was mainly performed to measure the liquidus temperature of all the alloys. The measured  $T_{liq}$  values of all the alloys were compared to the literature values. DTA was performed using a Perkin Elmer Diamond TG/DTA. Vit1, Vit106 and  $Pd_{43}Ni_{10}Cu_{27}P_{20}$  samples ranging from 20 to 30 mg were cleaned using acetone and ethanol and then placed in graphite pans for testing. Scan rates of 60 K/s from 373 to 1500 K under the flow of 99.999% pure nitrogen were used.

## **3.2 Viscosity Measurements**

### **3.2.1 Measurement Equipment**

The viscosity measurements are performed in a custom build high-temperature couette rheometer designed by Tyler Shaw [49]. The design and the

details of the equipment can be found in Tyler Shaw's thesis. This rheometer consists of a concentric cylinder shear cell that is mounted vertically inside a high-vacuum induction furnace as shown schematically in Fig. 8.

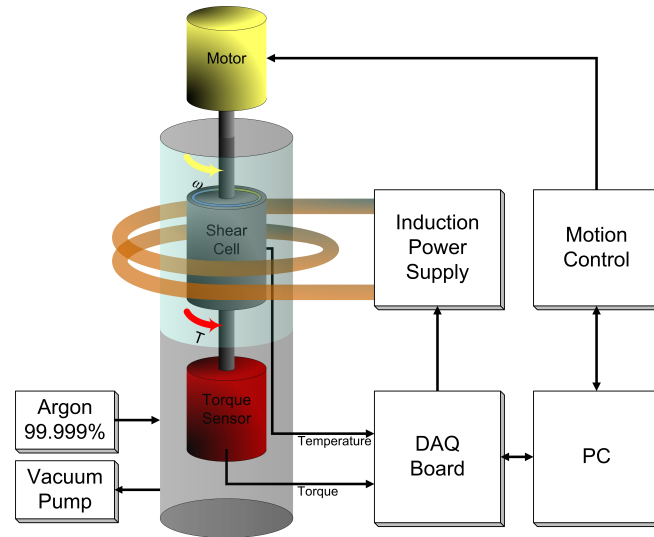


**Figure 8:** Schematic of high-temperature high-vacuum viscometer (from Tyler Shaw [49]).

The material is kept in the outer cylindrical cup where it is inductively melted. The outer cylinder is attached to a torque sensor and the temperature is measured with a thermocouple mounted inside the cylinder wall of the outer cylinder. The inner cylinder is connected to a stepper motor and is used to shear the material. Once the material is melted in the outer cylinder, the inner cylinder is lowered into the outer cylinder and the gap between the outer and inner cylinder contains the melt. By rotating the inner cylinder the desired shear rate,  $\Omega$ , in  $\text{rad}\cdot\text{s}^{-1}$  is

imposed on the molten alloys. This results in a shear field in the liquids which generates a torque on the outer cylinder [49, 50]. This torque signal,  $M$ , in N·m through the molten test sample is recorded with a torque sensor. Details of the equipment and procedures are described elsewhere [49, 50]. The final viscosity,  $\eta$ , in Pa·s is calculated using

$$\eta = \frac{\sigma}{\dot{\gamma}} \quad (17),$$

where  $\sigma$  is the shear stress given by

$$\sigma = \frac{M}{2\pi \cdot r_i^2 \cdot L} \quad (18),$$

where  $M$  is the torque,  $r_i$  is the radius of the inner cylinder in meters, and  $L$  is the immersion length in meters whereas,  $\dot{\gamma}$ , is the shear rate calculated by using:

$$\dot{\gamma} = \frac{2 \cdot r_i \cdot \Omega}{r_o^2 - r_i^2} \quad (19),$$

where  $\Omega$  is the angular velocity in  $\text{rad}\cdot\text{s}^{-1}$ ,  $r_i$  is the radius of the inner cylinder in meters, and  $r_o$  is the inner radius of the outer cylinder in meters.

Previous studies showed that the viscosity of Vit1 has a shear thinning behavior with increasing shear rate. Therefore a non-linear velocity profile in the testing material between the inner cylinder and the outer cylinder is generated which makes the material closest to the inner cylinder to be sheared faster than the material near the outer cylinder. Therefore a shear rate correction factor is applied and the corrected shear rate is given by

$$\dot{\gamma} = \frac{2 \cdot \Omega}{n \left(1 - b^{\frac{2}{n}}\right)} \quad (20),$$

where  $\Omega$  is the angular velocity,  $n$  is the fitted parameter which is obtained by fitting power law relationship to the plot of torque,  $M$ , in N·m with respect to the rotational velocity,  $\Omega$ , in  $\text{rad}\cdot\text{s}^{-1}$ . A power law relationship given by:

$$M = a \cdot \Omega^n \quad (21).$$

The details of the method used for shear rate correction can be found in Tyler Shaw and Christopher Way's thesis [49, 50].

### 3.3 Initial Work

Due to the difficulties described in section 2.6.2, the first effort was made to achieve the repeatability between the viscosity measurements of Vit1 and to measure its viscosity at the temperatures above 1156 K. Therefore the experimental methods used prior to this work were thoroughly investigated [49, 50]. The known factors affecting viscosity were the shear rate and temperature. The refinement of variables such as time, temperature and shear rate showed that the viscosity of Vit1 is immensely affected by the maximum experimental temperature and the amount of shearing experienced by the material. Since, the previous viscosity studies did not systematically investigate the effect of temperature history on the viscosity, a standard measurement procedure is developed. A stepwise approach in which the material is sheared from  $5 \text{ s}^{-1}$  to  $300 \text{ s}^{-1}$  (uncorrected shear rate) at every 25 K increment in temperature from 1075 K to 1300 K is now followed. At each measurement, it is made sure that the material is heated not to the higher temperature. By using this procedure repeatable measurements within the error bars are now achieved. The details could be found in Christopher Way doctoral thesis [50].

In order to obtain the measurements at high temperatures dehydrogenation of Vit1 was performed as explained in section 3.1. The samples were quenched to obtain the amorphous state. In addition to the dehydrogenated amorphous Vit1 samples, dehydrogenated fully micro-crystallized Vit1 samples, with an estimated average microstructure length scale of  $10^{-3}$  m [51], were also prepared by cooling the melt slower than the critical cooling rate of 1 K/s.

Viscosity measurements above and below the liquidus temperature,  $T_{liq}$ , were performed. For the measurements above  $T_{liq}$ , the above mentioned standard measurement procedure was used. The shear rate correction factor as described in section 3.2.1 was applied to the experimental data obtained at each investigated temperature which resulted in corrected shear rates from 6 to  $350\text{ s}^{-1}$ . For undercooling measurements below  $T_{liq}$ , the alloy was heated in the shear cell to an initial temperature above  $T_{liq}$  and then sheared in a clockwise direction at a constant shear rate. At this point the shear cell was cooled at an average cooling rate of 2 K/s until the generated torque signal,  $M$ , reached 95% of the maximum measurement capabilities of the torque sensor. The shear rate correction for the undercooling experiment was obtained by performing several undercooling experiments using uncorrected shear rates from 5 to  $20\text{ s}^{-1}$ . This resulted in corrected shear rates from 7 to  $34\text{ s}^{-1}$ .

The uncertainty in viscosity was determined by calculating the statistical standard deviation of the collected data after filtering instrumental noise using a running average method. Propagation of error through calculations was determined by applying the Kline-McClintock method [52].

*Experiments above  $T_{liq}$ :*

The results of the experiments conducted above  $T_{liq}$  on dehydrogenated initially amorphous and remelted Vit1 are shown in Fig. 9. The maximum measured viscosity of Vit1 is  $35.1 \pm 5.4$  Pa·s at 1075 K at a corrected shear rate of  $6 \text{ s}^{-1}$ . This viscosity decreases by an order of magnitude to  $3.6 \pm 0.5$  Pa·s by increasing the shear rate to  $350 \text{ s}^{-1}$ . By further increasing the temperature from 1075 to 1225 K the viscosity decreases an additional two orders of magnitude to  $0.05 \pm 0.01$  Pa·s. Also, at the temperature above 1225 K, no shear thinning behavior is observed.

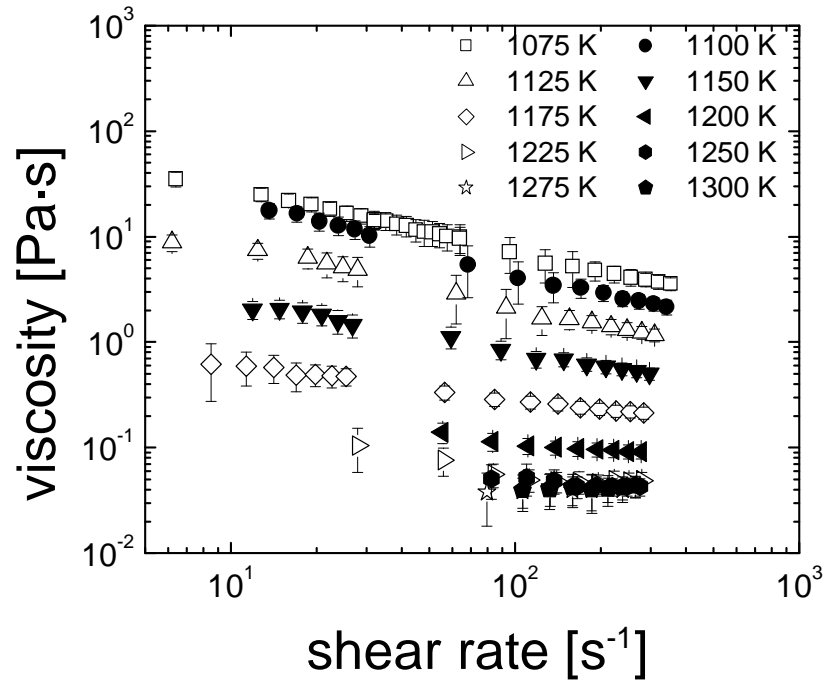


**Figure 9:** Isothermal viscosity vs. shear rate upon heating from 1075 K to 1300 K in 25 K increments. It shows the high viscosity and shear rate dependence above  $T_{\text{liq}}$  for this alloy. With increasing temperature both of these behaviors reduce and become constant above 1225 K.

To investigate a possible influence of thermal history, the same sample used in the previous experiment was cooled back to 1075 K and held isothermally for one hour. At that point the exact temperature and same shear profile that is described above were repeated. This experimental run is called the second temperature scan. Figure 10 shows the comparison of the first (depicted by red filled symbols) and the second (depicted by blue open symbols) temperature scans. The second temperature shows that the material stay Newtonian with the highest measured viscosity of  $0.26 \pm$

0.19 Pa·s at 1075 K, which is about two orders of magnitude lower than the viscosity obtained at 1075 K in the first temperature scan. With increasing temperature the viscosity of the sample continues to remain shear rate independent and the viscosity decreases to  $0.05 \pm 0.02$  Pa·s, which is in agreement with the lowest viscosity attained from the first temperature scan. This indicates that once the sample is exposed to high temperature, the viscosity does not increase upon cooling to temperature above  $T_{\text{liq}}$  to the values attained during the first temperature scan.

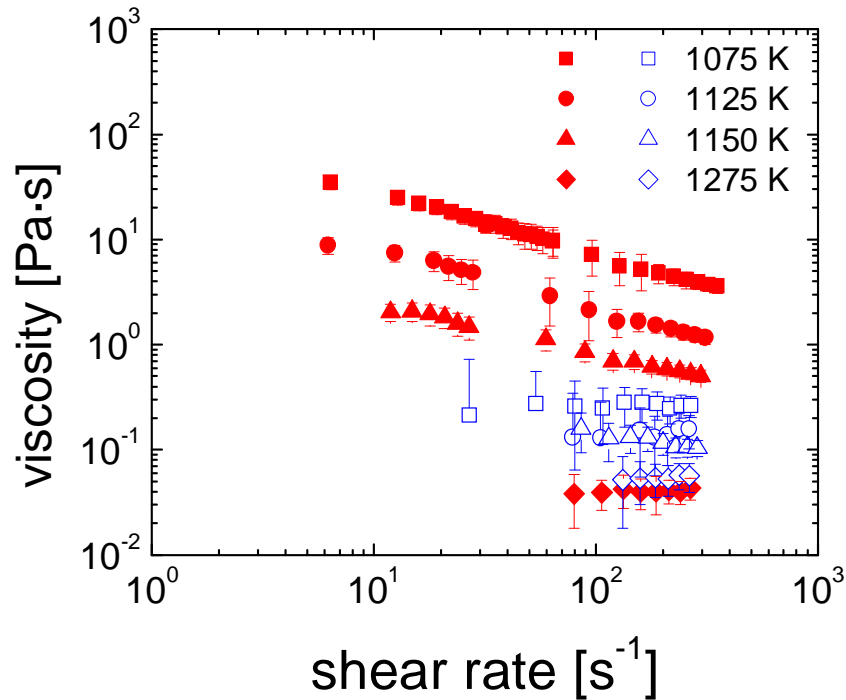


**Figure 10:** Comparison of the isothermal viscosity vs. shear rate on initially amorphous material shown for two different temperature scans. The solid red symbols represent first temperature scan in which the viscosity upon heating the initially amorphous alloy from 1075 to 1275 K. At this point the sample was cooled to 1075 K and held isothermally for one hour. A second temperature scan from 1075 K to 1300 K, indicated by the open blue symbols, was then performed.

Another set of experiments were performed on dehydrogenated initially micro-crystalline Vit1 with an average microstructure length scale of  $10^{-3}$  m. The same standard measurement procedure of isothermal viscosity measurements was performed to investigate the viscosity of these samples above  $T_{\text{liq}}$ . Figure 11 shows

the comparison of the results for the initially amorphous Vit1 from Fig. 9 and the data obtained from investigation of dehydrogenated initially micro-crystalline Vit1. Upon initially heating both samples to 1075 K the viscosity of the initially amorphous is  $25.0 \pm 3.6$  Pa·s at  $12 \text{ s}^{-1}$  while the initially micro-crystalline Vit1 sample has a viscosity of  $1.9 \pm 0.3$  Pa·s at the same shear rate. With increasing temperature this large difference in viscosity between the micro-crystalline and amorphous samples decreases and at the temperature of 1175 K, viscosity of both samples becomes equal within the error. Upon further heating, the viscosities continue to be the same and eventually shows Newtonian behavior above 1225 K with a viscosity of  $0.05 \pm 0.01$  Pa·s.

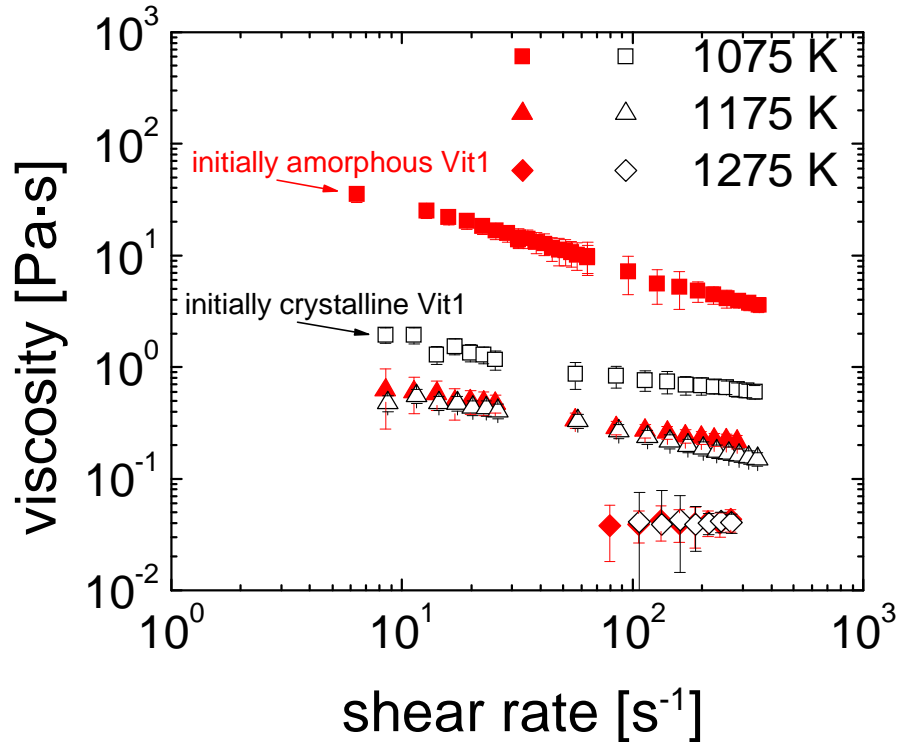


**Figure 11:** Comparison of the isothermal viscosity vs. shear rate between initially amorphous (solid red symbols) and initially micro-crystalline (open symbols) Vit1. At 1075 K there is a large difference between the viscosities of two samples, which decreases with increasing temperature. At 1175 K, the viscosities of both samples become the same and continue to be same with increasing temperature.

*Evaluation of Newtonian behavior as a function of temperature for initially amorphous and remelted Vit1:*

Evaluation of Newtonian behavior as a function of increasing temperature was done by using the power law which is given by [53]

$$\eta = A \cdot \dot{\gamma}^{(n-1)} \quad (22),$$

where  $\eta$  is the viscosity and  $\dot{\gamma}$  is the shear rate, respectively. The shear thinning exponent,  $n$ , is determined by fitting the above equation to the viscosity vs. shear rate data presented in Fig. 9 and Fig. 10. If this value is less than one, then the material exhibits a non-Newtonian shear thinning behavior whereas for  $n = 1$ , the viscosity has no shear rate dependence and Newtonian behavior is exhibited. Results of this analysis are shown in Fig. 12. Upon heating the initially amorphous Vit1, the shear thinning exponent, shown by (■), is 0.4 at 1075 K and increases to 1.0 above 1225 K, indicating increasing Newtonian behavior with increasing temperature. This indicates a thermal transition from a highly ordered to a less ordered state. The shear thinning exponent, depicted by (●), obtained by fitting power law to Fig. 10 (from the second temperature scan), when the material was cooled back to 1075 K, holding isothermal for one hour and reheating to 1300 K, shows that the viscosity remains non shear rate dependant over the entire tested temperature range.

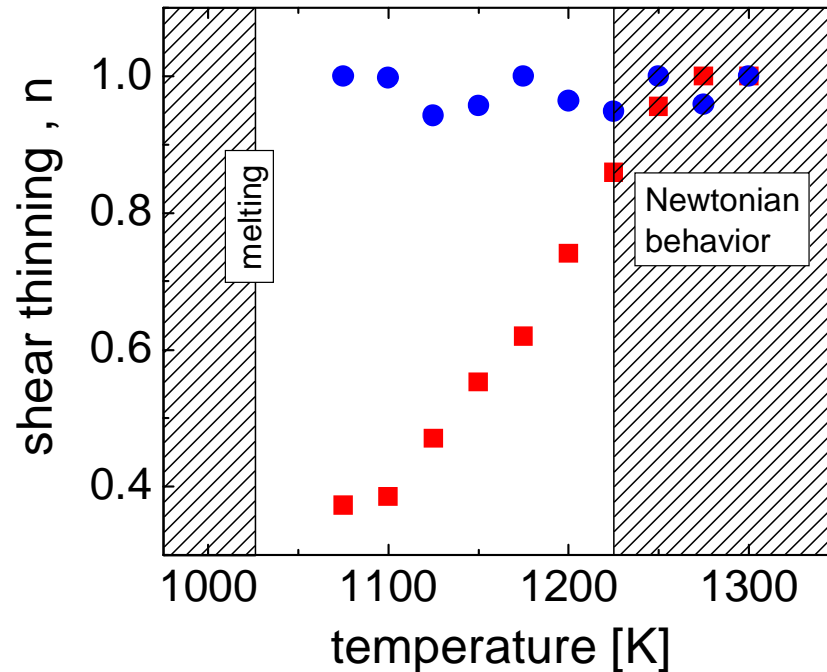


**Figure 12:** Non-Newtonian behavior vs. temperature of initially amorphous Vit1 for a first (■) and a second (●) temperature scans. After first melting from the initially amorphous state, the alloy exhibits a pronounced shear thinning behavior that weakens with increasing temperature. Above 1225 K there is no longer a shear rate dependence of the viscosity. After cooling back to 1075 K and holding isothermal for one hour, the material is still Newtonian over the investigated temperature range.

#### *Experiments below $T_{liq}$ :*

Two different undercooling experiments were performed. In the first run the sample was cooled from 1125 K and the sample was cooled from 1225 K in the second run. The measurement procedure for the undercooling experiments is

explained earlier in this section and the results are shown in Fig. 13. The initial measured viscosity by cooling from 1125 K ( $\square$ ) is 9 Pa·s which increases to 230 Pa·s upon cooling to 938 K. In another run shown by ( $\circ$ ), the sample was heated to 1225 K and then cooled. The viscosity of this sample stays far below the sample that was only heated to 1125 K. At 1045 K the viscosity of the sample cooled from 1225 K is 0.42 Pa·s which is over two orders of magnitude lower than the viscosity measured at 1045 K when cooled from 1125 K. In fact, by heating the sample to 1225 K the initial viscosity was too low to be measured accurately using a constant shear rate of  $5 \text{ s}^{-1}$ . Data between 1045 K and 1225 K has been replaced with data that was collected using isothermal viscosity measurements on initially amorphous Vit1 ( $\Delta$ ) heated above 1225 K that was shown earlier in Fig. 10. Upon cooling below  $T_{\text{liq}}$  the viscosity continues to increase until measurement limitations are reached at 907 K.

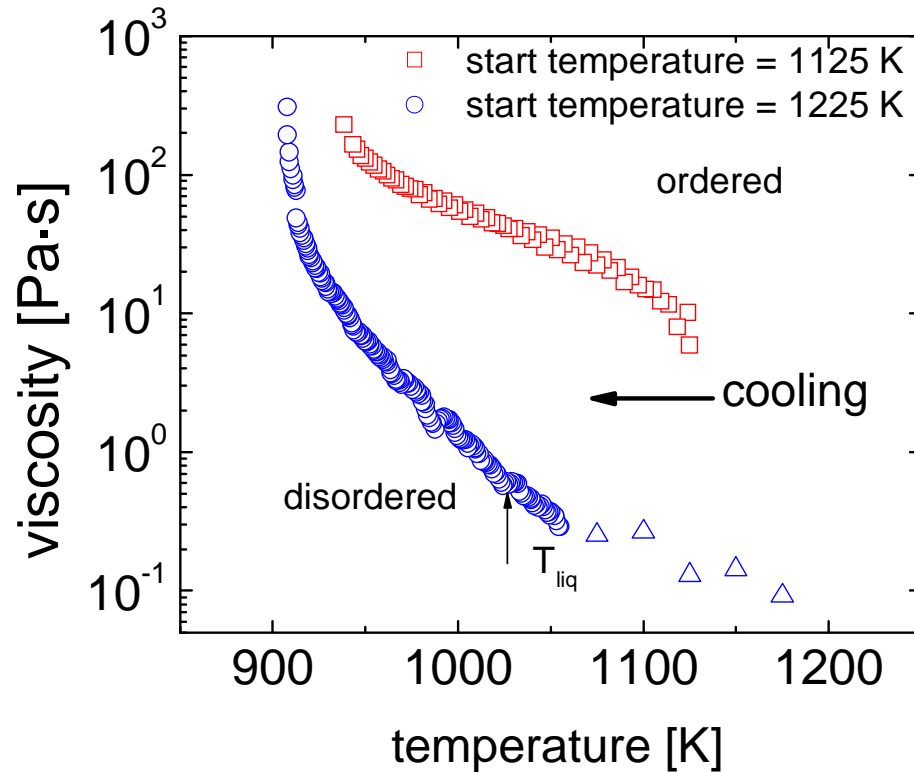


**Figure 13:** Viscosity vs. temperature during undercooling experiment with an average cooling rate of  $2 \text{ K}\cdot\text{s}^{-1}$  using a constant clockwise shear rate. When the material is cooled from 1125 K ( $\square$ ), the viscosity stays about two orders of magnitude higher than when cooled from 1225 K ( $\circ$ ). Data shown by ( $\Delta$ ) is represented by isothermal viscosity measurements.

The results of Vit1 shown in Fig. 9-11 indicate that not only the temperature and shear rates but also the initial sample's condition in terms of structure (amorphous or crystalline) affects the viscosity. Upon heating, the amorphous material retains its ordered state and show high viscosity whereas the initially

crystalline material is in a less ordered state and therefore has lower viscosity. Similar viscosity behavior with respect to temperature and shear rate has been observed in polymeric based systems and is addressed due to the interaction of highly ordered structures. Therefore, the high viscosity states are now called as ordered and low viscosity states as disordered states as depicted in Fig. 13.

This suggests that the initially amorphous and remelted material at 1075 K stays in an ordered state with high viscosity where it shows a non-Newtonian behavior and with increasing temperature this order is destroyed and a non-Newtonian behavior weakens. At the temperatures above 1225 K non-Newtonian behavior disappears. It is also seen that no reordering occurs upon cooling back to 1075 K and the sample remains in a disordered state as confirmed by second temperature scan.

Figure 14 shows the viscosity of initially amorphous and remelted Vit1 as a function of inverse temperature from both the isothermal and continuous cooling experiments on an Angell plot [37]. To compare the data of Vit1, also shown are the viscosity data of SiO<sub>2</sub> (strong liquid) and o-terphenyl (fragile liquid). Upon initial heating, the viscosity ( $\square$ ) is on the order of  $10^2$  Pa·s at an average corrected shear rate of  $8 \text{ s}^{-1}$ . This viscosity decreases continuously with increasing temperature showing a transition from a high viscosity (strong) to a low viscosity (fragile) state which is

completed at 1225 K. The drop in viscosity is about two orders of magnitude, and thus much larger than the regular temperature dependence for a liquid with a constant fragility parameter. Once the low viscosity above 1225 K has been reached it stays low even if the sample is cooled down to 1075 K. This is represented by the second set of isothermal data ( $\Delta$ ) in the temperature range between 1075 and 1225 K. These data were collected using a shear rate of  $100 \text{ s}^{-1}$  due to the low accuracy of the viscosity measurement at lower shear rates. In this case, it is reasonable to use a higher shear rate to represent the viscosity at lower shear rates because of the non-shear rate dependence of the viscosity that has been shown earlier in Fig. 10 and Fig. 13. This indicates a transition from a high to a low viscosity or from an ordered to a disordered state. In the continuous cooling experiment ( $\circ$ ) from 1225 K below  $T_{\text{liq}}$ , the viscosity measured at a shear rate of  $10 \text{ s}^{-1}$  increases until measurement limitations, given by the maximum allowable torque at the torque sensor, are reached at 907 K. At this point the viscosity is the same as the initially amorphous sample. This increase in viscosity can not be regarded to the crystallization of the sample. Although we could not follow the torque signal upon further undercooling, the temperature signal was monitored as shown in Fig. 15. Figure 15 shows the viscosity and temperature signal during undercooling experiment. The recalescence, which indicates the occurrence of crystallization, was detected at 840 K, which is approximately 60 K below the temperature at which the increase of the viscosity was

observed. The location of the recalescence on the temperature axis is in good agreement with the results by Kim et al. [54].

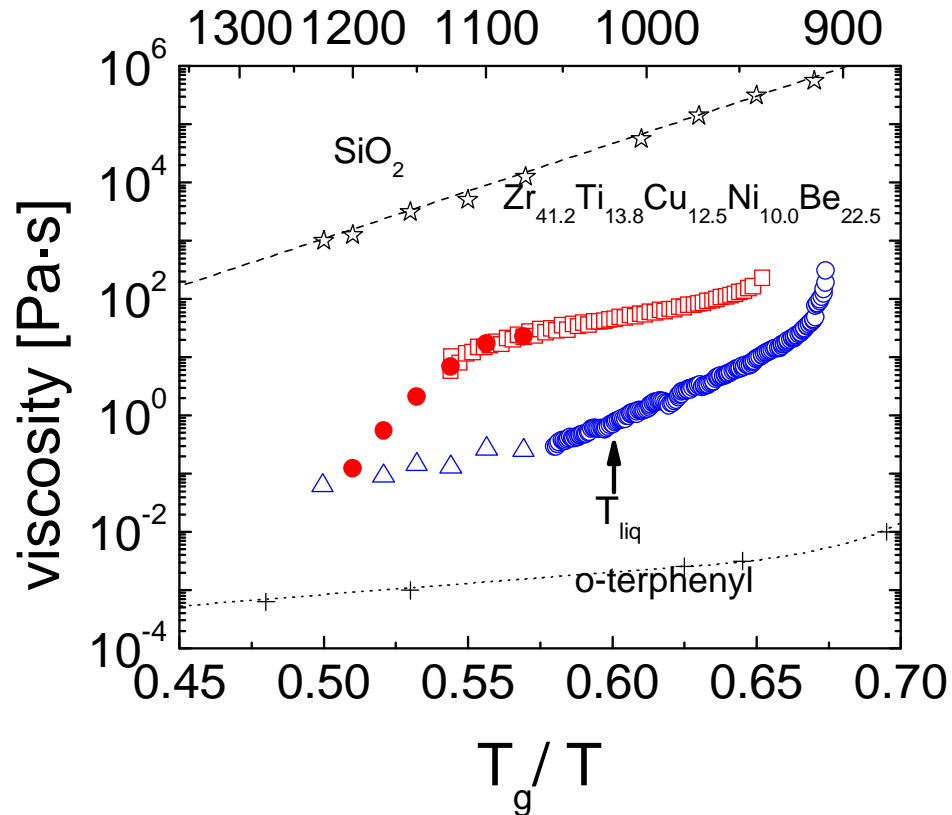


**Figure 14:** Angell plot showing the combined isothermal ( $\bullet$ ,  $\Delta$ ) and viscosity measurements obtained while cooling at  $2 \text{ K}\cdot\text{s}^{-1}$  from 1125 K ( $\square$ ) and 1225 K ( $\circ$ ). This shows the temperature hysteresis effect seen in the viscosity of Vit1. Also shown are the data of  $\text{SiO}_2$  and o-terphenyl. ( $\bullet$ ) represents data collected at a shear rate of  $10 \text{ s}^{-1}$  while ( $\Delta$ ) represents the viscosity collected at  $100 \text{ s}^{-1}$  upon cooling from 1300 K. This is done because the sensitivity of the torque sensor does not allow for accurate data at low shear rates.

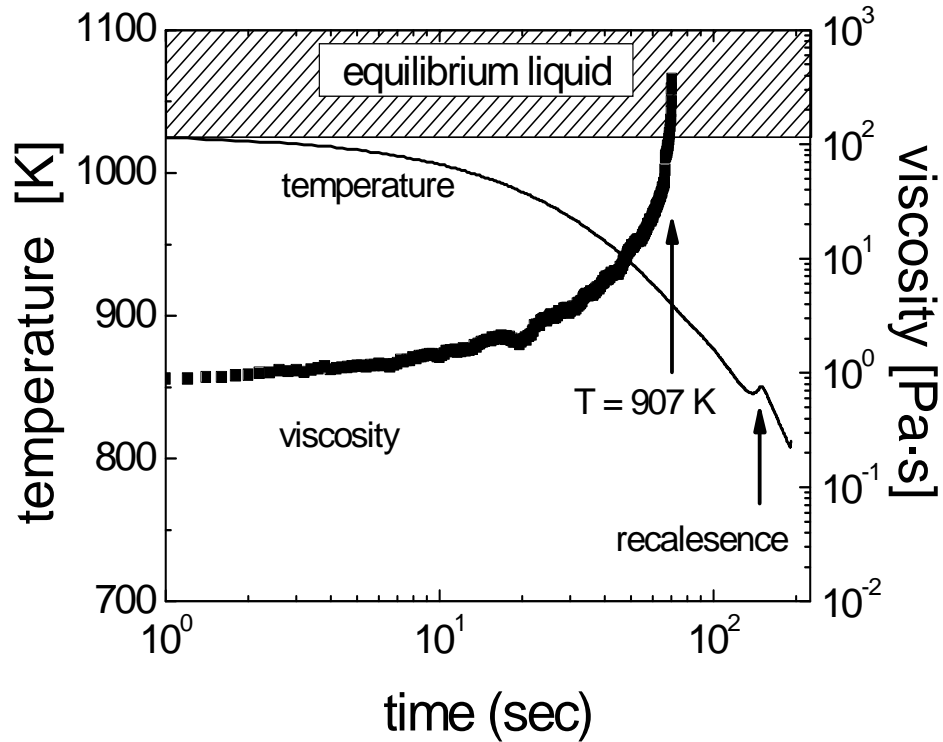


**Figure 15:** Viscosity (■) and temperature (-) signal with respect to recorded time upon cooling below  $T_{\text{liq}}$ . The onset of recalescence associated with crystallization occurs over 60 K below the temperature at which the increasing viscosity trips the torque sensor.

Hence, these observations can be summarized as a hysteresis curve (Fig. 14) in which “upon heating from the ordered (strong) state, the material makes a transition from the ordered (strong) state to the fragile (disordered) one (red symbols). This transition is complete at 1225K and upon cooling from the

temperatures  $\geq 1225\text{K}$  (blue symbols) the material starts to reorder in the supercooled liquid region and an ordered state is reached which is quantified by the high viscosity”.

The fragility of Vit1 for different ordered states is determined by fitting the Vogel-Fulcher-Tammann (VFT) relation, which is described in section 2.4.2.1. The VFT equation [37] is given by

$$\eta = \eta_0 \exp\left(\frac{D^* T_0}{T - T_0}\right) \quad (23),$$

where  $\eta_0 = 4 \times 10^{-5} \text{ Pa}\cdot\text{s}$  [55] is a constant pre-exponential factor,  $D^*$  is the fragility parameter, and  $T_0$  is the temperature at which the barrier to viscous flow would become infinite. By fitting equation 23 to the data for ordered state shown in Fig. 14 gives the  $D^* = 26.5$  and is the upper bound fragility parameters. Fitting the viscosity of the disordered state gives a lower bound  $D^* = 12$  of the fragility. Figure 16 shows the viscosity of the two different states of Vit1 above  $T_{\text{liq}}$  combined with the data obtained from three point beam bending viscosity experiments of Vit1 performed at an approximate shear rate of  $10^{-5} \text{ s}^{-1}$  close to the glass transition [56, 57] ( $\Delta$ ).

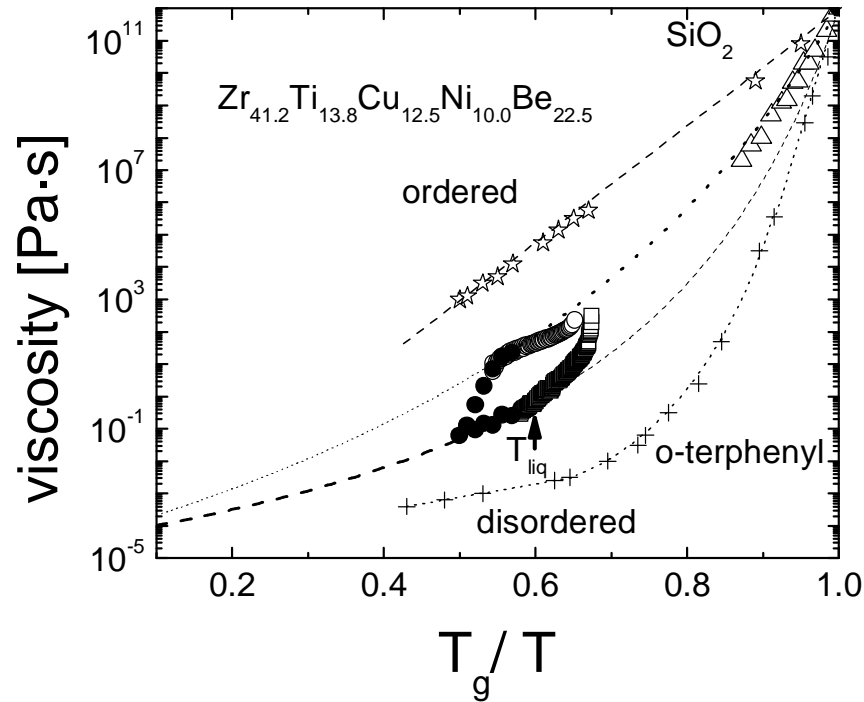


**Figure 16:** Expanded Angell plot of combined isothermal (●) and viscosity measurements obtained at a constant clockwise shear rate while cooling at  $2 \text{ K}\cdot\text{s}^{-1}$  from both  $1125 \text{ K}$  (○) and  $1225 \text{ K}$  (□). VFT fitting has been performed and shows the strong (---) and fragile (---) boundaries for Vit1. The viscosity hysteresis shows the transition between these two boundaries with respect to temperature. Also shown is TMA low viscosity measurements ( $\Delta$ ) obtained from three point beam bending experiments with an estimated shear rate of  $10^{-5} \text{ s}^{-1}$ . This viscosity data matches the predicted strong VFT fits thus indicating a similar ordered state both below and above  $T_{\text{liq}}$ .

The results presented in this section show that the pronounced shear rate and temperature effects of the viscosity in Vit1 must be due to retained order that is present above the liquidus temperature. The non-Newtonian behavior weakens with

increasing temperature and at the temperatures above 1225 K, material behaves like a Newtonian liquid. The structure of metallic systems has been recently investigated by D. Miracle [59] and E. Ma [60] to understand the structure of metallic systems. Their models suggest icosahedral short range ordered clusters (SRO) that form the building blocks for medium range order (MRO) in multicomponent systems. These (SRO) consist of a central atom of one species surrounded by several atoms of the other species. The (MRO) is then formed by placing this icosahedral (SRO) clusters on either a FCC lattice, in case of Miracle model, or icosahedral lattice in case of Ma model. The viscosity studies conducted in this work also indicate the presence of pronounced order present in the melt. This order can be reduced by shearing and more effectively destroyed by increasing the temperature leading to a much more fragile liquid.

The viscosity measurements on initially micro-crystalline Vit1 show much lower viscosities, which indicate that the medium and short range order is not present or at least significantly reduced, compared to the initially amorphous samples. The repeatability between the experiments is also achieved and the details could be found in Christopher Way's doctoral thesis [49].

In the next sections, the viscosity of other bulk metallic glass forming systems have been investigated to find if shear thinning behavior is seen in other

alloys. The effect of shear rate and ordering on the crystallization of Vit1 has also been investigated.

## References

- [1] H. A. Bruck, T. Christman, A. J. Rosakis and W.L. Johnson, *Scripta Mater* 30,429 (1994).
- [2] W. H. Petera, R. A. Buchanan, C. T. Liub, P. K. Liawa, M. L. Morrison, J. A. Hortonb, C. A. Carmichael, Jr. and J. L. Wright, *Intermetallics*, 10 (11-12), 1157 (2002).
- [3] A. Inoue, *Acta Mater*, 48, 279 (2000).
- [4] W. Clement, R. H. Willens and P. Duwez, *Nature (London)* 187, 869 (1960).
- [5] A. Inoue, T. Zhang and T. Masumoto, *Mater Trans. JIM*, 31, 425 (1991).
- [6] T. Zhang, A. Inoue, and T. Masumoto, *Mater Trans. JIM* 32, 1005 (1991).
- [7] A. Inoue, A. Kato, T. Zhang, S. G. Kim and T. Masumoto *Mater Trans. JIM* 32, 609 (1991).
- [8] A. Peker, W.L.Johnson, *Appl. Phys. Lett.* 63, 2342 (1993).
- [9] D. Xu, B. Lohwongwatana, G. Duan, W. L. Johnson and C. Garland, *Acta Mater.* 52, 2620 (2004).
- [10] J. Schroers and W.L.Johnson, *Appl. Phys. Lett.* 84, 3666 (2004).
- [11] A. Inoue, T. Nakamura, N. Nishiyama and T. Masumoto, *Acta mater.* 41, 915 (1993).
- [12] W.L.Johnson, *Bulk glass-forming metallic alloys*, MRS bulletin 42, (1999).
- [13] R. Busch and W.L. Johnson, *Appl. Phys. Lett.* 72, 2695 (1998).
- [14] T.A. Waniuk, R. Busch, A. Masuhr and W.L. Johnson, *Acta Mater* 46, 5229 (1998).
- [15] A. Masuhr, T. A. Waniuk, R. Busch and W. L. Johnson, *Phy. Rev. Lett.* 82 (11), 2290 (1999).

- [16] T. Shaw, C. Way and R. Busch, MRS Proc. 806, 215 (2004).
- [17] J. Jackle, "Models of the glass transition", Rep. Prog. Phys., 49, 171 (1986).
- [18] S. A. Miller and R. H. Murphy, Scr.Metall. 13, 673 (1979).
- [19] H. Cohen and D. Turnbull, *ibid* 189 (1960).
- [20] A. J. Drehman and A. L. Greer, Acta Metall. 32, 323 (1984).
- [21] X.H. Lin and W.L. Johnson, Mater. Trans. JIM.38, 475 (1997).
- [22] M. Ohring and A. Haldipur, Rev. Sci. Instrum. 42, 530 (1971).
- [23] R. Pond and R. Maddin, Trans. Met. Soc. AIME. 245, 2475 (1969).
- [24] Ivan McCracken, MS thesis, Oregon State University (2002).
- [25] M.D.Ediger, C.A.Angell, Sidney R. Nagel, J. Phys. Che., 100, 13200 (1996).
- [26] R. Busch, JOM, 52, 39 (2000).
- [27] H. S. Chen and D. Turnbull , Acta Mater. , 17, 1021 (1969).
- [28] D. Turnbull and J. C. Fisher, J. Chem. Phys., 17, 71 (1949).
- [29] A. Inoue, Acta Mater, 48, 279 (2000).
- [30] G. Wilde, G. P. Görler, R. Willnecker and G. Dietz, Appl. Phys. Lett. 65 (4), 397 (1994).
- [31] R. Busch, Y.J. Kim, and W.L. Johnson, J. Appl. Phys., 77, 4039 (1995).
- [32] R. Busch, W. Liu, and W.L. Johnson, J. Appl. Phys., 83, 4134 (1998).
- [33] S. C. Glade, R. Busch, D. S. Lee, and W. L. Johnson 87(10), 7242 (2000).
- [34] D. A. Porter and K. E. Esterling, Phase Transformations in Metals and Alloys, Chapman and Hall(1997).

- [35] R. Böhmer, K.L. Ngai, C.A. Angell and D.J. Plazek, *J. Chem. Phys.* 99, 4201 (1993).
- [36] T. Lida and R.I.L. Guuthrie, *The Physical Properties of Liquid Metals*, Clarendon, Oxford (1998).
- [37] C. A. Angell, *J. Non-Cryst. Solids* 13, 131 (1991).
- [38] E. Bakke, R. Busch and W. L. Johnson, *Appl. Phys. Lett.* 67 (22), 3260 (1995).
- [39] R. Busch, A. Masuhr, E. Bakke and W.L. Johnson, *Acta Mater.* 46, 4725 (1998).
- [40] G. J. Diennes and H. F. Klemm, *J. Appl. Phys.* 17, 458 (1946).
- [41] A. Masuhr, R. Busch and W. L. Johnson, *Mat. Sci. Forum* 269-272, 779 (1998).
- [42] T. Shaw, C. Way and R. Busch, *MRS Proc.* 806, 215 (2004).
- [43] G. Adam, J.H. Gibbs, *J. Che. Phys.*, 43, 139 (1965).
- [44] S.V. Nemilov, *Glass Physics and Chemistry*, 21, pp 91 (1995).
- [45] A. Masuhr, R. Busch, W.L. Johnson, *Journal of Non-Crystalline Solids*, 250-252, 250, (1999).
- [46] J. W. Christian, *The Theory of Transformations in Metals and Alloys*, Pergamon, Oxford, (2002).
- [47] K. F. Kelton, *Solid State Phys.* 45, 75 (1991).
- [48] T.A. Wanuik, R. Busch, A. Masuhr and W.L. Johnson, *Acta Mater* 46, 5229 (1998).
- [49] T.A. Shaw, PhD thesis, Oregon State University (2004).
- [50] C. Way, PhD thesis, Oregon State University (2005).
- [51] J. Schroers, R. Busch, A. Masuhr and W. L. Johnson, *Appl. Phys. Lett.*, 74, 2806 (1999).
- [52] S. J. Kline and F. A. McClintock, *Mech. Eng.*, 75, 3 (1953).

- [53] H.A. Barnes, J.K. Hutton, and K. Walters, *An Introduction to Rheology*, Elsevier Science, Amsterdam (1989).
- [54] Y. J. Kim, R. Busch, W. L. Johnson, A. J. Rulsion, and W.K Rhim, *Appl. Phys. Lett* 65, 2136 (1994).
- [55] S. V. Nemilov, *Glass Phys. Chem.*, 21, 91 (1995).
- [56] R. Busch, A. Masuhr, E. Bakke, W. L. Johnson, *Mater. Sci. Form.*, 269, 547 (1998).
- [57] T. A. Waniuk, R. Busch, A. Masuhr and W. L. Johnson, *Acta. Mater.* 46, 5229 (1998).
- [58] L.A. Shadovspeaker and Ralf Busch, *Mat. Res. Soc. Symp Proc.* 806, 233 (2004).
- [59] D. Miracle, *Nature Materials*, 3 (10), 697 (2004).
- [60] H.W. Sheng, W.K. Luo, F.M. Alamgir, J.M. Bai, and E. Ma, *Nature*, 439, 419 (2006).

#### 4. MANUSCRIPT I

### Ordering and shear rate induced crystallization of undercooled

### $\text{Zr}_{41.2}\text{Ti}_{13.8}\text{Cu}_{12.5}\text{Ni}_{10.0}\text{Be}_{22.5}$ metallic-glass-forming melts.

Prashant Wadhwa<sup>1,2,a</sup> and Ralf Busch<sup>1,2,b,\*</sup>

<sup>1</sup>Oregon State University, Department of Mechanical Engineering, Corvallis, OR

97331-USA

Tel.: 001-541-7377021; Fax: 001-541-7372600

<sup>2</sup>Universität des Saarlandes, Lehrstuhl für Metallische Werkstoffe, Postfach 151150,

66041 Saarbrücken, Germany

Tel.: 049-681-3023208; Fax: 049-681-3024385

<sup>a</sup>wadhwa@engr.orst.edu, <sup>b</sup>r.busch@mx.uni-saarland.de

\* Author to whom correspondence should be addressed; email: r.busch@mx.uni-saarland.de

To be submitted to: Physical Review Letter

## Abstract

The ordering and shear rate induced crystallization of undercooled  $\text{Zr}_{41.2}\text{Ti}_{13.8}\text{Cu}_{12.5}\text{Ni}_{10.0}\text{Be}_{22.5}$  (Vit1) metallic-glass-forming melts has been reported. We experimentally determined the time temperature transformation (TTT) diagrams of  $\text{Zr}_{41.2}\text{Ti}_{13.8}\text{Cu}_{12.5}\text{Ni}_{10.0}\text{Be}_{22.5}$ , which describes the occurrence of the reordering and crystallization events as a function of shear rate, isothermal annealing time and temperature in the undercooled liquid. In our study we measure the viscosity as well as the recalescence during crystallization at various shear rates ranging from  $10 \text{ s}^{-1}$  to  $150 \text{ s}^{-1}$  in order to develop these diagrams by using the high-temperature couette rheometer. With increasing shear rate the TTT diagram shifts to the left indicating the deterioration of glass forming ability of the alloy. It is quantified that the shear rate induced crystallization can not be explained by the classical nucleation theory. It is also shown that the amount of order present in the melt immensely influences the crystallization kinetics. We have put forward an approach which suggests that apart from viscosity the polymorphic transition from the short range ordered (SRO) state to the medium range ordered (MRO) state in the melt triggers crystallization. The formation of MRO is faster at higher shear rates and the crystallization occurs sooner.

Keywords: bulk metallic glass, ordering, shear thinning, short range order, viscosity

Over the last few decades bulk metallic glasses (BMGs) have gained much attention due to their interesting mechanical properties, lower solidification shrinkage, forming in a viscous state and higher corrosion resistance than their crystalline counterparts [1-3]. The first major breakthrough in metallic glass formation came in 1960 when Klement, Willens and Duwez processed amorphous  $\text{Au}_{80}\text{Si}_{20}$  by rapid quenching the melt with the cooling rate of about  $10^6\text{K/sec}$  [4, 5]. These conventional metallic glasses are usually processed in the form of thin ribbons or foils by melt spinning or splat quenching with extremely fast cooling rates but also at high shear rates.

In the recent years a number of alloy systems which can be processed in bulk amorphous form (thickness  $>1\text{mm}$ ), known as bulk metallic glass (BMG), have been developed. These alloys can be processed at much smaller cooling rates by copper mold casting. In contrast to rapid solidification methods, only little shear is involved during processing of bulk metallic glass. Many factors such as the number of components, composition of each element and the critical cooling rate of an alloy system to produce BMG, have been extensively studied in order to understand the glass forming ability (GFA) of a metallic glass [3].

However only recently, the fact got attention that high shear rates applied during quenching the alloy from the molten state might promote crystallization and hence make it more difficult to obtain a metallic glass. Some alloys, such as  $Zr_{50}Cu_{50}$  [6], which were conventionally processed in thin amorphous ribbons by melt spinning at high shear rates have been revisited in the last few years. It was believed that no bulk amorphous alloy can be processed in Cu-Zr binary alloy [7]. However, in recent years, several binary CuZr alloys have been successfully cast in amorphous form with the critical thickness between 0.5 and 2 mm in a copper mold casting at negligible shear rates [8]. These results raise the question if a high shear rate is detrimental to the glass forming ability of the metallic glass formers and can even overcompensate the positive effect of rapid quenching during fast shearing.

A first systematic qualitative study on the effect of shear rate on crystallization in BMG is reported recently by Johnson and co-workers [9] The solidification study on the  $Au_{49}Ag_{5.5}Pd_{2.3}Cu_{26.9}Si_{16.3}$  BMG-forming alloy experimentally showed the processing of fully amorphous rods of at least 5 mm in diameter using a conventional copper mold injection method, whereas amorphous samples could not be obtained when the alloy was processed by splat quenching under a high cooling rate and a high shear rate. Their results reveal that the large strain rate during splat cooling induces crystallization and the effect of shearing on the crystallization becomes less pronounced with increasing processing temperature

[9]. In their work, they suggested to consider a shear rate dependent critical cooling rate in order to completely characterize the glass forming ability of the material. Therefore, it is significantly important to quantify the shear rate dependence of crystallization in glass forming alloys in order to verify if the shear rate (flow rate) of the melt is another important parameter that determines glass forming ability and that has been overlooked so far.

In this letter, we present the experimentally determined time temperature transformation (TTT) diagrams of  $\text{Zr}_{41.2}\text{Ti}_{13.8}\text{Cu}_{12.5}\text{Ni}_{10.0}\text{Be}_{22.5}$ , which describes the occurrence of the reordering and crystallization events as a function of shear rate, isothermal annealing time and temperature in the undercooled liquid. In our study we measure the viscosity as well as the recalescence during crystallization at various shear rates in order to develop these diagrams.

Pellets of  $\text{Zr}_{41.2}\text{Ti}_{13.8}\text{Cu}_{12.5}\text{Ni}_{10.0}\text{Be}_{22.5}$  (Vit1) were obtained from Liquid Metal Technologies and dehydrogenated by melting them under a high vacuum of  $10^{-3}$  Pa. The samples were quenched to attain an amorphous state. The dehydrogenation was necessary to prevent hydrogen from emerging from the molten sample during the subsequent viscosity measurement and adversely affecting the viscosity measurements.

The viscosity measurements were performed in a high-temperature couette rheometer. This rheometer consists of a concentric cylinder graphite shear cell that is mounted vertically inside a high-vacuum induction furnace. The material was kept in the outer cylindrical cup where it was melted by inductive heating. The outer cylinder is attached to a torque sensor and the temperature was measured with a thermocouple mounted inside the cylinder wall. The inner cylinder was lowered into the outer cylinder and the gap between the outer and inner cylinder contained the melt. Under continuous rotation of the inner cylinder the molten material was sheared and the torque on the outer cylinder was generated via the shear field in the melt [10]. This torque signal,  $M$ , in  $\text{N}\cdot\text{m}$  through the molten test sample was subsequently recorded with a torque sensor. Details of the equipment and procedures are described elsewhere [10-12].

Viscosity measurements were performed both above and below liquidus temperature ( $T_{\text{liq}}$ ) by using the following procedure. For experiments above  $T_{\text{liq}}$ , the shear cell was heated to a constant temperature of 1075 K and the material was sheared in a clockwise and counter clockwise direction in order to obtain an average torque signal. A shear scan from 5 to 300  $\text{s}^{-1}$  was then performed at 25 K increments from 1075 K to 1300 K. Two different undercooling measurements below  $T_{\text{liq}}$  were performed. (I) For continuous cooling experiment, the alloy was heated in the shear cell to an initial temperature above  $T_{\text{liq}}$  and then sheared at a clockwise constant

shear rate. At that point the temperature of the shear cell was decreased using an average cooling rate of 2 K/s. The sample was then undercooled until the viscosity increased to a value where the generated torque signal, reached 95% of the maximum measurement capabilities of the torque sensor. At that point the experiment was terminated and the sample reheated again. (II) To determine the TTT diagram, the material was cooled below the  $T_{liq}$  and held isothermal at the desired temperature. The material was then sheared at a constant rotation speed until the generated torque signal, (again) reached 95% of the maximum measurement capabilities of the torque sensor due to the increase of the viscosity with time. It should be noted that it has been shown earlier that heterogeneous surface nucleation at graphite containers does not affect structural changes and crystallization of the Vit1 melts [13, 14].

We have found a strong non-Newtonian shear thinning behavior and high melt viscosity in Vit1 which we have reported earlier [12]. The study shows that the non-Newtonian behavior decreases with increasing temperatures and at the temperatures above 1225 K, the material behaves like a Newtonian liquid. The study suggests that this high melt viscosity and non Newtonian behavior is due to the presence of pronounced order in the strong liquid of Vit1 which is preserved upon first heating above  $T_{liq}$ . Here we do not explicitly show the shear thinning effect itself but show the temperature dependence of the viscosity that exhibits a pronounced hysteresis effect.

Figure 1 shows the results obtained from the isothermal viscosity measurements above  $T_{\text{liq}}$  and continuous cooling measurements below  $T_{\text{liq}}$  plotted on an Angell plot [15]. The figure exhibits four different sets of viscosity data at the shear rates of  $10 \text{ s}^{-1}$  and  $100 \text{ s}^{-1}$ . The samples were first heated to 1125 K and then the initial viscosity was measured during continuous cooling of sample below  $T_{\text{liq}}$ . The data obtained is shown by hollow squares ( $\square$ ). The data shown by ( $\bullet$ ), is obtained from isothermal measurements with a shear rate of  $10 \text{ s}^{-1}$  from 1125 K to 1250 K in 25 K increments. In another run, shown by ( $\circ$ ), the sample was heated to 1250 K and then the viscosity was measured during continuously cooling the material below  $T_{\text{liq}}$ . The viscosity from 1250 to 1045 K could not be measured accurately at a shear rate of  $10 \text{ s}^{-1}$  due to the limitations of our torque sensor. Therefore, the data between 1045 and 1250 K shown by ( $\Delta$ ) was measured by isothermal viscosity measurements at  $100 \text{ s}^{-1}$  by cooling the sample from 1250 K to 1075 K.

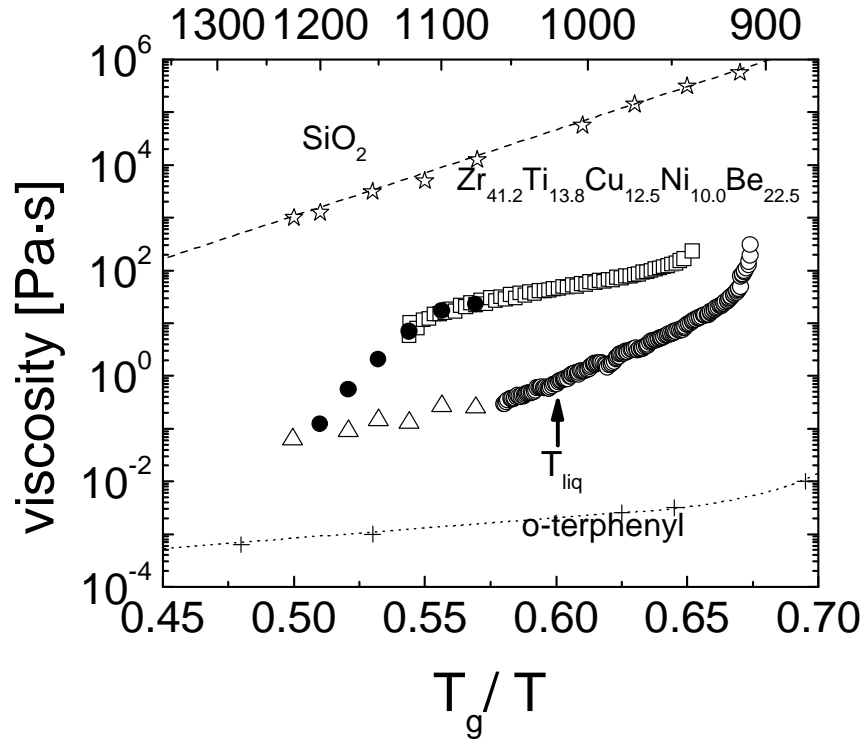


**Figure 1:** Angell plot showing the isothermal ( $\bullet$ ,  $\Delta$ ) viscosity data and viscosity measurements obtained upon continuous cooling at  $2 \text{ K}\cdot\text{s}^{-1}$  from 1125 K ( $\square$ ) and 1250 K ( $\circ$ ). ( $\bullet$ ) represents data collected at a shear rate of  $10 \text{ s}^{-1}$  while ( $\Delta$ ) represents the viscosity collected at  $100 \text{ s}^{-1}$  upon cooling from 1300 K. This is done because the sensitivity of the torque sensor does not allow for accurate data at low shear rates. The viscosity hysteresis can be seen upon heating and cooling. Upon heating the material makes a transition from a strong liquid to a weak liquid ( $\bullet$ ) where as upon cooling a reverse transition from fragile to strong in the supercooled liquid region can be seen ( $\circ$ ). The plot also shows the viscosity of  $\text{SiO}_2$  (strong liquid) and o-terphenyl (fragile liquid) plotted as a function of inverse temperature normalized by the glass transition

The substantial decrease in viscosity with increasing temperature ( $\bullet$ ) shown in Fig.1, indicates a transition from a strong (high viscosity) to a more fragile (low viscosity) liquid, which we refer to as a transition from an medium range ordered (MRO) to a short range ordered state (SRO) in the remainder of this letter. It is

important to note that the strong liquid exhibits pronounced shear thinning with shear thinning exponents as low as 0.4, whereas the fragile liquid behaves virtually Newtonian ( $n \sim 1$ ) (see ref [12] for details). By heating the sample from 1075 K to 1250 K it undergoes a transition from a strong and highly viscous to a more fragile liquid with a lower viscosity.

Recently structural considerations on the amorphous solid state of multicomponent metallic systems have been addressed by D. Miracle [16] and E. Ma [17]. Models have been developed that account for order in amorphous solids through icosahedral SRO clusters that form the building blocks for MRO in multicomponent systems. These SRO clusters consist of a central atom of one species surrounded by several atoms of the other species. The MRO is then formed by placing this icosahedral SRO clusters on either a FCC lattice [16] or icosahedral lattice [17]. Both models are relatively simple and it is likely that there is a much larger variety of icosahedral SRO clusters than what has been assumed in these studies.

The observed strong to fragile transition in our study is likely due to breakdown of a MRO similar to that discussed by Miracle and Ma, with only SRO prevailing in the fragile liquid. The initial MRO clusters are preserved upon first heating and can be reduced in size by shearing and more effectively destroyed by

increasing the temperature leading to a much more fragile liquid. Once the low viscosity at 1250 K has been reached it stays low, if the sample is cooled down to 1075 K which is shown by the isothermally measured data ( $\Delta$ ) (Fig. 1). By continuing to cool below  $T_{liq}$  the viscosity ( $\circ$ ) increases until measurement limitations, given by the maximum allowable torque at the torque sensor, are reached at 907 K. At this point the viscosity is comparable to the viscosity measured upon cooling from 1125 K ( $\square$ ). This increase of the viscosity must be due to the reordering of the liquid into a strong MRO liquid, and not due to crystallization as is shown in Fig.2. In this plot the measured viscosity as well as the temperature are monitored simultaneously during undercooling. Even though the viscosity could only be measured as low as 907 K, the temperature signal was monitored further down. The recalescence, which indicates the crystallization, was detected at 840 K, which is more than 60 K below the temperature where the increase of the viscosity due to MRO was observed. The results shown Fig. 2 indicate strong structural changes occurring in the melt of Vit1 upon cooling and the material reorders in the undercooled liquid region, undergoing a transition from a fragile to a strong liquid. Such transitions from fragile to strong liquids have been observed in  $Al_2O_3 - Y_2O_3$  [18, 19] and other network forming systems such as Silica, Si and even water.

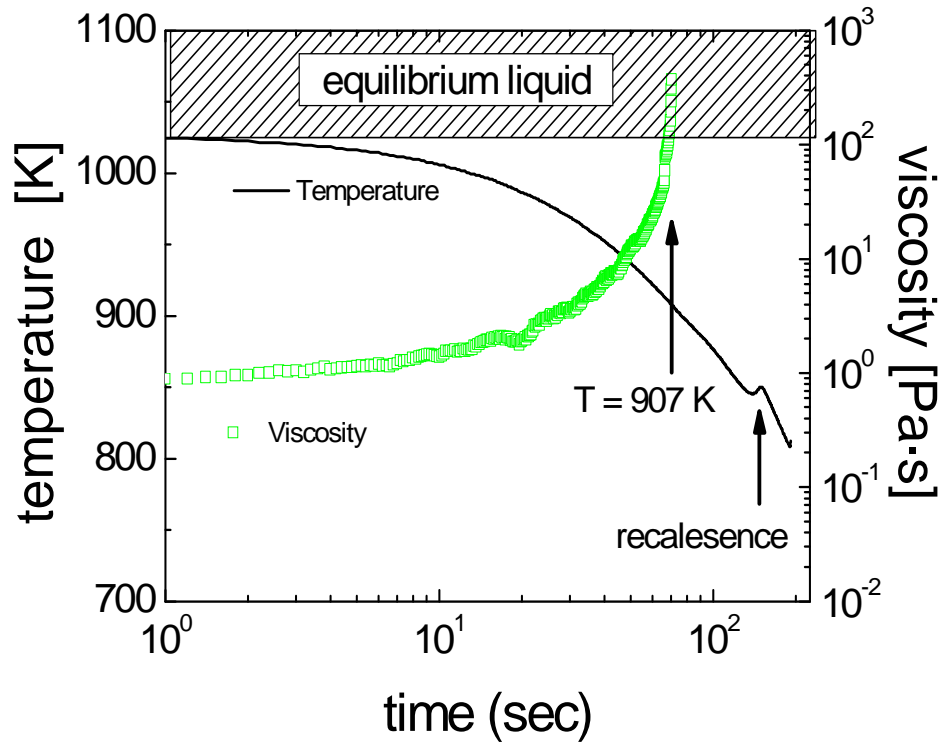


**Figure 2:** Viscosity (■) and temperature (-) during undercooling experiment are shown. The maximum measured viscosity related to maximum torque output is observed at 907 K whereas the recalescence associated with the onset of crystallization occurs more than 60 K below 907 K.

It should be noted that the observed behavior in Vit1 can not be attributed to the phenomenon of phase separation which has been recently revisited by Hono and coworkers [20], using three dimensional atom probe, transmission electron microscopy and small angle X-ray scattering. They have convincingly shown that as prepared Vit1 is chemically homogeneous and no phase separation occurs prior to crystallization. Since the alloy stays chemically homogenous, it is therefore most

likely that the observed fragile-strong transition is in deed a polyamorphism as it was found in network glass formers. Polyamorphism has been discussed e.g. by Angell [19] over the last decade. Angell has reported such transition in  $\text{Al}_2\text{O}_3 - \text{Y}_2\text{O}_3$  and water as a polymorphic transformation in which two glass phases of identical composition are formed by quenching.

It is interesting to note in Fig. 1 that the Vit1 possesses different melt viscosity at the same temperature depending on the initial temperature to which it was heated above the  $T_{\text{liq}}$ . For example when the material is heated to 1250 K into the fragile state and subsequently cooled, the sample has the viscosity of 0.289 Pa•s at 1054 K, whereas the sample heated to 1125 K and subsequently cooled, has a viscosity of 28.97 at 1054 K. Such a substantial difference in the viscosity of two orders of magnitude suggests a different crystallization behavior in Vit1 depending on the initial overheating temperature above  $T_{\text{liq}}$ . From a purely kinetic point of view one would, in fact, expect that the fragile Vit1 would crystallize easier than the strong alloy, since the viscosity is inversely proportional to the diffusion constant, which kinetically governs both nucleation and growth of crystals. However, the opposite is the case.

In order to investigate the effect of initial state of the sample (fragile or strong) on the crystallization, two samples were cooled from two different

temperatures. The results are presented in Fig. 3. The sample cooled from 1125 K, at which the material has a high viscosity, crystallizes at 881 K in 132 s, whereas the sample cooled from 1250 K, with much lower viscosity can be undercooled almost 40K lower to 845 K where it starts to crystallize after 210 s. This shows that the structural differences between the two melts must influence the crystallization much more than the overall kinetics given by the viscosity. It has been realized as early as 1994 that one has to heat the Vit1 sample to much higher temperatures than  $T_{\text{liq}}$  in order to obtain a good glass forming ability [21]. At that time, it was believed that the presence of oxide or other particles causes nucleation and the sample was to be heated much higher than  $T_{\text{liq}}$  to dissolve these particles into the liquid solution during processing in order to obtain the glassy samples. However, the observed change of the viscosity of two orders of magnitude in our study can not be due to crystalline particles in the melt even in a substantial amount of several percent. With Einstein's equation [22] for the flow of mixtures,  $\eta_{\text{eff}} = \eta(1 + 2.5\xi)$ , in which,  $\eta_{\text{eff}}$ , is the viscosity of the mixture,  $\eta$  is the viscosity of the liquid medium and  $\xi$  is the volume fraction of the particles, one estimates with a volume fraction of 0.1 (10%) particles an increase in viscosity of less than 30%. Our findings can only be due to substantial change in the structure of the melt as a whole. Apparently, the high MRO present in a melt acts as a precursor for the nucleation of long range ordered crystals and hence the sample in which the MRO has not been destroyed, crystallizes earlier. Therefore, for the following isothermal undercooling measurements, the material was first heated to the

$T_{\text{newtonian}}$  ( $>1250$  K) and subsequently undercooled to the desired isothermal temperature.

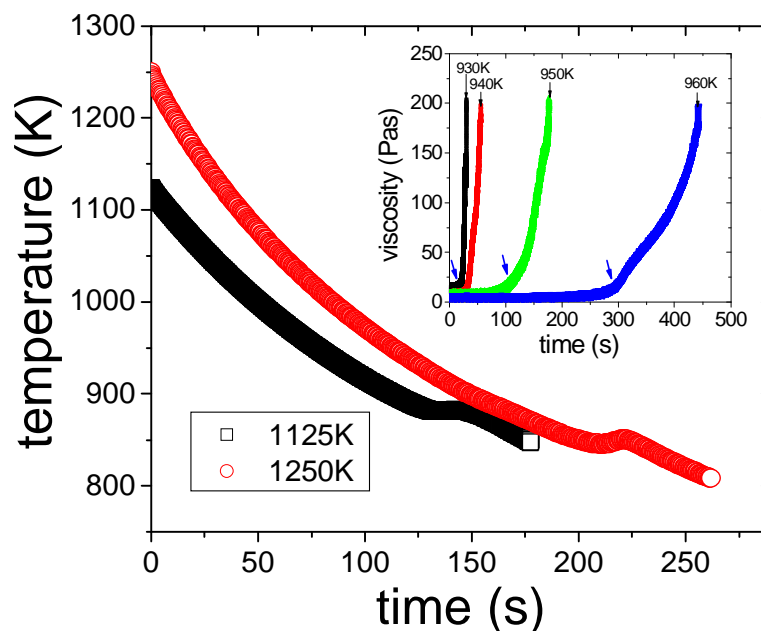


**Figure 3:** Continuous cooling data shown for two different samples cooled from 1125 K and 1250 K. The data reported by Schroers et al is also shown. The recalescence at different time and temperature are measured. Inset in the figure shows the isothermal measurements from 930 K to 970 K in the increments of 10 K at the shear rates of 10, 50 and 150  $\text{s}^{-1}$ . The initial increase in viscosity shows the onset of reordering and maximum viscosity reached indicates the crystallization event.

Figure 3 inset shows isothermal viscosity measurement between 930 and 970 K in 10 K increments at the shear rate of 10  $\text{s}^{-1}$ . The viscosity stays constant for a certain period of time at each isotherm and then starts to increase at a faster rate. This increase in viscosity is similar to the increase observed in Fig.1 and we believe that the material is reordering prior to crystallization. Therefore, the initial increase in

viscosity depicts the onset of reordering. Similar experiments at the shear rates of 50 and 150  $s^{-1}$  were performed. The different times for the onset of reordering at different shear rates and temperatures are tabulated in table I.

**Table I:** Table showing the viscosity at various temperatures and shear rates. Time for onset of ordering are also depicted.

Temp	viscosity(Pa•s )			time (s)		
	[10hz]	[50hz]	[150hz]	[10hz]	[50hz]	[150hz]
930	12.13	10.80	9.13	21.7	8	4.83
940	9.62	8.43	8.29	32.63	14.29	7.05
950	8.59	7.42	6.32	92.39	44.97	33.92
960	5.69	5.21	4.36	273.79	81.6	69.5

Figure 4 summarizes all the measured times for the onset of reordering and crystallization at various isothermal temperatures as a TTT diagram. The onset times for crystallization for a shear rate of 0Hz have been taken from Masuhr et al [14]. The are compared with the onset of the increase of viscosity for 10, 50, and 150 Hz in the viscometer. Only the upper portion of typical ‘‘C’’ shape of the TTT curve is shown in the figure since it was not possible to by Pa•s s the nose of the TTT diagram with the viscometer setup. At the lowest isothermal temperature of 930 K,

the onset of viscosity increase at the shear rate of  $10\text{s}^{-1}$  is observed at 22.48 s, which we attribute to the onset of reordering of the fragile liquid to the strong liquid, whereas shearing at 50 and  $150\text{ s}^{-1}$  shortens the onset time to 7.6 s and 4.5 s, respectively. Similarly, a pronounced shear rate dependence of reordering and crystallization at other isothermal temperatures can also be noticed in the figure.

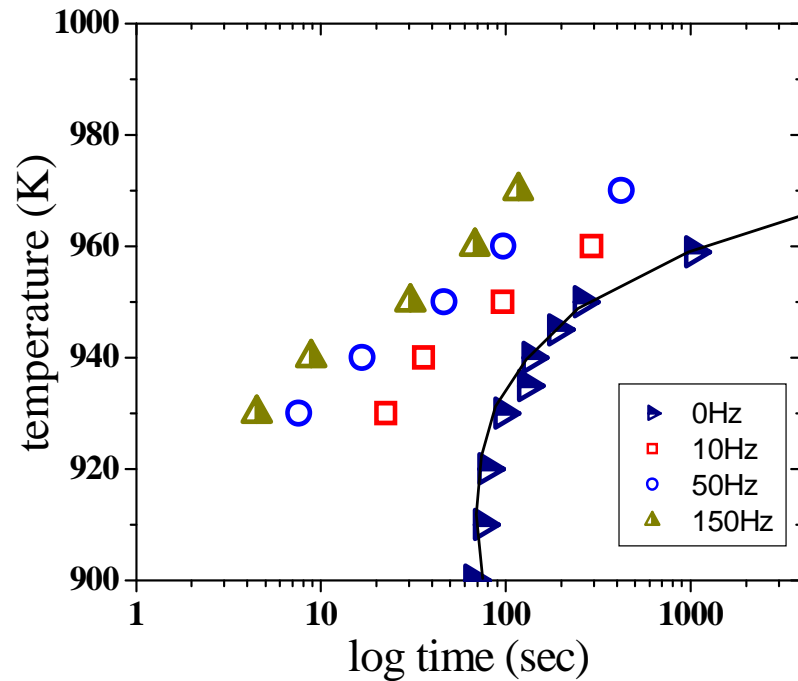


**Figure 4:** Time–temperature–transformation as a function for different shear rates reflecting the onset of reordering and crystallization. A strong impact of shear rate on the reordering and crystallization are observed.

At this point we need to analyze if nucleation and growth of crystal might be affected by the shearing process. The TTT diagram for crystallization under zero shear has been successfully analyzed previously [14] using classical nucleation theory as, e.g. described by Uhlman [23]. The fit to the TTT diagram is added in Fig 5, According to the classical nucleation theory, the time for the crystallization,  $t_x$ , is given by

$$t_x = \left( \frac{3 \cdot x}{\pi \cdot I_{ss} \cdot u^3} \right)^{1/4} \quad (1),$$

where  $x$  is a small volume fraction to crystallize,  $I_{ss}$  is the steady state nucleation rate and  $u$  is the growth velocity. The steady state nucleation rate,  $I_{ss}$ , can be described by,

$$I_{ss} = A \cdot D_{eff} \cdot \exp(-\Delta G^*/k_B T) \quad (2),$$

where  $D_{eff}$  is the effective diffusivity,  $A$  is a constant,  $k_B$  is a Boltzmann's constant and  $\Delta G^*$  is the activation energy barrier for nucleation,

$$G^* = 16\pi\sigma^3/(3\Delta G^2) \quad (3),$$

whereas the growth velocity,  $u$ , is given by

$$u = D_{\text{eff}}/l \cdot (1 - \exp(v_m \cdot \Delta G / k_B \cdot T)) \quad (4),$$

where  $k_B$  is the Boltzmann constant,  $T$  is the temperature and  $\Delta G$  is the Gibbs free energy difference between the liquid and crystalline phase (driving force), which can be described as

$$\Delta G_{l-x}(T) = \Delta H_f - \Delta S_f \cdot T - \int_T^{T_f} \Delta c_p^{l-x}(T) dT + T \int_T^{T_f} \frac{\Delta c_p^{l-x}(T)}{T} dT \quad (5),$$

where  $\Delta c_p(T)$  is the specific heat capacity difference between undercooled liquid and crystalline mixture and  $\Delta H_m$  and  $\Delta S_m$  the enthalpy and entropy of fusion, respectively. These latter three quantities have been previously determined calorimetrically in ref. [24] and were used in ref. [14] for the modelling of the TTT diagram.

It thus has to be evaluated, if the shearing process effectively alters the diffusivity and the driving force to account for the observed change in the TTT diagram. In ref.[14]  $D_{\text{eff}}$  was assumed to be inversely proportional to the viscosity,  $\eta$ . In that case, according to eq. 1-4,  $t_x$  is directly proportional to the  $\eta$ . This suggests that shear thinning which is associated with a decrease in viscosity could account for a shorter time for solidification by crystallization. However, the melt that we

investigate in the undercooling experiment is the fragile modification of Vit1, that shows no shear thinning above the liquidus temperature and only a weak thinning effect upon undercooling. Table I shows the viscosity and the time measured at the onset of reordering for different shear rates at the isothermal temperatures from 930 to 960 K. In this temperature range, a decrease in viscosity between 15-25% with changing shear rate is measured before the viscosity increase due to ordering is observed, whereas the time for the onset of reordering is shortened by about half orders of magnitude. Therefore, the small decrease in viscosity can not explain the substantial shortening of the time for ordering.

We therefore investigate the other factors that could influence the crystallization kinetics under shear. It can be seen from eq.(1) to eq.(4) that the other factor which influences crystallization time is the activation energy barrier ( $G^*$ ) which depends on the interfacial energy ( $\sigma$ ) and the Gibbs free energy difference between the liquid and crystalline ( $\Delta G$ ).  $\Delta G$  depends on the entropy change ( $\Delta S$ ), enthalpy change ( $\Delta H$ ) and the temperature. The entropy change ( $\Delta S$ ) as a function of viscosity can be described by the Adam Gibbs entropy model [25],

$$S_c = \frac{C}{T \cdot \ln(\eta/\eta_0)} \quad (6),$$

where  $\eta_0 = 4 \times 10^{-5}$  Pa·s [26] is a pre-exponential factor,  $S_c$  is the configurational entropy of the system and  $C$  represents an effective free enthalpy barrier for cooperative rearrangement. Since  $\eta$  changes by 15-25% depending on the shear rate as shown in table I, we estimated a small change in  $\Delta S$ . Such small change in  $\Delta S$  will not make a large change in  $\Delta G$  to account for a large change in  $t_x$ .

Another factor that could change the activation energy barrier for nucleation,  $G^*$ , is the amount of work introduced into the system by shearing. The effect of work done on the system under different flow conditions has been investigated in polypropylene by Kriegl et al [27, 28]. The work applied to the unit volume of sample under flow can be calculated by the following equation [27]

$$w = \eta \cdot \dot{\gamma}^2 \cdot t \quad (7),$$

where  $\gamma$  is the shear rate and  $t$  is the time for shearing. The amount of work introduced due to shearing is calculated by eq. (7). From all the shear rates, the maximum amount of work introduced in the system is approximately equal to 9 J/mol. This small work introduced into the melt is too small to make a considerable change in enthalpy. Therefore the effect of shearing on the driving force is not enough and can be neglected.

At this point the effect of order in Vit1 needs to be addressed. As discussed earlier the pronounced shear rate and temperature effects of the viscosity must be due to the retained MRO that is present above  $T_{liq}$  [12]. This MRO can be destroyed to SRO upon heating and reestablished on deeply undercooling the material below the  $T_{liq}$  as described earlier in Fig. 2. Therefore it is reasonable to assume that upon shearing the Vit1 during isothermal measurements, the material first forms preferred MRO structures and then crystallizes. These MRO structures act as precursor for the nucleation and trigger the crystallization. Upon shearing the material, the structural changes occur faster and preferred MRO is formed sooner at higher shear rate. This makes the TTT diagram to shift to the left at the higher shear rates.

In this letter we reported the ordering and shear rate induced crystallization of undercooled  $Zr_{41.2}Ti_{13.8}Cu_{12.5}Ni_{10.0}Be_{22.5}$  metallic-glass-forming melts. We quantitatively showed the shift in the TTT diagram of Vit1 at different shear rates. When the material was sheared at higher shear rate, it ordered and subsequently crystallized much sooner than the one sheared at smaller shear rates. The shift in the  $t_x$  can not be completely described with classical nucleation theory by taking  $\eta$  and  $G^*$  into consideration. We have put forward a qualitative approach which suggests that apart from viscosity the polymorphic transition from the SRO state to the MRO

state in the melt induces crystallization. These MRO clusters are formed faster at higher shear rates and the material crystallizes sooner.

This work was supported by DARPA (Grant No. DAAD-19-01-1-0525). This Material is also based upon work supported by the National Science Foundation under Grant No. DMR-0205940.

## References

- [1] A. Inoue, Trans. Tech Publications, Mat. Sci. Found., 6, (1999).
- [2] W. L. Johnson, MRS bulletin, 24, 2342 (1993).
- [3] A. Inoue Acta Mater, 48, 279 (2000).
- [4] Klement, W., Willens, R.H., Duwez, P.: Nature (London) 187, 869 (1996).
- [5] H. Cohen and D. Turnbull, *ibid* 189 (1960).
- [6] K. Dini and R. Dunlap, J. Phys. F., 15, 273 (1985).
- [7] A. Inoue, W. Zhang, Mater Trans JIM, 43, 2924 (2002).
- [8] S. W. Lee, M. Y. Huh, E. Fleury and J. C. Lee, Acta Mater, 54, 349 (2006).
- [9] B. Lohwongwatana, J. Schroers, W. L. Johnson, Phys. Rev. Lett., 96, 075503 (2006).
- [10] T. Shaw, C. Way and R. Busch, MRS Proc. 806, 215 (2004).
- [11] C. Way, T. Shaw, P. Wadhwa and R. Busch, J. Alloys and Comp., 434, 88 (2007).
- [12] C. Way, P. Wadhwa and Ralf Busch, Acta Mater., 55(9), 2977 (2007).
- [13] A. Masuhr, R. Busch, and W.L. Johnson, Mater. Sci. Forum 269-272, 779 (1998).
- [14] A. Masuhr, T.A. Waniuk, R Busch, and W.L. Johnson, Phys Rev. Lett. 82, 2290 (1999).
- [15] C.A. Angell, Science, 267, 1924 (1995).
- [16] Miracle D. Nat Mater, 3, 697 (2004).

- [17] H. W. Sheng, W. K. Luo, F. M. Alamgir, J. M. Bai, E. Ma, *Nature*, 439, 419 (2004).
- [18] S. Aasland and P.F. McMillan, *Nature*, 369 (6482), 633 (1994).
- [19] C. A. Angell, *Annu. Phys. Chem.*, 55, 559 (2004).
- [20] I. Martin, T. Ohkubo, M. Ohnuma, B. Deconihout, K. Hono, *Acta Mater*, 52, 27 (2004).
- [21] Y. J. Kim, R. Busch, Rulison A. J. and W. L. Johnson, *Appl. Phys. Lett.*, 65(17), 2136 (1994).
- [22] A. Einstein, *Ann. Phys.* 34, 592 (1911).
- [23] D.R. Uhlmann, *J. Non-Cryst. Solids* 7, 337 (1972).
- [24] R. Busch, Y.J. Kim, and W.L. Johnson, *J. Appl. Phys.* 77, 4039 (1995).
- [25] G. Adam, J.H. Gibbs, *J. Chem. Phys.*, 43, 139 (1965).
- [26] S.V. Nemilov, *Glass Phys. and Chem.*, 21, 91 (1995).
- [27] H. J. Kriegl, E. Ratajski and M. Stadlbauer, *Rheol. Acta.*, 42, 355 (2003).
- [28] H. Janeschitz-Kriegl, *Monatshefte fur Chemie*, 138, 327 (2007).

## 5. MANUSCRIPT II

**Non Newtonian viscosity of the  $\text{Zr}_{41.2}\text{Ti}_{13.8}\text{Cu}_{12.5}\text{Ni}_{10}\text{Be}_{22.5}$ ,  
 $\text{Zr}_{57}\text{Cu}_{15.4}\text{Ni}_{12.6}\text{Al}_{10}\text{Nb}_5$  and  $\text{Pd}_{43}\text{Ni}_{10}\text{Cu}_{27}\text{P}_{20}$  bulk metallic glass  
forming liquids**

Prashant Wadhwa<sup>1,2,a</sup> and Ralf Busch<sup>1,2,b,\*</sup>

<sup>1</sup>Oregon State University, Department of Mechanical Engineering, Corvallis, OR-  
97331, USA

Tel.: 001-541-7377021; Fax: 001-541-7372600

<sup>2</sup> Saarland University, Department of Materials Science, Chair for Metallic  
Materials, Saarbrücken 66041-Germany

Tel.: +49-681-3023208; Fax: +49-681-3024385

<sup>a</sup>wadhwa@engr.orst.edu, <sup>b</sup>r.busch@mx.uni-saarland.de

\* Author to whom correspondence should be addressed; email: r.busch@mx.uni-  
saarland.de

To be submitted to: Scripta Materialia

## Abstract

The viscosity of the  $\text{Zr}_{41.2}\text{Ti}_{13.8}\text{Cu}_{12.5}\text{Ni}_{10}\text{Be}_{22.5}$ ,  $\text{Zr}_{57}\text{Cu}_{15.4}\text{Ni}_{12.6}\text{Al}_{10}\text{Nb}_5$  and  $\text{Pd}_{43}\text{Ni}_{10}\text{Cu}_{27}\text{P}_{20}$  has been measured above the liquidus temperature as a function of temperature and shear rate in a high temperature couette rheometer. All these glass formers show both much higher viscosities than monoatomic metallic liquids and non-Newtonian shear thinning behavior.  $\text{Zr}_{41.2}\text{Ti}_{13.8}\text{Cu}_{12.5}\text{Ni}_{10}\text{Be}_{22.5}$  exhibits a strong shear thinning behavior on shearing from  $0.1\text{s}^{-1}$  to  $300\text{s}^{-1}$  at the temperatures above the liquidus temperature. This non-Newtonian behavior gets weaker with increasing temperature and the material starts to behave like a Newtonian liquid at temperatures above 1225 K.  $\text{Zr}_{57}\text{Cu}_{15.4}\text{Ni}_{12.6}\text{Al}_{10}\text{Nb}_5$  shows a strong non-Newtonian behavior on shearing from  $0.1\text{ s}^{-1}$  to  $143\text{ s}^{-1}$  at the temperatures between 1130 K and 1330 K. This non-Newtonian behavior disappears at higher shear rates where the viscosity stays constant. The melt viscosity of the Pd alloy is lower than the Zr-based alloys. The non-Newtonian behavior of the alloys is characterized by fitting a power law to the viscosity data as a function of shear rate. Both Zr-based alloys show a stronger shear rate dependence of the viscosity than the Pd alloy which is characterized by a significant difference in the shear thinning exponent.

Keywords: bulk metallic glass, ordering, shear thinning, short range order, viscosity

Metallic glasses are amorphous materials with a unique combination of interesting mechanical properties, higher corrosion resistance in the domain of high-strength metals and processability like plastics [1-3]. Metallic glass formation from the liquid state was first reported by Duwez et. al. in 1960 by rapid quenching of  $\text{Au}_{80}\text{Si}_{20}$  melt with the cooling rate of about  $10^6\text{K/sec}$  [4] . Since then, many glass-forming alloys with smaller critical cooling rate have been discovered [5-8]. Several attempts have been made to understand the glass forming ability (GFA) of the alloys by both thermodynamic and kinetic principles [2, 9, 10]. Among many factors, viscosity has been understood as one of the most important factors influencing the GFA of the alloys [11]. Viscosity reflects the kinetic slowdown, when a liquid is supercooled below its melting point. If we assume that the diffusivity,  $D$  is inversely proportional to the viscosity ( $D \propto 1/\eta$ ), it is apparent that the crystallization kinetics is substantially retarded in a material possessing high viscosity. Although viscosity near the glass transition temperature has been reported for several alloys [12, 13], only limited data is available above the liquidus temperature.

Contrary to the monatomic and binary simple metallic liquids, which exhibit low viscosities of about  $10^{-3}\text{ Pa}\cdot\text{s}$  [14] at the melting point , bulk metallic glass forming liquids (BMGs, thickness  $> 1\text{ mm}$ ) are expected to possess much higher viscosities, for example the viscosity of  $\text{Zr}_{41.2}\text{Ti}_{13.8}\text{Cu}_{12.5}\text{Ni}_{10.0}\text{Be}_{22.5}$  (Vit1) is more

than 3 orders of magnitude higher than that of a simple liquid. The previous studies estimated small relaxation times and high atomic mobility above the liquidus temperature ( $T_{\text{liq}}$ ) and in the supercooled liquid region. It was therefore assumed that the atomic mobility and viscosity would be constant with respect to shear [15]. However, our most recent studies on the viscosity of Vit1 above the liquidus temperature showed a very high melt viscosity and surprisingly a non Newtonian behavior [16, 17, 18]. It was found that the non-Newtonian behavior decreases with increasing temperatures and at the temperatures above 1225 K, the material behaves like a Newtonian liquid. It was suggested that this high melt viscosity and non Newtonian behavior is due to the presence of pronounced order in the strong liquid of Vit1 which is preserved upon first heating above  $T_{\text{liq}}$ . It was also shown that the initial state of the sample (amorphous or crystalline) substantially effect the viscosity due to the presence of different order in the melt.

In this paper, we compare the viscosity of,  $\text{Zr}_{41.2}\text{Ti}_{13.8}\text{Cu}_{12.5}\text{Ni}_{10}\text{Be}_{22.5}$  (Vit1), with the viscosity of the two alloys,  $\text{Zr}_{57}\text{Cu}_{15.4}\text{Ni}_{12.6}\text{Al}_{10}\text{Nb}_5$  (Vit106) and  $\text{Pd}_{43}\text{Ni}_{10}\text{Cu}_{27}\text{P}_{20}$  over a large temperature range above their respective liquidus temperatures. It will be shown by using Couette Concentric Cylinder viscosity measurements that there exists a shear rate dependence of the viscosity in all these alloys that strongly affects the fragility of the alloys.

Pellets of  $Zr_{41.2}Ti_{13.8}Cu_{12.5}Ni_{10.0}Be_{22.5}$  (Vit1) were obtained from Liquid Metal Technologies and dehydrogenated by melting them under a high vacuum of  $10^{-3}$  Pa. The samples are quenched to attain an amorphous state. The dehydrogenation is necessary to prevent hydrogen from emerging from the molten sample during the subsequent viscosity measurement and adversely affecting the viscosity measurements. Amorphous master alloys of Vit106 with the nominal composition of  $Zr_{57}Cu_{15.4}Ni_{12.6}Al_{10}Nb_5$ , are prepared by mixing the elements of high purity ranging from 99.9 % to 99.995% in a Bühler MAM Arc melter. Amorphous pieces of  $Pd_{43}Ni_{10}Cu_{27}P_{20}$  are prepared by melting the elements in quartz tubes under boron oxide flux. The glass transition temperatures ( $T_g$ ) and liquidus temperature ( $T_{liq}$ ) of all the alloys are measured in differential scanning calorimeter (DSC) and differential thermal analyzer (DTA) and verified with the literature data [ 19, 20, 21].

The viscosity measurements are performed in a high-temperature couette rheometer, which consists of a concentric cylinder shear cell that is mounted vertically inside a high-vacuum induction furnace. The material is kept in the outer cylindrical cup where it is melted by inductive heating. The outer cylinder is attached to a torque sensor and the temperature is measured with a thermocouple mounted inside the cylinder wall. The inner cylinder is lowered into the outer cylinder and the gap between the outer and inner cylinder contains the melt. By rotating the inner cylinder the desired shear rate is imposed on the molten alloys. The resulting shear

field in the liquids generates a torque on the outer cylinder [16]. This torque signal,  $M$ , in  $N\cdot m$  through the molten test sample is recorded with a torque sensor. Details of the equipment and procedures are described elsewhere [16-18]. In the case of Vit1 and Vit106 the shear cells are manufactured from graphite whereas for  $Pd_{43}Ni_{10}Cu_{27}P_{20}$  the shear cells are made of molybdenum (Mo). Different materials are used for shear cells in order to minimize the reaction of melt with the shear cells. In the case of Zr based alloys (Vit1 and Vit106) it has been shown that a thin ZrC layer forms at the interface between container and melt which acts as an effective diffusion barrier [18, 22]. The compatibility of Mo as a crucible material for  $Pd_{43}Ni_{10}Cu_{27}P_{20}$  is tested by processing  $Pd_{43}Ni_{10}Cu_{27}P_{20}$  and block of Mo in quartz tube at 1173 K for 20 min. Subsequent chemical analysis using EDX reveal that Mo does not get dissolved in the alloy.

Due to the non Newtonian shear thinning behavior in the materials a non linear shear profile develops in the melt between the concentric walls of the cylinder. Material that is closest to the inner cylinder is more rapidly sheared in comparison to the material near the wall of the outer cup. Therefore a shear rate correction factor [23, 24] is applied. The appropriate procedure is explained elsewhere [18]. The actual shear rate deviates from the uncorrected shear rate between 0 and 60 % depending on the magnitude of the shear thinning effect.

For Vit1 it has been shown in previous studies that the initial state of the alloy, i.e. whether it is amorphous or crystalline, influences the viscosity when the alloy is melted [18]. Therefore in all the experiments we start with completely glassy samples which we melt in the viscometer and only compare data of alloys that have been amorphous before processing. The liquidus temperatures of Vit1, Vit106 and  $\text{Pd}_{43}\text{Ni}_{10}\text{Cu}_{27}\text{P}_{20}$  are measured as 1026K, 1115K and 815K respectively. For all the alloys, the viscosity measurements are obtained starting approximately 45-60 K above their respective liquidus temperature.

Each sample is sheared first in a clockwise and then a counter clockwise direction in order to obtain an average torque signal. The (uncorrected) shear rate is then increased from 5 to 300  $\text{s}^{-1}$  while obtaining an average torque signal at each shear rate. At this point the shear cell temperature is increased by 25 K and the sample is held isothermally and again sheared using shear rates from 5 to 300  $\text{s}^{-1}$ . This method is continued until 1275 K for Vit1, 1330K for Vit106 and 1025 K for  $\text{Pd}_{43}\text{Ni}_{10}\text{Cu}_{27}\text{P}_{20}$  are reached. Another set of experimental run is performed only on Vit1 in which the material is cooled back to 1075 K and the same shear profile at same temperatures from 1075 K to 1275 K is applied. The shear rate correction factor is applied to all the viscosity data obtained at each isothermal temperature for all the three alloys.

Figure 1 shows the viscosity data (open symbols) obtained from the experiment on initially amorphous and remelted Vit1 sheared from 5 to 300 s<sup>-1</sup> at the temperatures from 1075 K to 1250 K. The maximum measured viscosity of Vit1 which is  $35.1 \pm 5.4$  Pa·s at 1075 K at a corrected shear rate of  $6 \text{ s}^{-1}$  decreases by an order of magnitude to  $3.6 \pm 0.5$  Pa·s by shearing the melt at  $350 \text{ s}^{-1}$ . By further increasing the temperature from 1075 to 1225 K the viscosity decreases an additional two orders of magnitude to  $0.05 \pm 0.01$  Pa·s. Above 1225 K no measurable decrease in viscosity with increasing temperature is observed indicating a Newtonian behavior and a transformation into a fragile liquid [18]. Also shown are the viscosity data (solid symbols) obtained by cooling the sample back to 1075 K and repeating the experimental routine up to 1250 K. The material stays Newtonian and fragile. It only transforms back into the strong liquid, when it gets deeply undercooled [18].

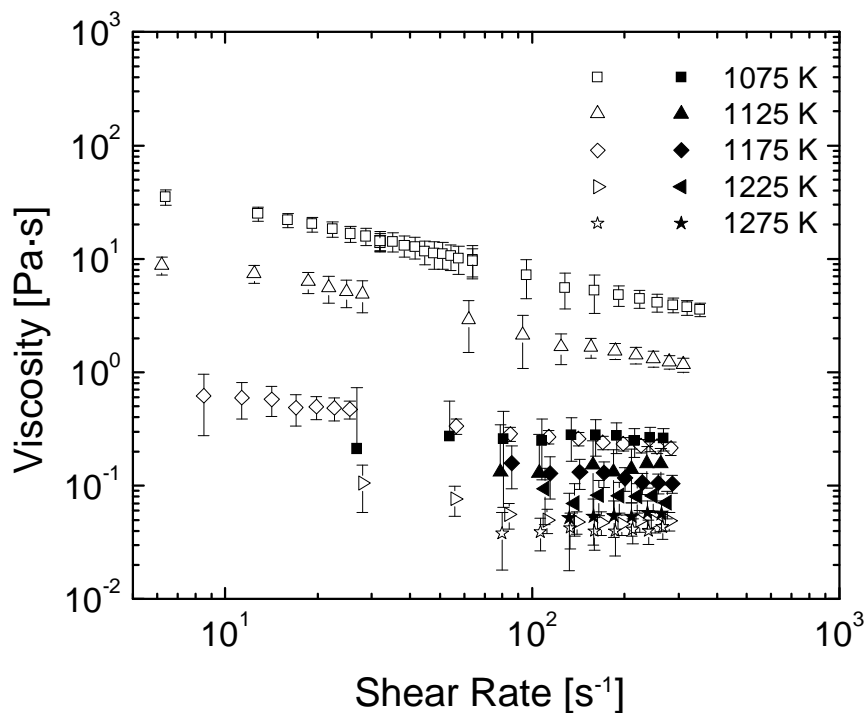


**Figure 1:** Viscosity as a function of shear rate at isothermal temperatures from 1075 K to 1275 K in 25 K increments for initially amorphous and remelted Vit1 (hollow symbols). The high viscosity and shear rate dependence above  $T_{\text{liq}}$  for this alloy decreases with increasing temperature. Solid symbols show the viscosity data obtained by cooling the sample to 1075 and reheating to 1275 by 25 K increments. The difference between the first and second temperature scans show a strong temperature dependence of the viscosity.

The results of the viscosity measurements obtained by shearing the melt of initially amorphous Vit106 between 1155 K and 1330 K are shown in Fig. 2. The maximum measured viscosity of Vit106 is  $0.5 \pm 0.12$  Pa·s at 1155 K at a corrected shear rate of  $22.05 \text{ s}^{-1}$ . At the same temperature, this viscosity decreases to  $0.15 \pm$

0.06 Pa·s at a shear rate of  $143 \text{ s}^{-1}$  and at further higher rates reaches a steady state value. On further increasing the shear rate at 1155 K, the viscosity does not decrease significantly and at the shear rate of  $205.2 \text{ s}^{-1}$  the viscosity is measured as  $0.149 \pm 0.034 \text{ Pa}\cdot\text{s}$ . This indicates that at a fixed temperature, the melt of Vit106 shows a shear thinning behavior up to a certain shear rate and upon further increasing the shear rate there is no measurable change in viscosity. At this point the viscosity becomes constant and Newtonian behavior is observed. By further increasing the temperature from 1155 K to 1330 K, the same behavior is observed up to 1280 K. In this whole temperature range a transition from non Newtonian behavior at low shear rates to Newtonian behavior at high shear rates is observed. Above 1280 K, only the viscosities at high shear rates can be measured due to the sensitivity of our torque sensor. At 1330 K, a Newtonian viscosity of approximately  $0.029 \pm 0.011 \text{ Pa}\cdot\text{s}$  is observed.

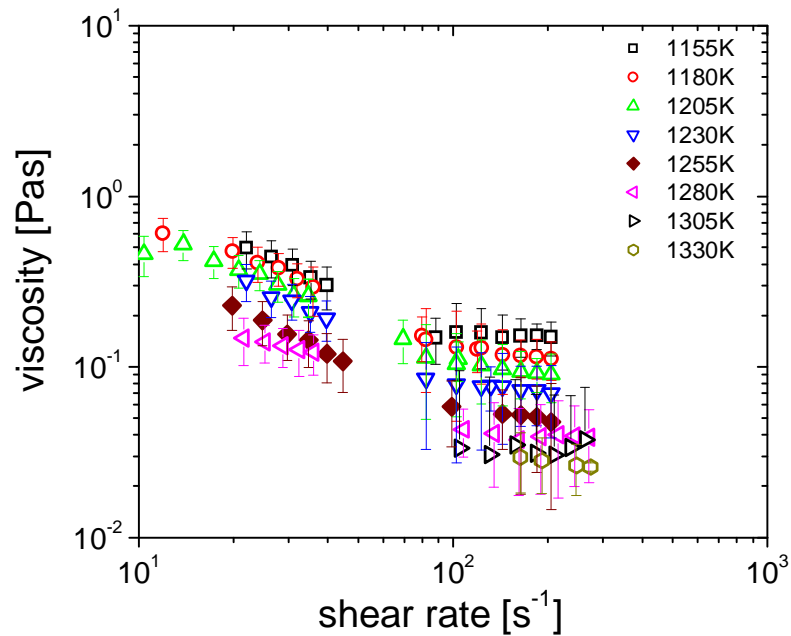


**Figure 2:** Isothermal viscosity vs. shear rate upon heating from 1155 K to 1335 K in 25 K increments for initially amorphous and remelted Vit106. It shows strong shear rate dependence above  $T_{\text{liq}}$  for this alloy. At the shear rate of above  $143 \text{ s}^{-1}$ , the viscosity approximately reaches a constant value and non Newtonian behavior disappears. The non Newtonian behavior disappears completely at the temperatures equal to and above 1305 K.

For the  $\text{Pd}_{43}\text{Ni}_{10}\text{Cu}_{27}\text{P}_{20}$  alloy the viscosity has been measured between 875 K and 1000 K. The results are shown in Fig. 3 as a function of shear rate. The maximum measured viscosity of  $\text{Pd}_{43}\text{Ni}_{10}\text{Cu}_{27}\text{P}_{20}$  which is  $0.17 \pm 0.03 \text{ Pa}\cdot\text{s}$  at 875 K at a corrected shear rate of  $16 \text{ s}^{-1}$  decreases only by 33 % to  $0.116 \pm 0.02 \text{ Pa}\cdot\text{s}$  on shearing the melt at  $136 \text{ s}^{-1}$ . On further increasing the shear rate the viscosity does not change significantly and a Newtonian behavior is observed. This behavior in

$\text{Pd}_{43}\text{Ni}_{10}\text{Cu}_{27}\text{P}_{20}$  is similar to Vit106 but the rate of decrease of viscosity with respect to shear rate is much faster in Vit106 than in the Pd alloy. At the temperatures above 975 K, no measurable decrease in viscosity with increasing shear rate and temperature is observed indicating a Newtonian behavior.

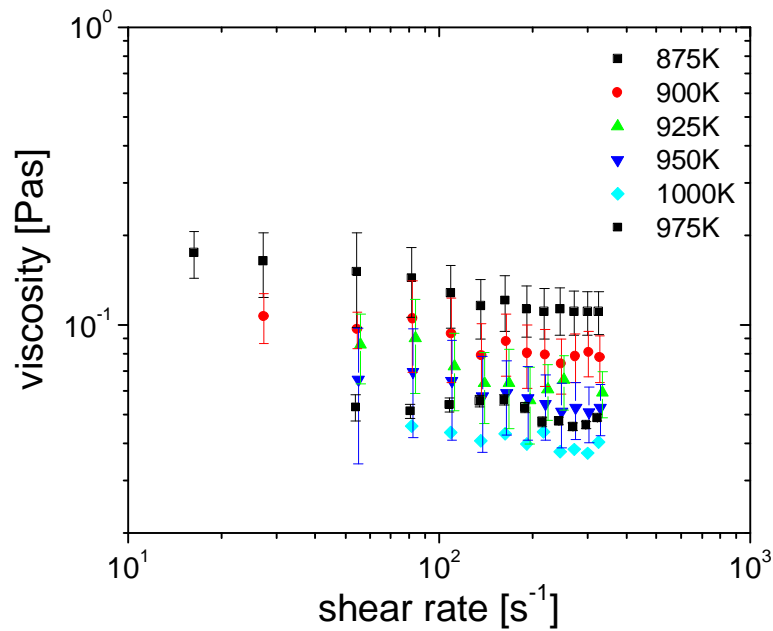


**Figure 3:** Isothermal viscosity vs. shear rate upon heating from 875 K to 1100 K in 25 K increments for initially amorphous and remelted  $\text{Pd}_{43}\text{Ni}_{10}\text{Cu}_{27}\text{P}_{20}$ . This alloy shows relatively smaller shear rate dependence above  $T_{\text{liq}}$  in comparison to Vit1 and Vit106. Similar behavior like Vit106 in which the viscosity reaches a constant value and non Newtonian behavior disappears can be seen.

The shear rate dependence of the viscosity can be described using the power law [24]

$$\eta = A \cdot \dot{\gamma}^{(n-1)} \quad (1),$$

where  $\eta$  and  $\dot{\gamma}$  represent viscosity and shear rate, respectively. The shear thinning exponent,  $n$ , is determined by fitting equation 1 to the viscosity as a function of shear rate data depicted in Fig. 1, Fig. 2 and Fig. 3 for the three alloys. If this value is less than one, then the liquid exhibits a decrease in viscosity with increasing shear rate or non-Newtonian shear thinning behavior. When  $n = 1$ , the viscosity has no shear rate dependence and exhibits Newtonian behavior. Since the viscosity of Vit106 and Pd<sub>43</sub>Ni<sub>10</sub>Cu<sub>27</sub>P<sub>20</sub> show a Newtonian behavior at higher shear rates we have applied the power law up to the temperature, at which non Newtonian behavior is observed.

The results of this analysis are shown in figures 4(a), 4(b) and 4(c). Figure 4(a) shows that upon heating Vit1 above  $T_{liq}$ , the shear thinning exponent is 0.4 at 1075 K and increases to 1.0 above 1225 K (■), revealing increasing Newtonian behavior with increasing temperature. This indicates a thermal transition from an ordered to less ordered state. Figure 4(b) shows the shear thinning exponent of Vit106 as a function of temperature. A small shear thinning exponent of 0.2 at 1155 K which increases to 1.0 above 1305 K (□) can be seen. This indicates that the viscosity of Vit106 depicts an even stronger shear thinning behavior than Vit1 within a temperature range of about 200K above the  $T_{liq}$  for both alloys, respectively. A

similar trend as Vit106 is observed in  $\text{Pd}_{43}\text{Ni}_{10}\text{Cu}_{27}\text{P}_{20}$  as shown in Fig. 4(c).

However  $\text{Pd}_{43}\text{Ni}_{10}\text{Cu}_{27}\text{P}_{20}$  show much larger shear thinning exponent of 0.83 indicating a weak shear thinning behavior. Moreover this behavior is prevalent in much smaller temperature range from 875 K to 950 K and above 975 K the material behaves like a Newtonian liquid and the viscosity is not shear rate dependent.

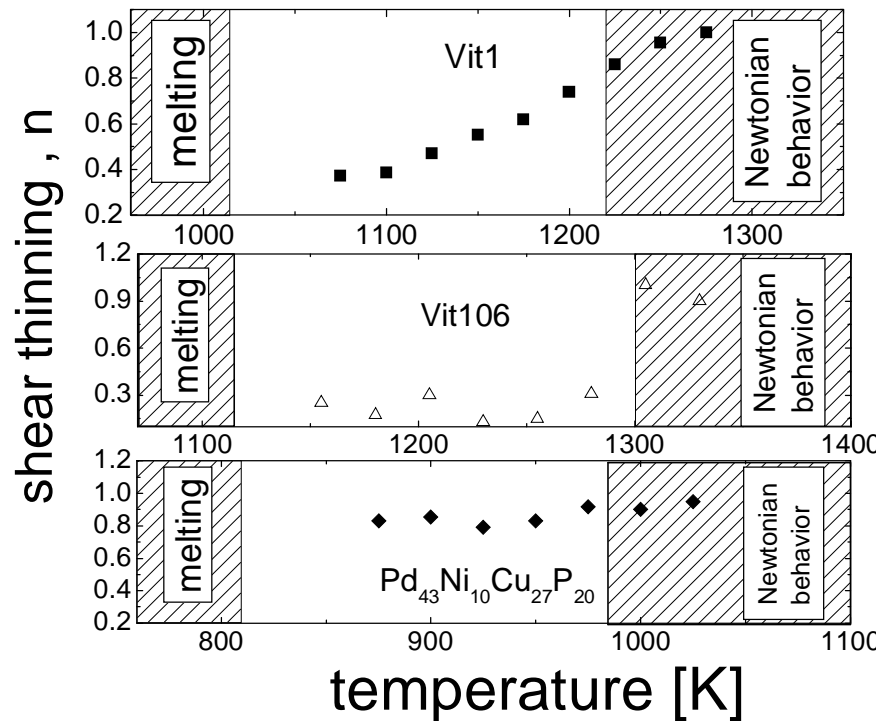


**Figure 4a** (top): Shear thinning exponent  $n$  vs. temperature of initially amorphous and remelted Vit1 obtained by fitting the power law to the data shown in Fig. 1. After melting the alloy exhibits a pronounced shear thinning dependence of the viscosity which vanishes above 1225 K. **Figure 4b** (middle): Shear thinning exponent,  $n$ , vs. temperature of initially amorphous and remelted Vit106 obtained by fitting the power law to the data shown in Fig. 2. At each isotherm, the power law was applied to the range to which the shear rate dependence of viscosity is seen. After melting the alloy exhibits much stronger shear thinning behavior which vanishes above 1305 K. **Figure 4c** (bottom): A much larger shear thinning exponent, vs. temperature of initially amorphous and remelted Pd<sub>43</sub>Ni<sub>10</sub>Cu<sub>27</sub>P<sub>20</sub>. The larger value to  $n$  indicates much smaller shear rate dependence. At the temperature above 975 K the material becomes completely Newtonian.

Figure 5 shows the shear rate dependence of the viscosity for the three alloys at a temperature that is about 50 K higher than the liquidus temperature of the

respective alloy. Plotted are the fits to the experimental data extracted from Figs1-3. All the alloys show shear thinning but to a different extent. Vit1 in its strong modification has the highest viscosity with drastic change in viscosity with increasing shear rates. This trend is followed by Vit106 and then  $\text{Pd}_{43}\text{Ni}_{10}\text{Cu}_{27}\text{P}_{20}$ , which shows the smallest change in viscosity with increasing shear rates. Another interesting point to note is that at each temperature, the non-Newtonian behavior of Vit106 and  $\text{Pd}_{43}\text{Ni}_{10}\text{Cu}_{27}\text{P}_{20}$  disappears at higher shear rates where the viscosity stays constant. It was earlier shown in Fig. 2 that a transition from non Newtonian to Newtonian behavior also occurs at higher shear rates in Vit106. However both transitions are of different kinds, (I) the transition from non Newtonian to Newtonian liquid behavior due to shear rate indicates a small structural changes because a similar behavior is again seen at next higher temperature until 1285 K whereas (II) a transition to Newtonian liquid due to temperature indicate larger structural changes occurring in the melt. This is because as the liquid becomes Newtonian, it stays Newtonian at higher temperatures and cooling does not restores the non Newtonian behavior. This temperature for Vit106 is 1305 K.

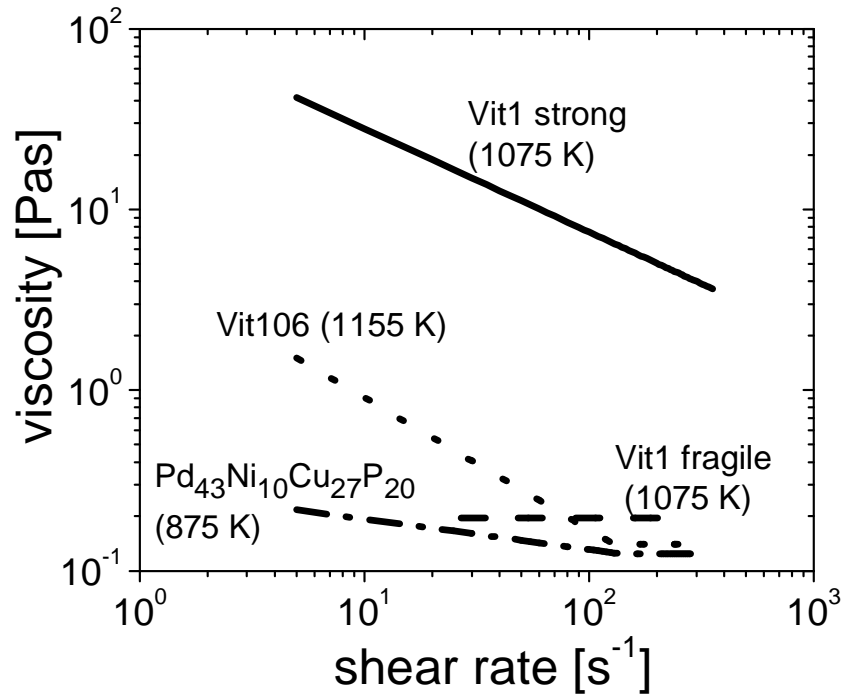


**Figure 5:** Isothermal viscosity vs. shear rate of all the three alloys upon heating above the  $T_{liq}$ . Vit1 strong shows the higher viscosity than Vit106 and  $Pd_{43}Ni_{10}Cu_{27}P_{20}$

Similar viscosity behaviors with respect to temperature and shear rate have been observed in polymer based systems and are primarily due to the interaction of highly ordered structures. Recently, the structural considerations in the amorphous solid state of metallic systems have gained much attention. Two such studies have been reported by D. Miracle [25] and E. Ma [26] and they have developed models which describe the order present in multicomponent amorphous metals. Both models

suggest that they are composed of icosahedral short range ordered (SRO) clusters that form the building blocks for medium range order (MRO) in multicomponent systems. These icosahedral short range order clusters consist of a central atom of one species surrounded by several atoms of the other species. The MRO is then formed by placing this icosahedral SRO on either a FCC lattice [25] or icosahedral lattice [26]. It is clear from our results that a pronounced order must exist in the investigated BMGs which is responsible for high melt viscosities and shear thinning behavior. The smaller viscosity of Vit106 and  $\text{Pd}_{43}\text{Ni}_{10}\text{Cu}_{27}\text{P}_{20}$  and a smaller decrease indicate less pronounced order in the melt as compared to Vit1. Moreover the shear rate dependence of viscosity disappears at the shear rates higher than  $143 \text{ s}^{-1}$  and  $136 \text{ s}^{-1}$  respectively. Since Vit1 is much stronger liquid than the other two BMGs we can expect a similar transition in Vit1 but at much larger shear rates as indicated by arrows in Fig. 1. It is also interesting to note from Fig.1 to Fig.3 that the amount of decrease in viscosity with increasing shear rates is different for different alloys. In case of Vit1 the viscosity decreases by an order of magnitude at a smaller rate and a drop of only 70 and 30 % is observed in Vit106 and  $\text{Pd}_{43}\text{Ni}_{10}\text{Cu}_{27}\text{P}_{20}$  respectively. This indicates that Vit1 has the highest order present above  $T_{\text{liq}}$  followed by Vit106 and  $\text{Pd}_{43}\text{Ni}_{10}\text{Cu}_{27}\text{P}_{20}$  although in all the three alloys we see that the non Newtonian behavior completely vanishes at higher temperatures. This Newtonian temperature ( $T_{\text{newtonian}}$ ) is different for three alloys depending on their  $T_{\text{liq}}$  and GFA. Therefore it is likely that this MRO present in the melt can be reduced by

shearing and more effectively destroyed to SRO by increasing the temperature.

This transition from MRO to SRO leads to a Newtonian liquid with smaller viscosity (fragile).

An empirical concept to describe the sensitivity of the viscosity to temperature changes for different materials is developed by Angell [27]. Angell plot (or fragility plot) shows the viscosity change as a function of inverse temperature for different materials. Figure 6 shows the fragility plot for the alloys investigated in this work. The high temperature viscosity data obtained in this study above the  $T_{liq}$  of initially amorphous and remelted Vit106 [□] and  $Pd_{43}Ni_{10}Cu_{27}P_{20}$  [○] are plotted as a function of inverse temperature. The high temperature viscosity data for Vit106 [□] and  $Pd_{43}Ni_{10}Cu_{27}P_{20}$  [○] as shown in the plot were taken at 22 s<sup>-1</sup> and 53 s<sup>-1</sup> respectively. However the data above 1280 K in case of Vit106 and 1000 K in case of  $Pd_{43}Ni_{10}Cu_{27}P_{20}$  were taken at higher shear rates ( $> 136$  s<sup>-1</sup> and  $143$  s<sup>-1</sup>) due to the sensitivity associated with our torque sensor. This substitution is viable because it has been seen in this study that there is no shear rate dependence of the viscosity at those elevated temperatures. Also shown are the viscosities of Vit106 and  $Pd_{43}Ni_{10}Cu_{27}P_{20}$  close to the glass transition temperature ( $T_g$ ) measured by using three point beam bending method. Figure 6 includes the viscosity of  $SiO_2$  which is a strong glass former, showing Arrhenius temperature dependence of

viscosity. The fragility of materials is determined by fitting the Vogel-Fulcher-Tammann (VFT) equation [28] given by

$$\eta = \eta_0 \cdot \exp [D^* T_0 / (T - T_0)], \quad (2),$$

where  $\eta_0 = 4 \times 10^{-5}$  Pa·s [29] is a constant pre-exponential factor,  $D^*$  is the fragility parameter, and  $T_0$  is the temperature, at which the barrier to viscous flow would go to infinity. The low temperature viscosity point used for fitting is fixed at the glass transition temperature at  $10^{12}$  Pa·s. The fragility of initially amorphous and remelted Vit1 (strong) and fragile Vit1 has been previously published by the authors and is also shown in the figure. Therefore in this work we determined the fragility parameter of Vit106 and  $\text{Pd}_{43}\text{Ni}_{10}\text{Cu}_{27}\text{P}_{20}$  and compared it with that of Vit1. The scope of this paper is limited to initially amorphous and remelted samples only. The  $D^*$  and  $T_0$  obtained for these alloys are tabulated in table I.

**Table I:** The fragilities of three different bulk metallic glass formers are obtained by fitting the viscosity data as a function of inverse temperature using VFT equation [2].

BMG	$T_g$	$T_l$	$\eta_0$	$D^*$	$T_0$
Initially amorphous Vit1	620	1026	4.00E-05	26.5	360
Initially amorphous Vit106	682	1115	4.00E-05	10.4	538
Initially amorphous Pd <sub>43</sub> Ni <sub>10</sub> Cu <sub>27</sub> P <sub>20</sub>	584	815	4.00E-05	7.7	484

We can see in the table that the  $D^*$  is maximum for Vit1 followed by Vit106 with  $D^*$  value of 10.4 and Pd<sub>43</sub>Ni<sub>10</sub>Cu<sub>27</sub>P<sub>20</sub> with  $D^*$  of 7.7. Clearly these values indicate that a stronger glass former possess higher  $D^*$  values and the high viscosity. At the temperature 50 K above the  $T_{liq}$  Vit1 has the viscosity of about 2 orders of magnitude higher than Vit106 whereas the viscosity of Vit106 is about half order of magnitude higher than Pd<sub>43</sub>Ni<sub>10</sub>Cu<sub>27</sub>P<sub>20</sub>.

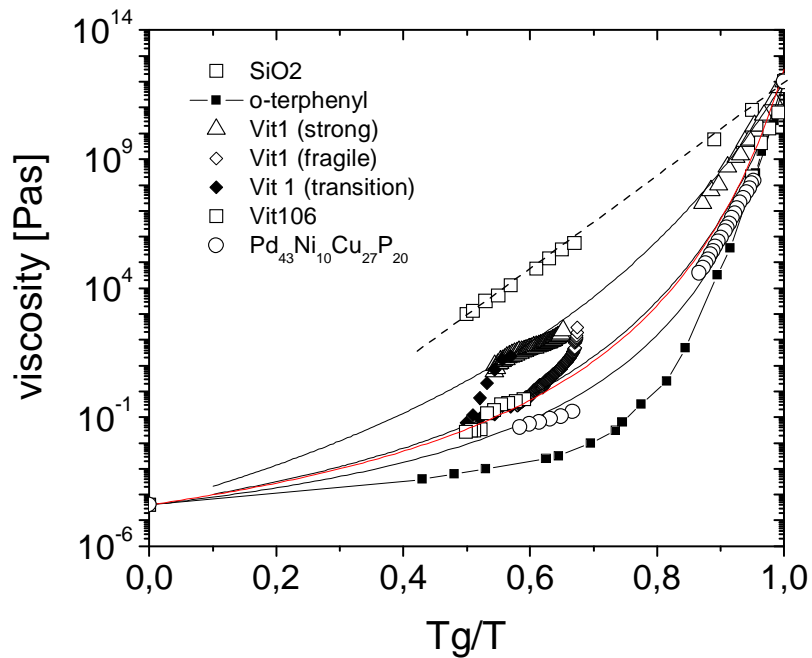


Figure 6: Fragility plot of viscosity of Vit106 ( $\square$ ) and  $\text{Pd}_{43}\text{Ni}_{10}\text{Cu}_{27}\text{P}_{20}$  ( $\circ$ ). The viscosities of  $\text{SiO}_2$  and o-terphenyl. ( $\Delta$ ) shows a strong and a weak behavior. The data was fitted by VFT relations as indicated by the solid lines and the results are tabulated in table I.

In summary, we showed the viscosity data of  $\text{Zr}_{41.2}\text{Ti}_{13.8}\text{Cu}_{12.5}\text{Ni}_{10}\text{Be}_{22.5}$  (Vit1),  $\text{Zr}_{57}\text{Cu}_{15.4}\text{Ni}_{12.6}\text{Al}_{10}\text{Nb}_5$  (Vit106) and  $\text{Pd}_{43}\text{Ni}_{10}\text{Cu}_{27}\text{P}_{20}$  BMG forming liquids above the liquidus temperature as a function of temperature and shear rate. All these glass formers show higher viscosities than monoatomic metallic liquids and the non-Newtonian shear thinning behavior. Vit1 exhibits a largest drop in viscosity on

shearing from  $0.1\text{s}^{-1}$  to  $250\text{s}^{-1}$  at the temperatures above  $T_{\text{liq}}$ . Vit106 shows lower viscosities than Vit1, however, a strong non-Newtonian behavior on shearing from  $0.1\text{ s}^{-1}$  to  $143\text{ s}^{-1}$  at the temperatures between 1130 K and 1330 K is seen. Surprisingly, this non-Newtonian behavior disappears at higher shear rates where the viscosity stays constant. We believe that if we apply high enough shear rates to the melt of Vit1 at each isotherm, a constant viscosity could be achieved. The melt viscosity of the  $\text{Pd}_{43}\text{Ni}_{10}\text{Cu}_{27}\text{P}_{20}$  shows a lower viscosity and much smaller shear thinning behavior than the Zr-based alloys. In all the three alloys, this non-Newtonian behavior gets weaker with increasing temperature and the material starts to behave like a Newtonian liquid. This behavior is attributed to the presence of MRO and SRO in the melt of these alloys. The MRO present in the melt can be reduced by shearing and more effectively destroyed to SRO by increasing the temperature which leads to a Newtonian liquid with smaller viscosity.

This work was supported by DARPA (Grant No. DAAD-19-01-1-0525). Some of the work reported in this work was also supported by the National Science Foundation under Grant No. DMR-0205940.

## References

- [1] A. Inoue, Trans. Tech Publications, Mat. Sci. Found., 6, (1999).
- [2] W. L. Johnson, MRS bulletin, 24, 2342 (1993).
- [3] A. Inoue Acta Mater, 48, 279 (2000).
- [4] W. Clement, R. H. Willens and P. Duwez, Nature (London) 187, 869 (1960).
- [5] A. Inoue, T. Zhang and T. Masumoto, Mater Trans. JIM, 31, 425 (1991).
- [6] A. Inoue, A. Kato, T. Zhang, S. G. Kim and T. Masumoto Mater Trans. JIM 32, 609 (1991).
- [7] A. Peker, W. L. Johnson, Appl. Phys. Lett. 63, 2342 (1993).
- [8] D. Xu, B. Lohwongwatana, G. Duan, W. L. Johnson and C. Garland, Acta Mater. 52, 2620 (2004).
- [9] R. Busch, Y. J. Kim and W. L. Johnson, J. Appl. Phys. 77 (8) 4039 (1995)
- [10] G. Wilde, G. P. Gorler, R. Willnecker and H. J. Fecht, 87, 1141 (2000)
- [11] Turnbull, Contemp. Phys. 10, 473 (1969).
- [12] H. Kato, Y. Kawamura, A. Inoue, and H. S. Chen, Appl. Phys. Lett. 73, 3665 (1998).
- [13] T. G. Nieh, C. A. Schuh, J. Wadsworth, and Y. Li, Intermetallics 10, 1177 (2002).
- [14] T. Iida, R.I.L. Guthrie, The Physical Properties of Liquid Metals, Clarendon Press, Oxford (1998).
- [15] A. Masuhr, T.A. Waniuk, R. Busch, and W.L. Phys. Rev. Lett., 82 (1999).
- [16] T. Shaw, C. Way and R. Busch, MRS Proc. 806, 215 (2004).

- [17] C. Way, T. Shaw, P. Wadhwa and R. Busch, *J. Alloys and Comp.*, 434, 88 (2007).
- [18] C. Way, P. Wadhwa and Ralf Busch, *Acta Mater.*, 55(9), 2977 (2007)
- [19] A. Masuhr, R. Busch, and W.L. Johnson, *Mat. Sci. For.*, 269-272, 779 (1998).
- [20] S. Mukherjee, J. Schroers, W. L Johnson and W. K. Rhim, *Phys. Rev. Let.* 94, 245501 (2005).
- [21] M. Kuno, L. A. Shadowspeaker, J. Schroers, and R. Busch *MRS Proc.* 806, 215 (2003).
- [22] J. Schroers, K. Samwer, F. Szuecs, W. L. Johnson, *J. Mater. Res.* 15, 1617 (2000).
- [23] I.M. Krieger, S.H. Maron, *Journal of Applied Physics*, 25, 72 (1954).
- [24] H.A. Barnes, J.K. Hutton, and K. Walters, *An Introduction to Rheology*, Elsevier Science, Amsterdam, (1989).
- [25] D. Miracle, *Nature Matl.*, 3 (10), 697 (2004).
- [26] H.W. Sheng, W.K. Luo, F.M. Alamgir, J.M. Bai, and E. Ma, *Nature*, 439, 419 (2006).
- [27] C. A. Angell, *J. Non-Cryst. Solids* 13, 131 (1991).
- [28] C.A. Angell, *Science*, 267, 1924 (1995).
- [29] S.V. Nemilov, *Glass Physics and Chemistry*, 21, 91 (1995).

## 6. SUMMARY AND CONCLUSIONS

Following is the summary of the work presented in this dissertation

(I) The influence of shear rate and temperature on the viscosity and fragility of the  $Zr_{41.2}Ti_{13.8}Cu_{12.5}Ni_{10.0}Be_{22.5}$  metallic glass forming liquid is shown in the first part. The results show a complex rheological behavior of Vit1. The viscosity of Vit1 is very high with strong shear thinning behavior upon first heating from the amorphous state. The shear thinning behavior decreases with increasing temperature and this kinetically strong liquid transforms to a more fragile liquid with no shear rate dependence of viscosity. The Newtonian temperature ( $T_{Newtonian}$ ) for Vit1 is measured as 1225 K. Upon cooling this liquid the strong liquid behavior is only re-established when the melt is deeply undercooled below the liquidus temperature. This gives rise to the “hysteresis effect” in the viscosity of Vit1 as a function of temperature. The difference in viscosity and the shear thinning behavior is also seen depending on the initial state of the material (amorphous or crystalline). The shear thinning and strong to fragile transition is attributed to the destruction of medium range order in the liquid state whereas the reformation of order in the supercooled region is much more complex.

The recent work by Hono and coworkers [1, 2] shows that as prepared glassy Vit1 is chemically homogeneous and no phase separation occurs prior to crystallization indicating that fragile-strong transition can not be due to phase separation. It is therefore most likely that the observed fragile-strong transition is a polyamorphism in which the fragile liquid polymorphically transforms into a strong liquid. Polyamorphism has been observed in  $\text{Al}_2\text{O}_3 - \text{Y}_2\text{O}_3$  [3] and other network forming systems such as Silica, Si and even water [4]. In glass forming alloys the possibility of phase separation into two strong liquids or the precipitation of the strong liquid from the fragile liquid has to be added to the general picture. This is done in the following.

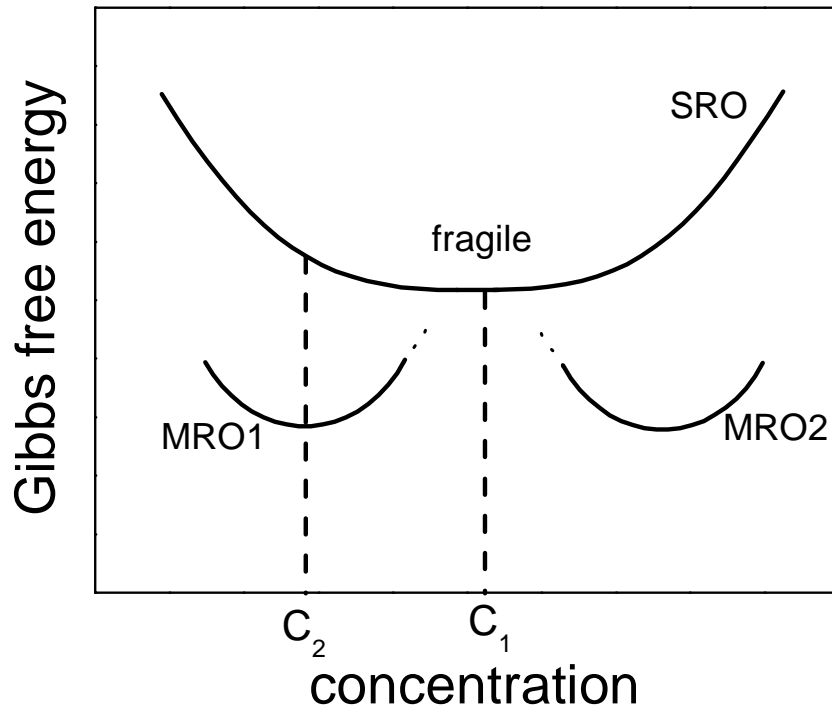


**Figure 1:** Schematic quasibinary Gibbs free energy diagram for a fragile strong transition below the critical temperature. At concentration  $C_1$  polyamorphism occurs, whereas at  $C_2$  the fragile liquid decomposes into two strong liquids with different medium range orders.

Figure 1 depicts schematically quasibinary Gibbs free energy curves for a fragile-strong transition below the critical temperature of 900 K. This is one scenario, in which the fragile liquid has a higher Gibbs free energy and entropy than the strong states. The fragile liquid may exhibit short range order (SRO) but no medium range order. It is further assumed, that two medium range ordered states, MRO1 and MRO2, exist at two different compositions. This creates a miscibility gap between the two MRO states. If the high temperature fragile liquid has a composition within the miscibility gap ( $C_1$ ), the fragile liquid will decompose into

the two strong MRO liquids. There will, in fact, exist an invariant eutectic-like point, in which the fragile liquid is in equilibrium with both strong liquids. Figure 2a shows a binary cut through the metastable fragile strong phase diagram, which would result from the Gibbs free energy curves drawn in Fig. 1.

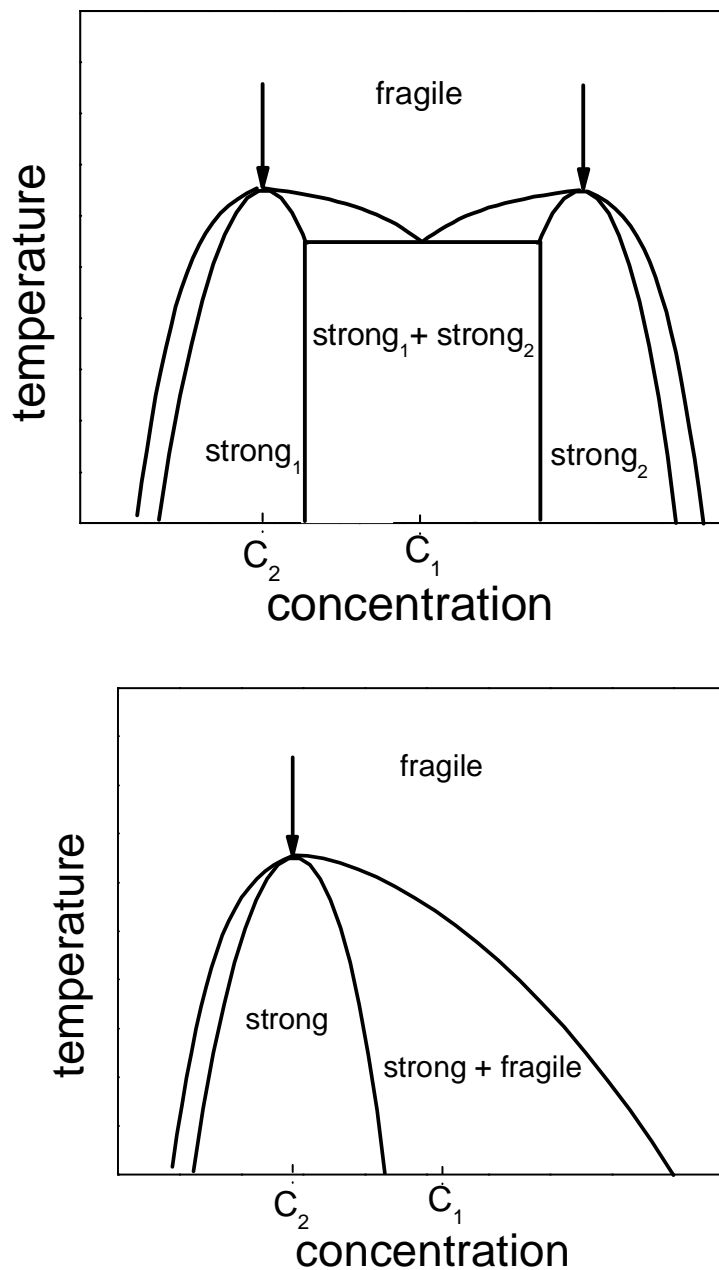


**Figure 2:** a) Schematic binary cut through the metastable fragile-strong liquid phase diagram that would result from the Gibbs free energy curves drawn in Fig. 1 with two medium range ordered states. b) Schematic binary cut through metastable fragile-strong phase diagram with only one strong liquid. There is a large region in which the fragile liquid decomposes into a strong and a fragile liquid. The arrows in both figures indicate where polyamorphism is possible.

If there is no phase separation present, as we assume in Vit1, our concentration is consistent with the concentration  $C_2$  in Fig. 1 or Fig. 2. The fragile liquid transforms polymorphically into the strong liquid. This is strictly only possible at the two congruent points marked by arrows in Fig 2a. If there is only one medium range ordered strong liquid e.g. only MRO1 in Fig. 1 the phase diagram would look like Fig 2b. There is a large composition range, in which the strong liquid precipitates out of the fragile liquid e.g. at the composition  $C_1$ . Only at the composition  $C_2$  is a polyamorphism possible.

(II) In the second part, the ordering and shear rate induced crystallization of undercooled  $Zr_{41.2}Ti_{13.8}Cu_{12.5}Ni_{10.0}Be_{22.5}$  metallic-glass-forming melts is investigated. The study quantitatively shows the shift of the TTT diagram of Vit1 to shorter crystallization times with increasing shear rates. The classical nucleation and growth theory is applied by incorporating the change in various factors such as viscosity, driving force for crystallization and entropy change as a function of shear rate. It is found that the change in crystallization kinetics can not be explained quantitatively by the classical nucleation and growth theory. The order present in the melt immensely influences the crystallization and the material with higher order crystallizes sooner than the material with smaller order. The ordered clusters are formed faster at higher shear rates and hence the material crystallizes sooner at higher shear rates making the TTT diagram shift to the left.

(III) In the third part, the viscosities of two bulk metallic glass forming liquids  $Zr_{57}Cu_{15.4}Ni_{12.6}Al_{10}Nb_5$  (Vit106) and  $Pd_{43}Ni_{10}Cu_{27}P_{20}$  are measured and compared with the viscosity of Vit1. The main goal of this study was to investigate whether high viscosity and shear thinning behavior is just associated with Vit1 or the other BMG forming liquids also show such behavior. It is shown that all these glass formers show both higher viscosities than monoatomic metallic liquids and non-Newtonian shear thinning behavior.

Vit1 exhibits the highest viscosity with the largest drop in viscosity on shearing from  $0.1 \text{ s}^{-1}$  to  $250 \text{ s}^{-1}$  at the temperatures above  $T_{liq}$ . Vit106 shows lower viscosities than Vit1, however, a stronger non-Newtonian behavior on shearing from  $0.1 \text{ s}^{-1}$  to  $143 \text{ s}^{-1}$  at the temperatures between 1130 K and 1305 K is seen. Surprisingly, this non-Newtonian behavior disappears at higher shear rates where the viscosity stays constant. The viscosity data of Vit106 and  $Pd_{43}Ni_{10}Cu_{27}P_{20}$  apparently indicate that if high enough shear rates are applied to the melt of Vit1 a similar steady state viscosity state could be found at the temperatures between 1075 K and 1225 K. The melt viscosity of the  $Pd_{43}Ni_{10}Cu_{27}P_{20}$  shows a lower viscosity and much smaller shear thinning behavior than the Zr-based alloys. In all the three alloys, this non-Newtonian behavior gets weaker with increasing temperature and the material starts to behave like a Newtonian liquid. This Newtonian temperature is found to be 1225K for Vit1, 1330 K for Vit106 and 1000 K for  $Pd_{43}Ni_{10}Cu_{27}P_{20}$ . This behavior is

attributed to the presence of MRO and SRO in the melt of these alloys. The MRO present in the melt can be reduced by shearing and more effectively destroyed to SRO by increasing the temperature which leads to a Newtonian liquid with smaller viscosity.

## References

- [1] W.H. Wang, Q. Wei, S. Friedrich, et al., *Appl. Phys. Lett.*, 71 (8), 1053 (1997).
- [2] I. Martin, T. Ohkubo, M. Ohnuma, B. Deconihout, and K. Hono, *Acta Mater.*, 52, 4427 (2004).
- [3] S. Aasland and P.F. McMillan, *Nature*, 369 (6482), 633 (1994).
- [4] J.L. Yarger, C.A. Angell, S.S. Borick, and G.H. Wolf, *Supercooled Liquids ACS Symp.*, Series 676, 214 (1997).

## 7. REFERENCES

### References (Chapters 1-3)

- [1] H. A. Bruck, T. Christman, A. J. Rosakis and W.L. Johnson, *Scripta Mater.* 30, 429 (1994).
- [2] W. H. Petera, R. A. Buchanan, C. T. Liub, P. K. Liawa, M. L. Morrison, J. A. Hortonb, C. A. Carmichael, Jr. and J. L. Wright, *Intermetallics*, 10 (11-12), 1157 (2002).
- [3] A. Inoue, *Acta Mater*, 48, 279 (2000).
- [4] W. Clement, R. H. Willens and P. Duwez, *Nature (London)* 187, 869 (1960).
- [5] A. Inoue, T. Zhang and T. Masumoto, *Mater Trans. JIM*, 31, 425 (1991).
- [6] T. Zhang, A. Inoue, and T. Masumoto, *Mater Trans. JIM* 32, 1005 (1991).
- [7] A. Inoue, A. Kato, T. Zhang, S. G. Kim and T. Masumoto *Mater Trans. JIM* 32, 609 (1991).
- [8] A. Peker, W.L.Johnson, *Appl. Phys. Lett.* 63, 2342 (1993).
- [9] D. Xu, B. Lohwongwatana, G. Duan, W. L. Johnson and C. Garland, *Acta Mater.* 52, 2620 (2004).
- [10] J. Schroers and W.L.Johnson, *Appl. Phys. Lett.* 84, 3666 (2004).
- [11] A. Inoue, T. Nakamura, N. Nishiyama and T. Masumoto, *Acta mater.* 41, 915 (1993).
- [12] W.L.Johnson, *Bulk glass-forming metallic alloys*, MRS bulletin 42, (1999).
- [13] R. Busch and W.L. Johnson, *Appl. Phys. Lett.* 72, 2695 (1998).
- [14] T.A. Wanuik, R. Busch, A. Masuhr and W.L. Johnson, *Acta Mater* 46, 5229 (1998).

- [15] A. Masuhr, T. A. Waniuk, R. Busch and W. L. Johnson, *Phy. Rev. Lett.* 82 (11), 2290 (1999).
- [16] T. Shaw, C. Way and R. Busch, *MRS Proc.* 806, 215 (2004).
- [17] J. Jackle, "Models of the glass transition", *Rep. Prog. Phys.*, 49, 171 (1986).
- [18] S. A. Miller and R. H. Murphy, *Scr. Metall.* 13, 673 (1979).
- [19] H. Cohen and D. Turnbull, *ibid* 189 (1960).
- [20] A. J. Drehman and A. L. Greer, *Acta Metall.* 32, 323 (1984).
- [21] X.H. Lin and W.L. Johnson, *Mater. Trans. JIM.*38, 475 (1997).
- [22] M. Ohring and A. Haldipur, *Rev. Sci. Instrum.* 42, 530 (1971).
- [23] R. Pond and R. Maddin, *Trans. Met. Soc. AIME.* 245, 2475 (1969).
- [24] Ivan McCracken, MS thesis, Oregon State University (2002).
- [25] M.D.Ediger, C.A.Angell, Sidney R. Nagel, *J. Phys. Che.*, 100, 13200 (1996).
- [26] R. Busch, *JOM*, 52, 39 (2000).
- [27] H. S. Chen and D. Turnbull , *Acta Mater.* , 17, 1021 (1969).
- [28] D. Turnbull and J. C. Fisher, *J. Chem. Phys.*, 17, 71 (1949).
- [29] A. Inoue, *Acta Mater*, 48, 279 (2000).
- [30] G. Wilde, G. P. Görler, R. Willnecker and G. Dietz, *Appl. Phys. Lett.* 65 (4), 397 (1994).
- [31] R. Busch, Y.J. Kim, and W.L. Johnson, *J. Appl. Phys.*, 77, 4039 (1995).
- [32] R. Busch, W. Liu, and W.L. Johnson, *J. Appl. Phys.*, 83, 4134 (1998).
- [33] S. C. Glade, R. Busch, D. S. Lee, and W. L. Johnson 87(10), 7242 (2000).
- [34] D. A. Porter and K. E. Esterling, *Phase Transformations in Metals and Alloys*, Chapman and Hall(1997).

- [35] R. Böhmer, K.L. Ngai, C.A. Angell and D.J. Plazek, *J. Chem. Phys.* 99, 4201 (1993).
- [36] T. Lida and R.I.L. Guuthrie, *The Physical Properties of Liquid Metals*, Clarendon, Oxford (1998).
- [37] C. A. Angell, *J. Non-Cryst. Solids* 13, 131 (1991).
- [38] E. Bakke, R. Busch and W. L. Johnson, *Appl. Phys. Lett.* 67 (22), 3260 (1995).
- [39] R. Busch, A. Masuhr, E. Bakke and W.L. Johnson, *Acta Mater.* 46, 4725 (1998).
- [40] G. J. Diennes and H. F. Klemm, *J. Appl. Phys.* 17, 458 (1946).
- [41] A. Masuhr, R. Busch and W. L. Johnson, *Mat. Sci. Forum* 269-272, 779 (1998).
- [42] T. Shaw, C. Way and R. Busch, *MRS Proc.* 806, 215 (2004).
- [43] G. Adam, J.H. Gibbs, *J. Che. Phys.*, 43, 139 (1965).
- [44] S.V. Nemilov, *Glass Physics and Chemistry*, 21, pp 91 (1995).
- [45] A. Masuhr, R. Busch, W.L. Johnson, *Journal of Non-Crystalline Solids*, 250-252, 250, (1999).
- [46] J. W. Christian, *The Theory of Transformations in Metals and Alloys*, Pergamon, Oxford, (2002).
- [47] K. F. Kelton, *Solid State Phys.* 45, 75 (1991).
- [48] T.A. Wanuik, R. Busch, A. Masuhr and W.L. Johnson, *Acta Mater* 46, 5229 (1998).
- [49] T.A. Shaw, PhD thesis, Oregon State University (2004).
- [50] C. Way, PhD thesis, Oregon State University (2005).
- [51] J. Schroers, R. Busch, A. Masuhr and W. L. Johnson, *Appl. Phys. Lett.*, 74, 2806 (1999).

- [52] S. J. Kline and F. A. McClintock, *Mech. Eng.*, 75, 3 (1953).
- [53] H.A. Barnes, J.K. Hutton, and K. Walters, *An Introduction to Rheology*, Elsevier Science, Amsterdam (1989).
- [54] Y. J. Kim, R. Busch, W. L. Johnson, A. J. Rulsion, and W.K Rhim, *Appl. Phys. Lett* 65, 2136 (1994).
- [55] S. V. Nemilov, *Glass Phys. Chem.*, 21, 91 (1995).
- [56] R. Busch, A. Masuhr, E. Bakke, W. L. Johnson, *Mater. Sci. Form.*, 269, 547 (1998).
- [57] T. A. Waniuk, R. Busch, A. Masuhr and W. L. Johnson, *Acta. Mater.* 46, 5229 (1998).
- [58] L.A. Shadovspeaker and Ralf Busch, *Mat. Res. Soc. Symp Proc.* 806, 233 (2004)
- [59] D. Miracle, *Nature Materials*, 3 (10), 697 (2004).
- [60] H.W. Sheng, W.K. Luo, F.M. Alamgir, J.M. Bai, and E. Ma, *Nature*, 439, 419 (2006)

**References (Chapter 4)**

- [1] A. Inoue, Trans. Tech Publications, Mat. Sci. Found., 6, (1999).
- [2] W. L. Johnson, MRS bulletin, 24, 2342 (1993).
- [3] A. Inoue Acta Mater, 48, 279 (2000).
- [4] Klement, W., Willens, R.H., Duwez, P.: Nature (London) 187, 869 (1996).
- [5] H. Cohen and D. Turnbull, ibid 189 (1960).
- [6] K. Dini and R. Dunlap, J. Phys. F., 15, 273 (1985).
- [7] A. Inoue, W. Zhang, Mater Trans JIM, 43, 2924 (2002).
- [8] S. W. Lee, M. Y. Huh, E. Fleury and J. C. Lee, Acta Mater, 54, 349 (2006).
- [9] B. Lohwongwatana, J. Schroers, W. L. Johnson, Phys. Rev. Lett., 96, 075503 (2006).
- [10] T. Shaw, C. Way and R. Busch, MRS Proc. 806, 215 (2004).
- [11] C. Way, T. Shaw, P. Wadhwa and R. Busch, J. Alloys and Comp., 434, 88 (2007).
- [12] C. Way, P. Wadhwa and Ralf Busch, Acta Mater., 55(9), 2977 (2007).
- [13] A. Masuhr, R. Busch, and W.L. Johnson, Mater. Sci. Forum 269-272, 779 (1998).
- [14] A. Masuhr, T.A. Waniuk, R Busch, and W.L. Johnson, Phys Rev. Lett. 82, 2290 (1999).
- [15] C.A. Angell, Science, 267, 1924 (1995).
- [16] Miracle D. Nat Mater, 3, 697 (2004).
- [17] H. W. Sheng, W. K. Luo, F. M. Alamgir, J. M. Bai, E. Ma, Nature, 439, 419 (2004).

- [18] S. Aasland and P.F. McMillan, *Nature*, 369 (6482), 633 (1994).
- [19] C. A. Angell, *Annu. Phys. Chem.*, 55, 559 (2004).
- [20] I. Martin, T. Ohkubo, M. Ohnuma, B. Deconihout, K. Hono, *Acta Mater*, 52, 27 (2004).
- [21] Y. J. Kim, R. Busch, Rulison A. J. and W. L. Johnson, *Appl. Phys. Lett.*, 65(17), 2136 (1994).
- [22] A. Einstein, *Ann. Phys.* 34, 592 (1911).
- [23] D.R. Uhlmann, *J. Non-Cryst. Solids* 7, 337 (1972).
- [24] R. Busch, Y.J. Kim, and W.L. Johnson, *J. Appl. Phys.* 77, 4039 (1995).
- [25] G. Adam, J.H. Gibbs, *J. Chem. Phys.*, 43, 139 (1965).
- [26] S.V. Nemilov, *Glass Phys. and Chem.*, 21, 91 (1995).
- [27] H. J. Kriegl, E. Ratajski and M. Stadlbauer, *Rheol. Acta.*, 42, 355 (2003).
- [28] H. Janeschitz-Kriegl, *Monatshefte fur Chemie*, 138, 327 (2007).

**References (Chapter 5)**

- [1] A. Inoue, Trans. Tech Publications, Mat. Sci. Found., 6, (1999).
- [2] W. L. Johnson, MRS bulletin, 24, p.2342 (1993).
- [3] A. Inoue Acta Mater, 48, 279 (2000).
- [4] W. Clement, R. H. Willens and P. Duwez, Nature (London) 187, 869 (1960).
- [5] A. Inoue, T. Zhang and T. Masumoto, Mater Trans. JIM, 31, 425 (1991).
- [6] A. Inoue, A. Kato, T. Zhang, S. G. Kim and T. Masumoto Mater Trans. JIM 32, 609 (1991).
- [7] A. Peker, W. L. Johnson, Appl. Phys. Lett. 63, 2342 (1993).
- [8] D. Xu, B. Lohwongwatana, G. Duan, W. L. Johnson and C. Garland, Acta Mater. 52, 2620 (2004).
- [9] R. Busch, Y. J. Kim and W. L. Johnson, J. Appl. Phys. 77 (8) 4039 (1995)
- [10] G. Wilde, G. P. Gorler, R. Willnecker and H. J. Fecht, 87, 1141 (2000)
- [11] Turnbull, Contemp. Phys. 10, 473 (1969).
- [12] H. Kato, Y. Kawamura, A. Inoue, and H. S. Chen, Appl. Phys. Lett. 73, 3665 (1998).
- [13] T. G. Nieh, C. A. Schuh, J. Wadsworth, and Y. Li, Intermetallics 10, 1177 (2002).
- [14] T. Iida, R.I.L. Guthrie, The Physical Properties of Liquid Metals, Clarendon Press, Oxford (1998).
- [15] A. Masuhr, T.A. Waniuk, R. Busch, and W.L. Phys. Rev. Lett., 82 (1999).
- [16] T. Shaw, C. Way and R. Busch, MRS Proc. 806, 215 (2004).

- [17] C. Way, T. Shaw, P. Wadhwa and R. Busch, *J. Alloys and Comp.*, 434, 88 (2007).
- [18] C. Way, P. Wadhwa and Ralf Busch, *Acta Mater.*, 55(9), 2977 (2007)
- [19] A. Masuhr, R. Busch, and W.L. Johnson, *Mat. Sci. For.*, 269-272, 779 (1998).
- [20] S. Mukherjee, J. Schroers, W. L Johnson and W. K. Rhim, *Phys. Rev. Let.* 94, 245501 (2005).
- [21] M. Kuno, L. A. Shadowspeaker, J. Schroers, and R. Busch *MRS Proc.* 806, 215 (2003).
- [22] J. Schroers, K. Samwer, F. Szuecs, W. L. Johnson, *J. Mater. Res.* 15, 1617 (2000).
- [23] I.M. Krieger, S.H. Maron, *Journal of Applied Physics*, 25, 72 (1954).
- [24] H.A. Barnes, J.K. Hutton, and K. Walters, *An Introduction to Rheology*, Elsevier Science, Amsterdam, (1989).
- [25] D. Miracle, *Nature Matl.*, 3 (10), 697 (2004).
- [26] H.W. Sheng, W.K. Luo, F.M. Alamgir, J.M. Bai, and E. Ma, *Nature*, 439, 419 (2006).
- [27] C. A. Angell, *J. Non-Cryst. Solids* 13, 131 (1991).
- [28] C.A. Angell, *Science*, 267, 1924 (1995).
- [29] S.V. Nemilov, *Glass Physics and Chemistry*, 21, 91 (1995).

**References (Chapter 6)**

- [1] W.H. Wang, Q. Wei and S. Friedrich *Appl. Phys. Lett.*, 71 (8), 1053 (1997).
- [2] I. Martin, T. Ohkubo, M. Ohnuma, B. Deconihout, and K. Hono, *Acta Mater.*, 52, 4427 (2004).
- [3] S. Aasland and P.F. McMillan, *Nature*, 369 (6482), 633 (1994).
- [4] J.L. Yarger, C.A. Angell, S.S. Borick, and G.H. Wolf, *Supercooled Liquids ACS Symp.*, Series 676, 214 (1997).